CHAPTER 4

Stratospheric Aerosol Record and Climatology

Lead Authors:
Patrick Hamill
Colette Brogniez

Authors:
Juan Carlos Antuña
Darrel Baumgardner
Rich Bevilacqua
Christine Bingen
Greg Bodeker
Christine David
Terry Deshler
Didier Fussen
Mark Hervig
Chris A. Hostettler
John Mergenthaler
Thomas Peter
Graciela B. Raga
Larry Thomason
James C. Wilson

4.1 Introduction

In this chapter we present the stratospheric aerosol record obtained during the first three decades of quantitative measurements of its properties, and present a climatology of the stratospheric aerosol. The most intensely monitored property of the stratospheric aerosol layer is the extinction of solar radiation by the aerosol particles. This quantity has been measured by different satellite borne sensors for twenty-five years. Therefore, the principal parameter considered in this record is the aerosol extinction as a function of time, latitude, altitude, and wavelength.

The large amount of data obtained from satellite observations during the past quarter century forces us to limit ourselves to a few representative samples of the numerous plots and tables that have been generated for this report. A full set of the plots, tables and data sets that are described here are available at the SPARC Data Center web site *http://www.sparc.sunysb.edu* or at other web sites referenced below.

In Section 4.2 we present samples of the *primary* measured aerosol properties obtained by the various instruments: extinction, backscatter, absorption, and number density. The various measurements are characterized as follows:

(1) Global long term measurements of aerosol extinction and aerosol optical depth as obtained from the satellite systems SAM II, SAGE and SAGE II, HALOE, POAM II and POAM III.
(2) Global short term measurements of aerosol extinction from CLAES and ORA.
(3) Localized long term measurements of number density from the University of Wyoming balloon borne optical particle counter (OPC), and measurements of aerosol backscatter from a number of different lidar systems.
(4) Localized short term measurements from aerosol sensors on aircraft.

In Section 4.3 we present *derived* products from several of the data sets, specifically: aerosol surface area per unit volume of air (surface area density), aerosol volume (per unit volume of air), and particle effective radius, as derived from the SAGE II, HALOE and POAM II and III global long term measurements. We also discuss surface areas and effective radius from the University of Wyoming Optical Particle Counter (OPC), a localized long term measurement.

In Section 4.4 we *compare* primary and derived products as determined by various instruments. In particular, we present extinction comparisons for SAGE/HALOE, for SAGE/POAM and for SAGE/ORA. All of these instruments yield extinction as a primary product, although generally at different wavelengths. Extinction comparisons are also made for SAGE/OPC and SAGE/lidar. In these cases the extinctions for the OPC and the lidar systems are derived quantities. Furthermore, we present in that section comparisons of SAGE/HALOE/OPC derived values of surface area density, volume density, and effective radius.

Finally, some general conclusions are presented in section 4.6.

4.2 Primary Measured Aerosol Properties

Section 4.2.1 presents long term global measurements, that is extinction and optical depth measurements from the SAGE series of satellite instruments, the HALOE instrument, and the POAM satellite instruments. This is followed in Section 4.2.2 by aerosol extinction and optical depth from the global short term satellite instruments, namely CLAES and ORA. Section 4.2.3

gives localized long term measurements, specifically, the measurements of aerosol number density made with the University of Wyoming balloon borne optical particle counter (OPC), and measurements of aerosol backscatter from various lidar systems. Finally, Section 4.2.4 presents a number of short term measurements made by instruments mounted on aircraft, specifically lidars and particle counters.

4.2.1 Global Long-term Measurements of Extinction and Optical Depth

SAGE Series Aerosol Extinction and Optical Depth Measurements

The SAGE public release data is available on the NASA Langley Research Center's Atmospheric Sciences Data Center (*http://eosweb.larc.nasa.gov/*). With a few exceptions, as noted, this report is based on the release versions 6.1 for SAGE II and unnumbered versions for SAM II and SAGE. The recently released version 6.2 has an improved water vapor product but the aerosol products are essentially unchanged.

The dynamic range of extinction measurements (uncertainties < 100%) is instrument dependent. SAM II, SAGE, and SAGE II all have upper limits for extinction of around 0.02 km^{-1}, above which the line of sight optical depth is large enough for the atmosphere to be effectively opaque to the instruments. At 1000 nm wavelength, the lower extinction limits (due to instrument noise and limits on the digitizer) are 2×10^{-6} km^{-1} for SAGE and SAGE II but only about 5×10^{-5} km^{-1} for SAM II. At the shorter wavelengths the lower limit is 2-4 $\times 10^{-5}$ km^{-1}. The absolute precision of the measurements is relatively constant, thus the relative uncertainty decreases with increasing extinction. The precision is also dependent on the contribution of gas species to the total measured optical depth in the aerosol channels. For channels around 1000 nm, aerosol is by far the largest contributor except well above the tropopause where molecular scatter is important. On the other hand, molecular scatter and absorption by ozone strongly contribute in the shorter wavelength channels. As a result the precision in these channels is not as good as in the longer wavelength channels despite the short wavelength extinction being greater than the long wavelength extinction. In addition, since the magnitude of these effects is spatially and temporally variable, the precision has seasonal and latitudinal dependence. Figure 4.1 (a-d) shows the aerosol extinction measured vs. the relative uncertainty for the four SAGE II aerosol extinction channels in May of 1994. As this figure shows, the relative uncertainty at the upper end of the dynamic range is on the order of a few percent but increases significantly at the lower extinctions. The three shorter wavelength channels show a bifurcated structure in the relative error plots. The left wings of these plots correspond to data in the tropics where the Rayleigh contribution is smaller than for equivalent extinctions at mid and high latitudes since they occur at lower pressures. Due to the strong spectral dependence of the molecular scatter cross section ($\propto \lambda^{-4}$), molecular scatter at 386 nm is almost twice as large as it is at 452 nm and almost 50 times larger than it is at 1020 nm.

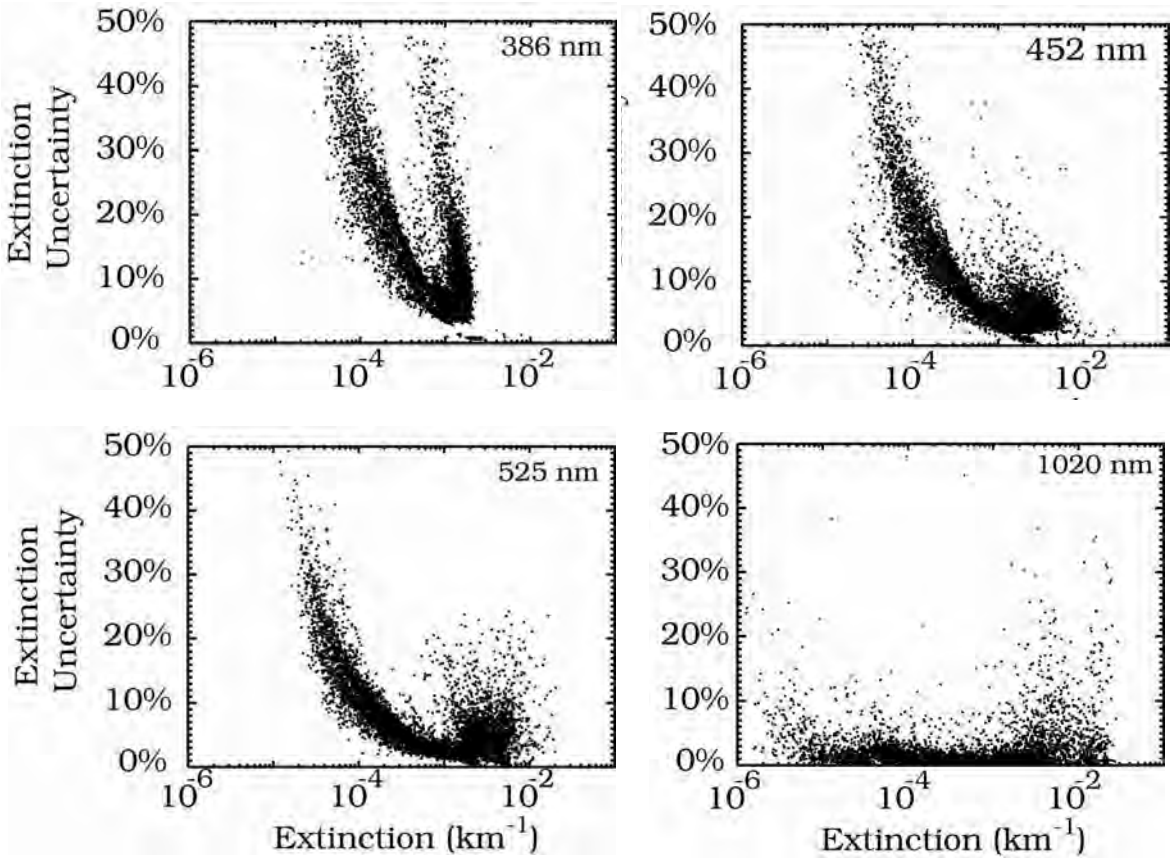

Figure 4.1 (a-d): Precision of SAGE II aerosol extinction in May 1994 as a function of extinction for 386, 453, 525, and 1020 nm, respectively.

Unlike measurements of most gas species, there is no standard measurement by which to assess systematic errors in the aerosol extinction measurements and efforts to evaluate this aspect of the measurements has been limited to comparisons with other satellite data sets [e.g., Burton et al., 1999; Randall et al., 2000, 2001]. These comparisons, and those later in this chapter, can establish the level of systematic bias between data sets but cannot establish an independent level of bias. For instance, comparisons of SAGE II and SAGE III extinction data in Thomason and Taha [2003], show mean differences less than 5% at the 3 short wavelength SAGE II channels, but nearly 15% at the 1020 nm channels which are generally considered to be the most robust measurements for both instruments. As of this writing, it is not clear what produces this difference. The optical depth measurements have a range of 0.0006 to 0.08 with precisions running from approximately 10% at the lower range to around 1% at the upper limit.

Figures 4.2a-d show the aerosol extinction as a function of latitude and altitude during January 1994 for 386, 452, 525, and 1020 nm, respectively. These figures were produced using 5-degree latitude bins and the native 0.5 km altitude bins and require at least 5 points per bin in order to create a value. The average tropopause altitude is calculated by NCEP, which also supplies the SAGE project with temperature profiles at measurement locations. The presence of cloud in individual profiles has been identified using the method of Kent et al. [1997a] and data determined to be clouds have been excluded from the archive and from the aerosol data sets discussed in the rest of this section. A brief discussion of the cloud clearing process and the statistics of cloud occurrences in the SAGE data sets is given in Section 4.3.1. All these figures show similar and familiar details [e.g., Trepte and Hitchman, 1993]. Aerosol extinction above 20 km has a maximum in the tropics where aerosol trapped within the tropical "pipe"

from the Pinatubo June 1991 eruption remains. (The tropical pipe model assumes the lower tropical stratosphere is isolated with respect to mixing from higher latitudes [Plumb, 1996].) Generally, away from low latitudes, lines of constant aerosol extinction gradually descend in altitude and, in fact, tend to be fairly homogeneous on surfaces of constant potential temperature (not shown). The exception is that within the winter/spring polar vortices (particularly in the Antarctic) aerosol extinction in the absence of polar stratospheric clouds (PSCs) is substantially less than outside the vortex as a result of diabatic subsidence and irreversible removal of aerosols through PSC formation [Thomason and Poole, 1993].

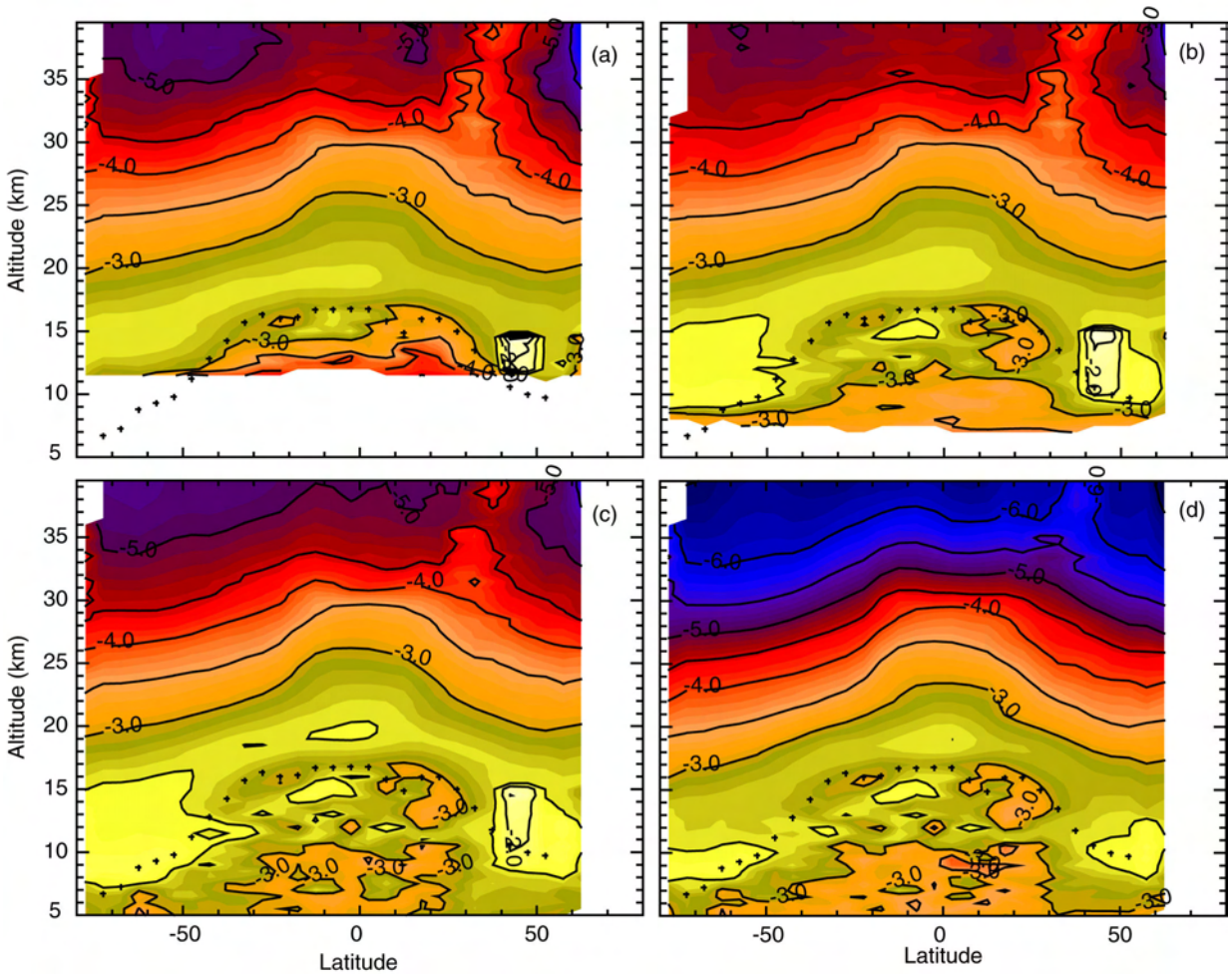

Figure 4.2: Zonal depictions of $\log_{10}$ aerosol extinction at (a) 386, (b) 452, (c) 525, and (d) 1020 nm measured by SAGE II during January 1994. The crosses represent the average tropopause altitude.

The two panels of Figures 4.3 show analyses typical of the data included in the ASAP (Assement of Stratospheric Aerosol Properties) data archive. In these figures, 1020 nm aerosol extinction from SAGE II is shown as a function of altitude and time for 40-45ºN and 0-5ºN. The data are shown at one month increments with a 3 month running median and requiring at least 5 points to produce a value in the data grid. In these figures, the effects of the eruptions of Nevado del Ruiz (Nov 1985), Kelut (Feb 1990), and Pinatubo (Jun 1991) can be seen. For the archive, data are produced for all four channels at 5 degree bins from 80ºS to 80ºN with both one and three month windows (called non-interpolated and interpolated, respectively). These analyses leave seasonally-based gaps at high latitudes as well as gaps at all latitudes during the period following the Pinatubo eruption and between the end of the SAGE mission in November 1981 and the beginning of the SAGE II mission in October 1984. SAM II, SAGE, and SAGE II data files are archived separately.

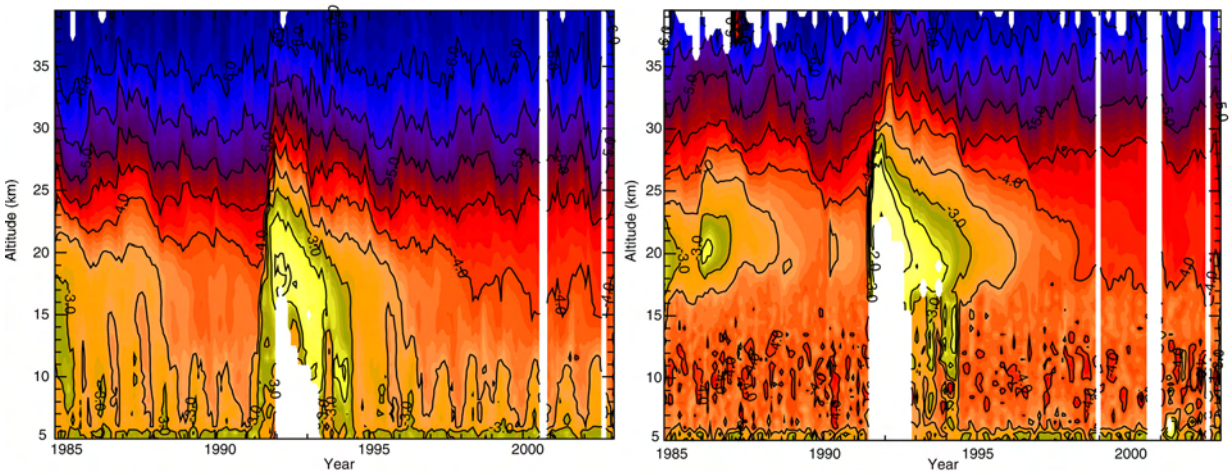

Figure 4.3: The SAGE II 1020 nm aerosol extinction (as $\log_{10}$) between 1984 and 2002 as a function of altitude for 40-45ºN (left) and 0 to 5ºN (right).

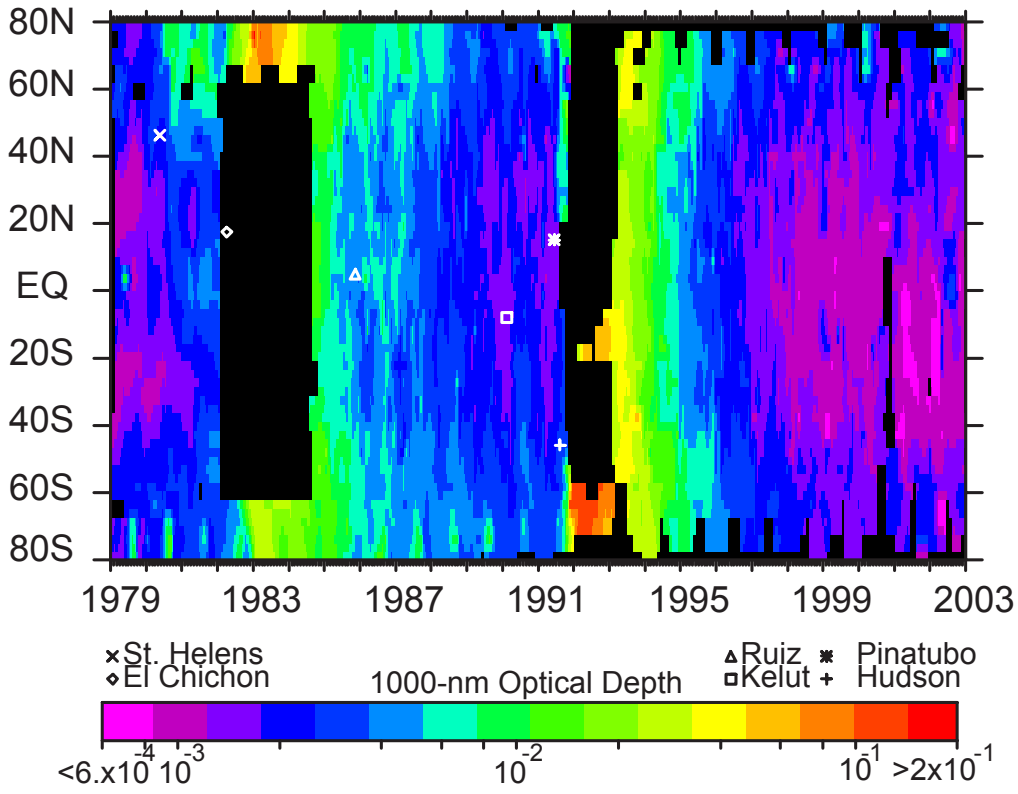

Figure 4.4: SAM II, SAGE, and SAGE II stratospheric aerosol optical depth at 1000 nm from 1979 through 2002. Profiles that do not extend to the tropopause are excluded from the analysis leading to a significant region of missing data following the eruption of Mt. Pinatubo in 1991. The earlier gap (1982-1984) was the period between SAGE and SAGE II.

Optical depth is so closely and simply related to extinction that we treat it as a primary product rather than a derived quantity. The optical depth data archived in the ASAP aerosol data set includes 1000-nm data from SAM II, SAGE, and SAGE II. Like the profile data, it is produced using a 3 month running median filter and 5-degree latitude bins. Aerosol optical depth at 1000 nm for 1979 through 2002 is shown in Figure 4.4 where all profiles that do not extend

down to the tropopause (due to the presence of cloud or high aerosol loading) are excluded. The persistent maximum in the tropical region is a result of the injection of aerosol (or its gaseous precursors) into the so-called tropical pipe by the powerful low latitude eruptions of El Chichón and Pinatubo. There are small wavelength differences between the instruments (1000 nm for SAM II and SAGE; 1020 nm for SAGE II) that can cause systematic differences in aerosol optical depth. Given the observed wavelength dependence of stratospheric aerosol optical depth, the differences should be less than 4%. The creation of a continuous, gap-free 1000 nm stratospheric optical depth data set is discussed in later sections.

HALOE Extinctions and Optical Depths

The current public release of HALOE data (V19) is available on the internet at http://haloedata.larc.nasa.gov/Haloe/home.html. Aerosol measurements are reported as extinction (units of km-1) profiles at four wavelengths (2.45, 3.40, 3.46, and 5.26 μm). Optical depths are not reported as a standard product but can be easily computed from the profiles as the vertical integral of extinction. Periodic measurement gaps are a result of variations in latitude coverage related to the UARS orbit, normal operational concerns, and (in some cases) spacecraft anomalies. For example, during normal operations HALOE measurements are paused if the instrument temperature is elevated due to increased sun exposure. During normal orbit progression, the angle between the orbit plane and earth-sun vector ("beta angle") oscillates between roughly -65° and +65°, and the greatest solar exposure (and therefore heating) occurs at large beta angles. Data gaps increased after the late 1990's due to spacecraft anomalies. Degradation of the UARS power and data systems has required duty cycling of the UARS instruments resulting in reduced operation time for HALOE.

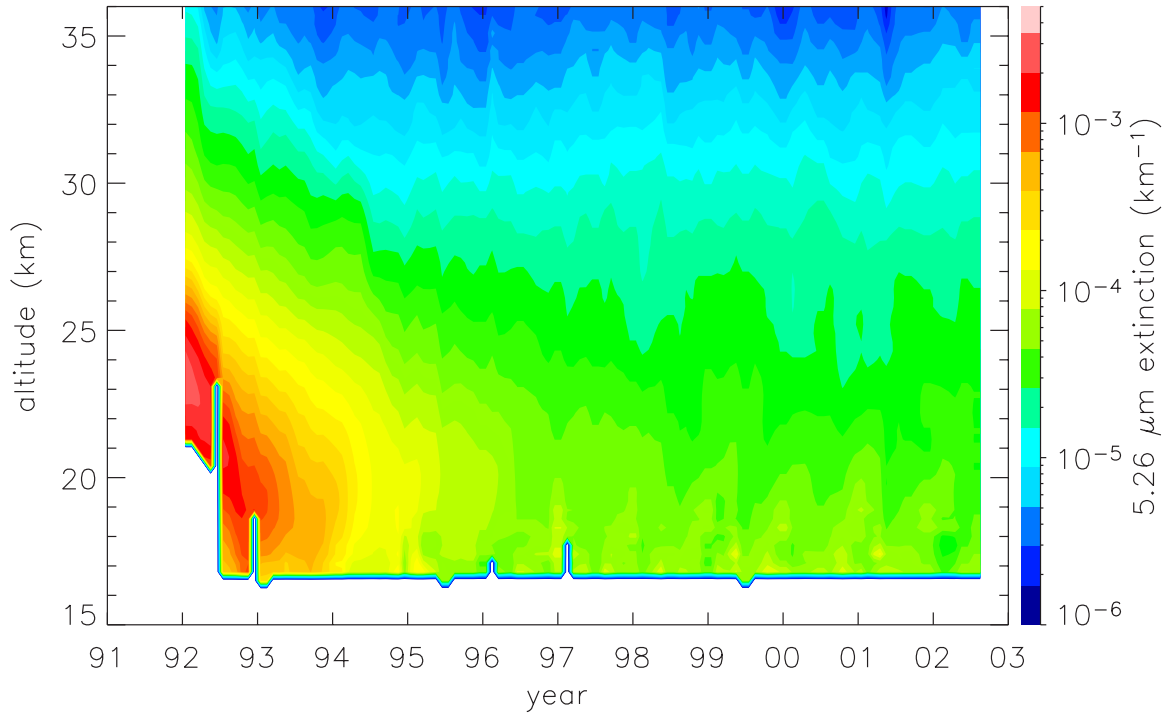

Figure 4.5: Time-height cross section of 5.26 μm HALOE aerosol extinction. The data are an average for latitudes from 2.5°S–2.5°N. White areas represent absent data. Measurements identified as affected by cirrus clouds were removed, resulting in the absence of data below 16 km altitude.

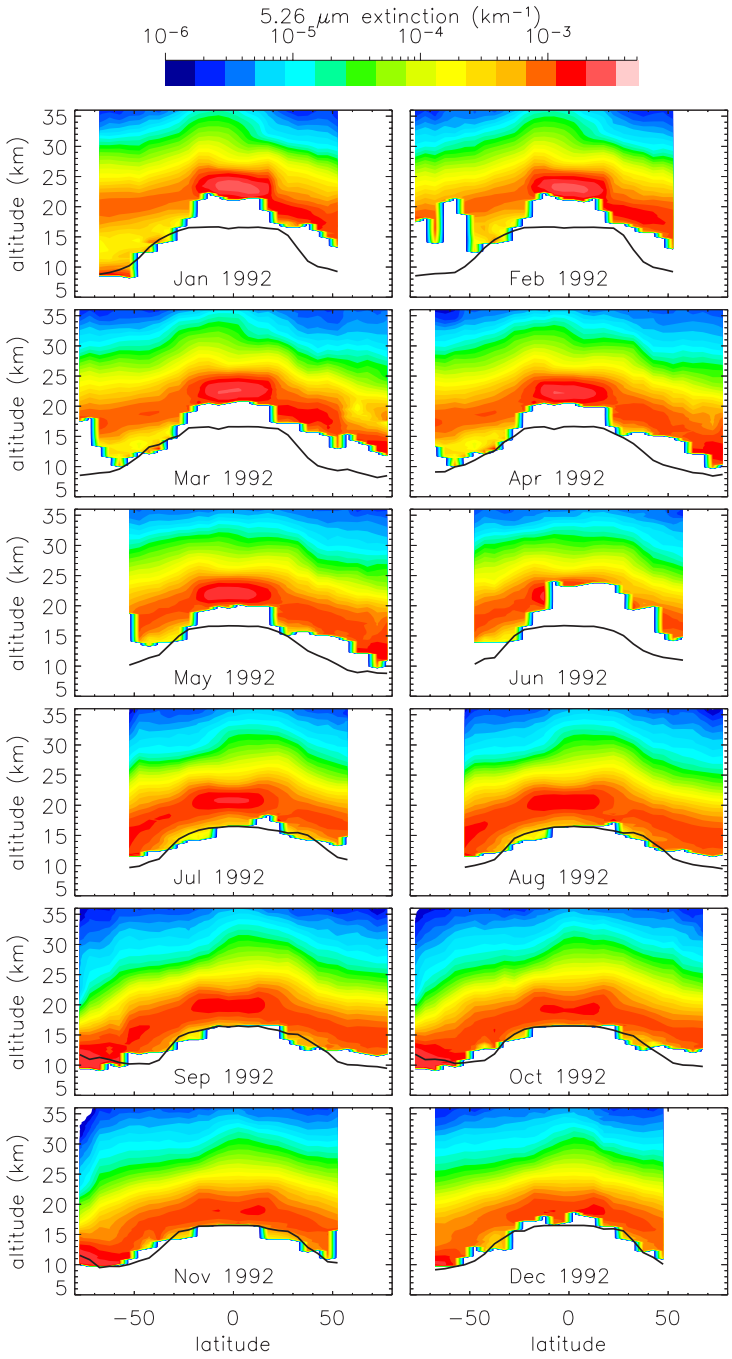

Figure 4.6: HALOE 5.26 μm aerosol extinctions as a function of altitude and latitude for each month in 1992, the year after the Pinatubo eruption. White areas represent missing data, and lines indicate average tropopause height. Measurements identified as cirrus were removed, resulting in the absence of data below the tropopause.

This section presents examples of stratospheric HALOE aerosol extinction and aerosol optical depths. The altitude history of 5.26 μm aerosol extinction near the equator is shown in Figure 4.5. Pinatubo aerosols are evident as enhanced extinctions at altitudes from the tropopause to over 35 km during the early 1990's. The enhanced aerosol loading decays rapidly until a near steady state is apparent after roughly 1997. During early 1992 the optical depth of the stratosphere was sufficient to cause complete opacity along the limb. The resulting saturation of the measurements accounts for data gaps in the lower stratosphere during early 1992. Latitude-

height cross sections of zonally averaged extinctions in 5 degree latitude bands are shown in Figures 4.6 and 4.7. Figure 4.6 shows 5.26 μm wavelength extinctions for each month in 1992. Pinatubo aerosols were concentrated at tropical latitudes during the early part of 1992, and spread towards polar latitudes as time progressed. Extinctions during the month of July for years from 1992 to 2002 are presented in Figure 4.7. The overall decrease in extinction from 1992 onward is due to decay of the Pinatubo aerosol cloud. Increasing data gaps after 1998 are due to duty cycling of the HALOE instrument.

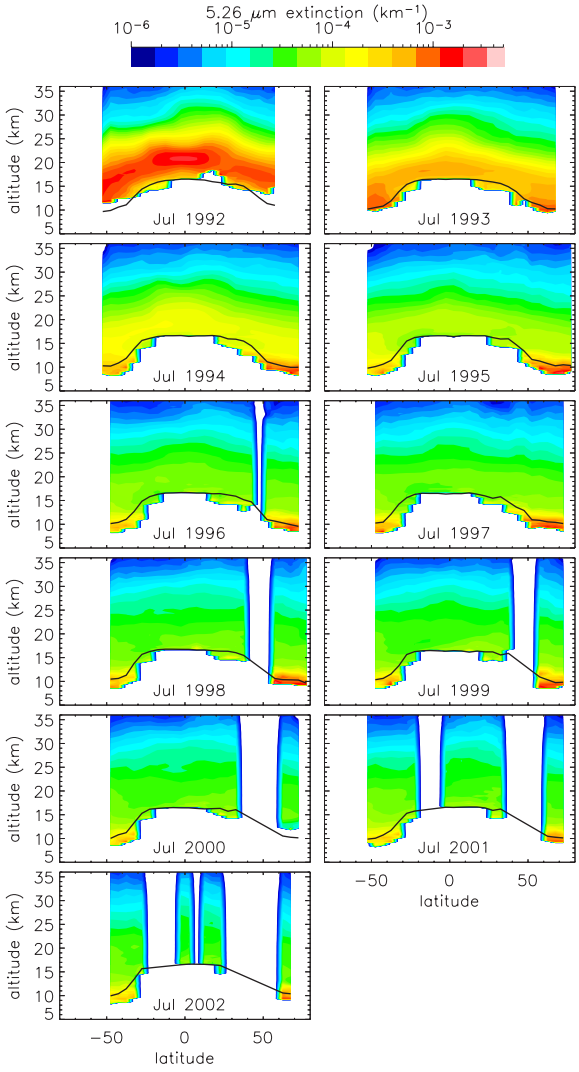

Figure 4.7: HALOE 5.26 μm aerosol extinctions as a function of latitude and altitude for the month of July during each year from 1992 to 2002. White areas represent missing data and lines indicate average tropopause height. Measurements identified as cirrus were removed, resulting in the absence of data below the tropopause.

HALOE optical depths at 5.25 μm are shown in Figure 4.8 as functions of latitude and time. Optical depths were calculated by integrating the extinction profiles from 2 km above the tropopause to 36 km and are presented as monthly averages. The steady removal of Pinatubo aerosols is observed in the early 1990s until an apparent steady state is reached after 1997.

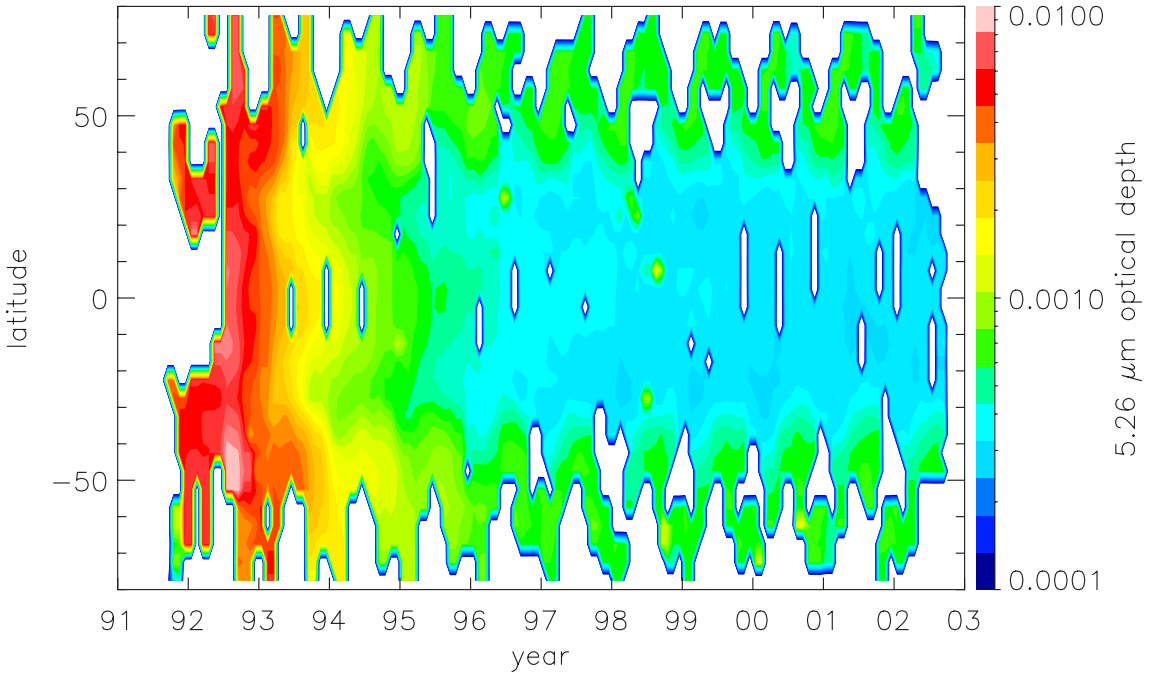

Figure 4.8: HALOE aerosol optical depth at 5.25 µm wavelength as a function of latitude and time for the period from 1991 to 2002. Optical depth was computed for altitudes from 2 km above the local tropopause (z_{trop} + 2 km) to 36 km. White areas represent missing data.

POAM II, POAM III Extinctions

As described in Chapter 3, as a consequence of satellite orbital properties, POAM II and POAM III only make measurements at high latitudes, The latitudinal variation of the POAM II and POAM III measurements is (exactly) annually periodic, as shown in Figure 4.9a (the POAM II and POAM III measurement coverage is identical).

In this section we present monthly averaged extinctions from the POAM instruments for the northern hemisphere (Figure 4.9b) and the southern hemisphere (Figure 4.9c). Extinction enhancements caused by PSCs were identified [e.g., Fromm et al., 1997, and 1999] and removed from the data to produce cloud free averages. PSCs occur intermittently in the POAM NH winter measurements, but are ubiquitous in the SH winter measurements. Data voids in the SH plots indicate periods where there were insufficient cloud free measurements to calculate a cloud free average. There are slight differences in the channel wavelengths of the POAM II and POAM III instruments. The extinction data shown for the first part of the time period 1994-1996 (POAM II) were obtained at wavelengths of 0.780 and 1.06 µm. The data during 1998-2004 (POAM III) were obtained at 0.779 and 1.02 µm.

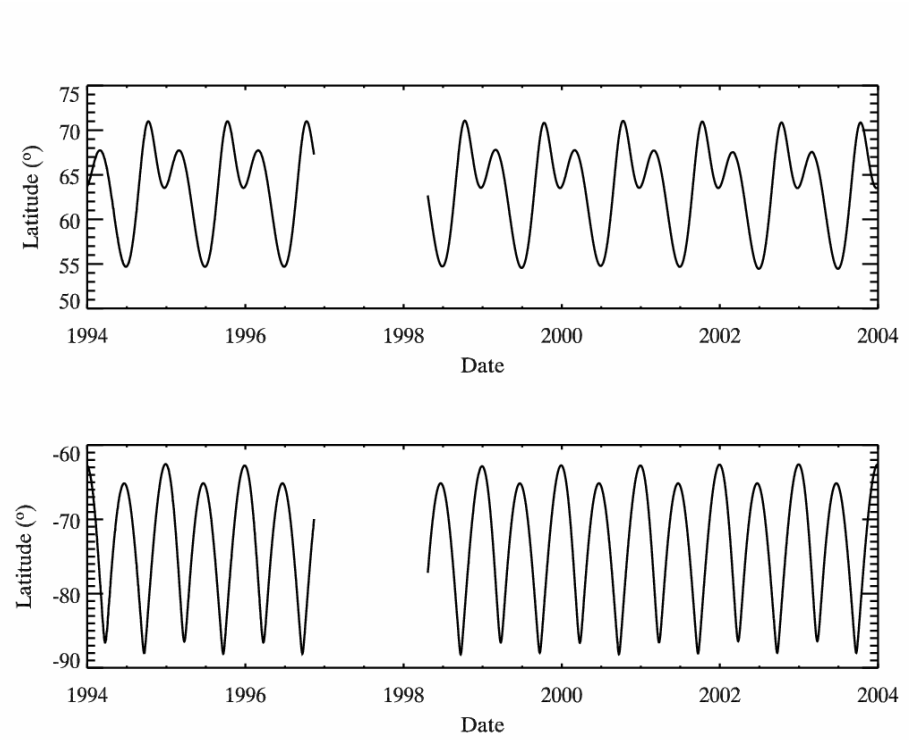

Figure 4.9a: POAM II and POAM III measurement coverage. For both instruments, the southern hemisphere measurements are obtained in spacecraft sunset, and the northern hemisphere measurements in spacecraft sunrise.

The northern hemispheric extinctions clearly show the residual effect of the Mt. Pinatubo eruption that caused elevated extinctions up to at least 23 km until late 1996. The periodic increases observed in the 10-13 km altitude region are most probably the result of enhanced horizontal transport during the summer of high aerosol extinction upper troposphere air from lower latitudes. Similar features were observed in the POAM water vapor and ozone mixing ratios as reported by Nedoluha et al. [2002] and Prados et al. [2003].

The POAM latitude variation is greater in the SH than the NH, and impacts the seasonal variation observed in the SH. The extinction maxima observed mainly in the late winter at low altitudes is probably the result of incomplete removal of PSC extinction enhancements (which extend down nearly to the tropopause late in the winter [Fromm et al., 1997]) from the data record.

The monthly averaged POAM extinction profiles were integrated vertically to calculate the total stratospheric optical depth, as shown in Figure 4.10. The vertical range of integration begins at 3 km above the tropopause and extends to 30 km altitude, using a tropopause defined by the 3 pvu potential vorticity level. The near constant aerosol optical depth after the decay of the residual Mt. Pinatubo aerosol suggests that background aerosol levels were reached in the polar regions in the measurement gap between 1996 and 1998.

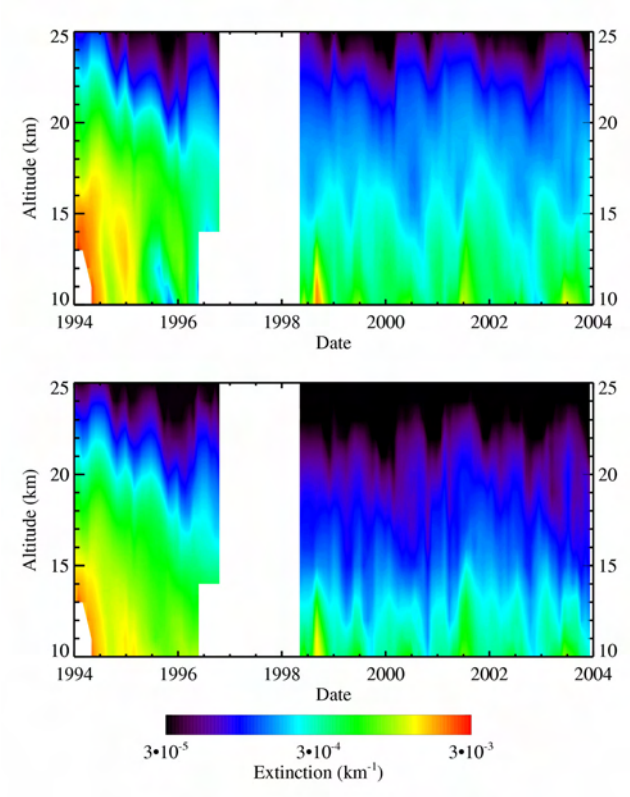

Figure 4.9b: POAM northern hemisphere aerosol extinction measurements for 1994 to 2003. (a) Extinction at 0.781 µm before gap and 0.779 µm after gap. (b) Extinction at 1.06 µm before gap and 1.02 µm after gap. Year labels denote the beginning (Jan 1) of each year.

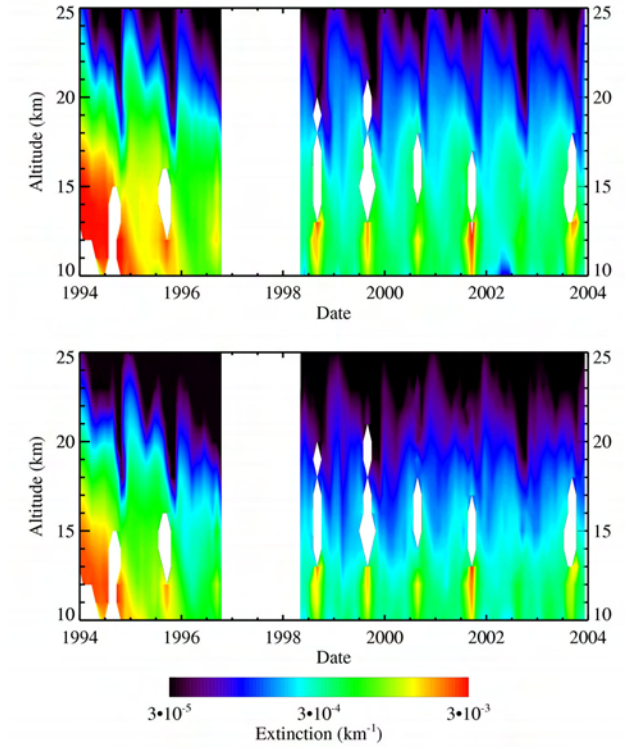

Figure 4.9c: POAM southern hemisphere aerosol extinction measurements for 1994 to 2003. (a) Extinction at 0.781 µm before gap and 0.779 µm after gap. (b) Extinction at 1.060 µm before gap and 1.020 µm after gap. Year labels denote the beginning (Jan 1) of each year.

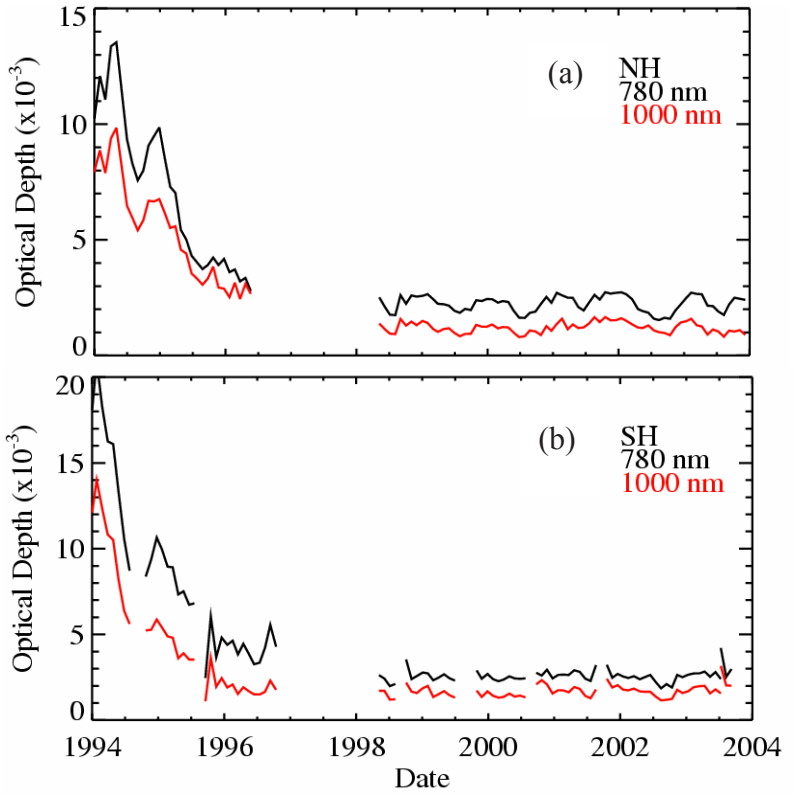

Figure 4.10: POAM stratospheric aerosol optical depth for the (a) northern hemisphere and (b) southern hemisphere. The optical depth was calculated by integrating the extinction profiles from 3 km above the tropopause to 30 km in altitude. The optical depth at 0.78 µm (black) and 1.0 µm (red) are shown.

4.2.2 Global Short-term Measurements

ORA

An overview of the ORA extinction profiles at 1013 nm is given in Figure 4.11 for the month of February 1993. The extinction profiles are defined at 26 altitude levels, with an increment of 1 km up to 25 km, and 2.5 km from 25 to 50 km. All profiles have been binned in latitude intervals of 5°, and cover most of the ORA latitudinal range (40°S to 40°N). Similar data are available over the whole duration of the ORA mission (August 1992 – May 1993) and for 6 spectral channels at 340, 385, 435, 442, 600 and 1013 nm. These data are available on the SPARC Data Center website.

CLAES

In this section we present plots of extinction *vs.* altitude and latitude as obtained from the CLAES data set. Figures 4.12 – 4.14 are examples of higher level aerosol products constructed from individual aerosol volume extinction coefficient profiles. Extinction and absorption coefficients are used interchangeably in discussions of CLAES aerosol data since they are essentially equal for the infrared wavelengths of interest here.

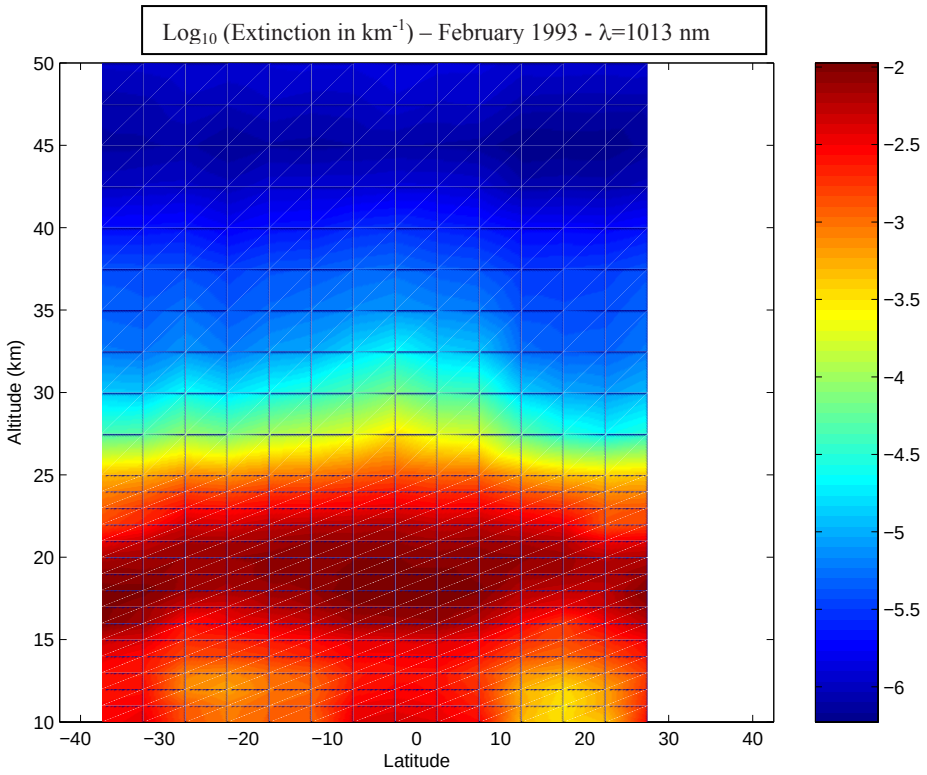

Figure 4.11: Dependence in latitude and altitude of the aerosol extinction (at 1013 nm) measured by the ORA instrument during February 1993. The color bar corresponds to the base 10 logarithm of the extinction measured in km^{-1}.

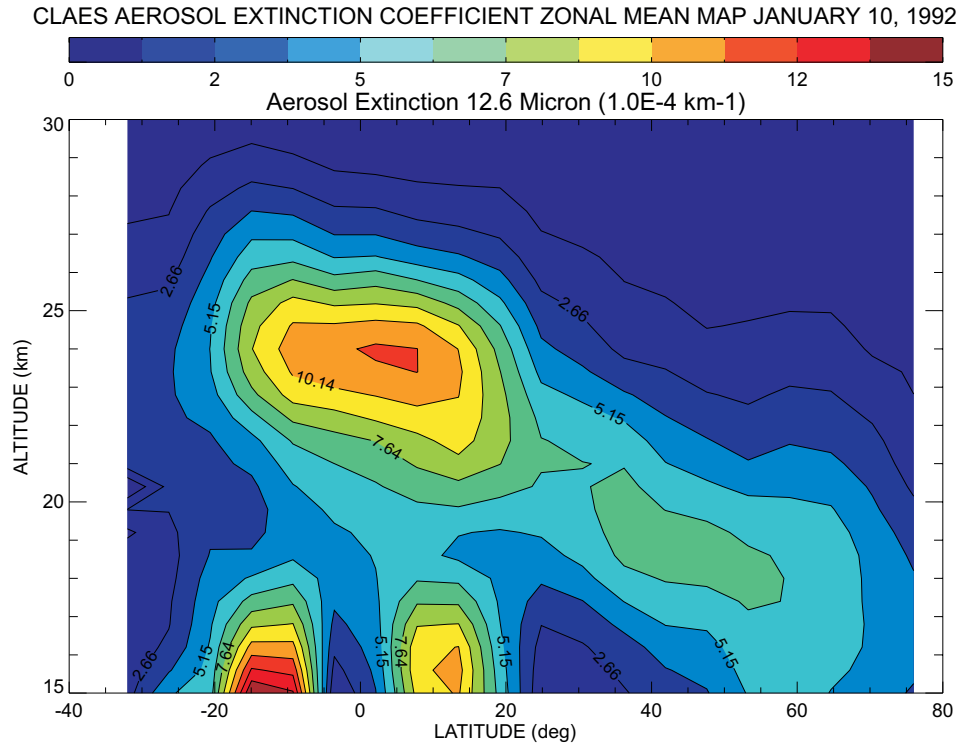

Figure 4.12: Extinction vs. latitude and altitude for one day (January 10, 1992) from the CLAES 12.6 µm measurements.

Figure 4.12 shows the zonal mean of aerosol extinction at 12.6 µm for January 10, 1992 (early winter NH). The tropical stratospheric "reservoir" region shows high aerosol extinction from

the Mt. Pinatubo eruption of June 15, 1991. Clearly, a significant amount of aerosol has been transported into the winter hemisphere at this time; nevertheless the stratosphere at very high northern latitude is relatively clean due to the barrier presented by the polar vortex. At low altitudes in the tropics, the high extinction patches are due to tropical cirrus near the tropopause (~16 km).

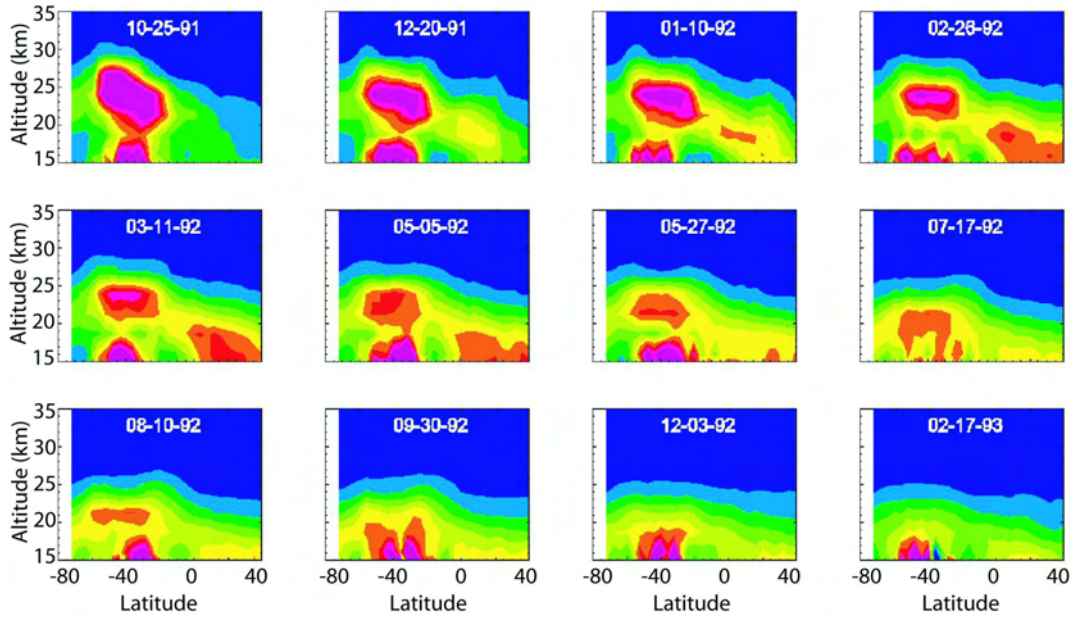

Figure 4.13a: CLAES zonal mean aerosol absorption as function of altitude (15-35 km). The orientation of the satellite yields this northward view, so the coverage is from 34°S to 80°N.

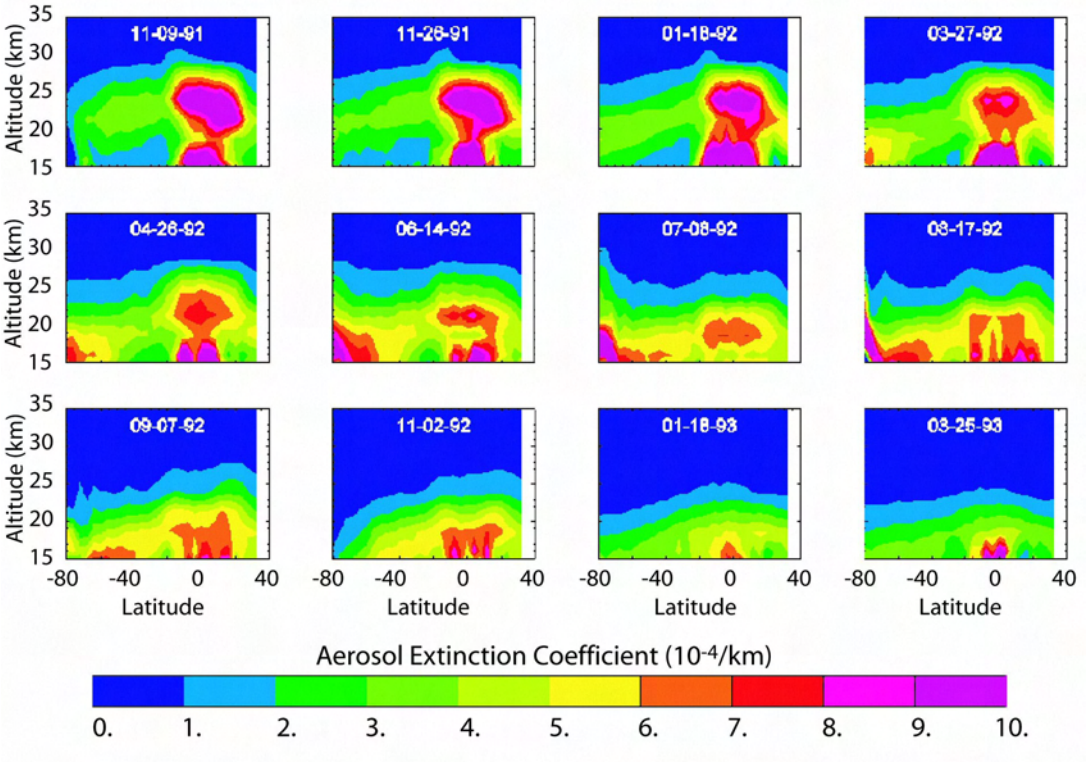

Figure 4.13b: CLAES zonal mean aerosol absorption as function of altitude (15-35 km). The orientation of the satellite yields this southward view, so the coverage is from 80°S to 34°N.

Figures 4.13a and 4.13b are a series of zonal mean aerosol extinction snapshots at 12.6 μm for north and south viewing, respectively. Taken together they reveal the evolution of the Mt. Pinatubo aerosol as observed over the entire CLAES lifetime. Polar stratospheric clouds are prominent as high extinction regions particularly in the SH winter. The parameter Z* is pressure equivalent altitude, given by

$$Z^* = 16.0 \times (3 - \log_{10}(p)),$$

with p in hPa and Z* in km.

Figure 4.14 shows the mean aerosol optical depth at 12.8 μm as constructed from the mission-long set of zonal mean averages. This composite was constructed by integrating mean aerosol extinction upward from 68 hPa in the tropics (20°S to 20°N) and upward from 100 hPa in the extratropics.

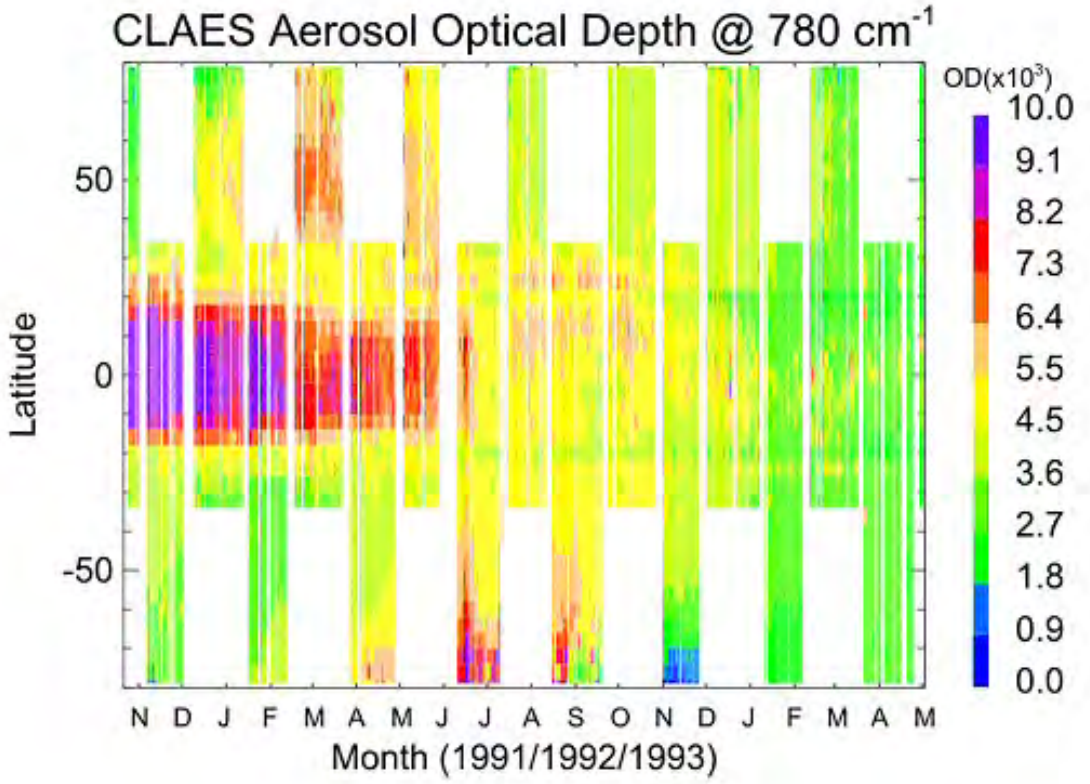

Figure 4.14: CLAES zonal mean optical depths at 12.8 μm for the entire mission.

4.2.3 Localized Long-term Measurements

University of Wyoming balloon borne in situ measurements

Balloon borne optical particle counters have been used by the University of Wyoming to measure stratospheric aerosol size and number density since 1970. Although the balloon borne sensors have been launched from many locations, regular long term flights have only been conducted from Laramie Wyoming. These have captured the major eruptions of Fuego, El Chichón and Pinatubo as well as a number of smaller eruptions. Example aerosol profiles for volcanically perturbed and quiescent periods are shown in Figure 4.15.

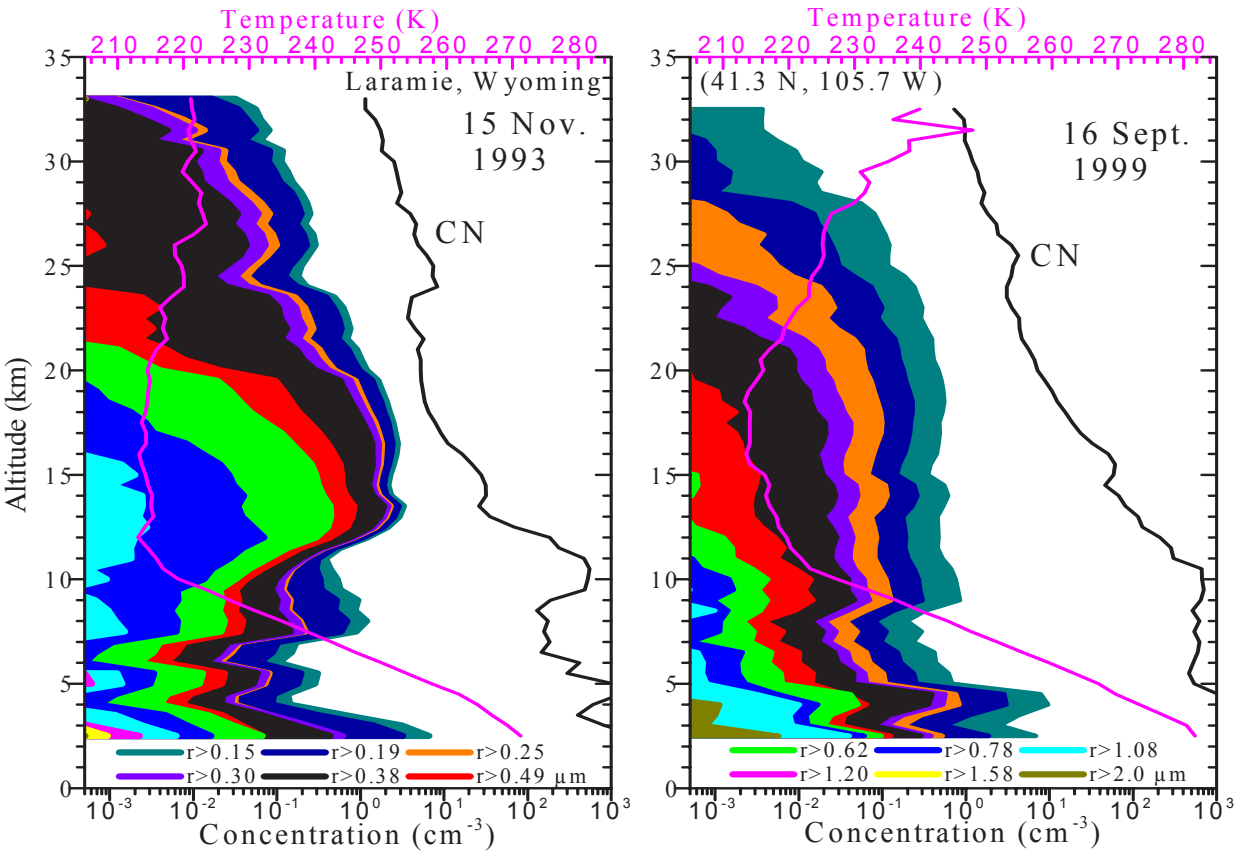

Figure 4.15: Vertical profiles of aerosol concentration above Laramie, Wyoming, for particles in twelve size classes ranging from radius $r > 0.15$ to $r > 2.0$ µm (in color), and condensation nuclei ($r > 0.01$ µm, black line). Temperature profile is also shown (pink line). The left hand panel was obtained 18 months after the eruption of Pinatubo when the stratosphere was still highly disturbed. The right hand panel is a typical profile during a volcanically quiescent period. The color codes for the twelve size ranges are presented at the base of the two panels.

The temporal history of the Laramie measurements is shown in Figure 4.16. The figure presents the history of the two fundamental sizes measured since the program began. Error bars represent the counting error, and are at times smaller than the data symbols. The Laramie measurements represent about 340 individual profiles. Also included in the figure are 12 measurements from Lauder, New Zealand using the same instrumentation. Eruption times for the nine stratospherically important volcanic eruptions occurring during the period are indicated.

Integrated Backscatter from Various Lidar Systems

Table 3.2 (in Chapter 3), gives a list of the various stratospheric aerosol lidars operated in the past or still running today, from Arctic to Antarctic latitudes. These lidar stations can provide suitable datasets for establishing a stratospheric aerosol climatology. Their location is shown in Figure 3.7 and their characteristics and integrated backscatter records are given below.

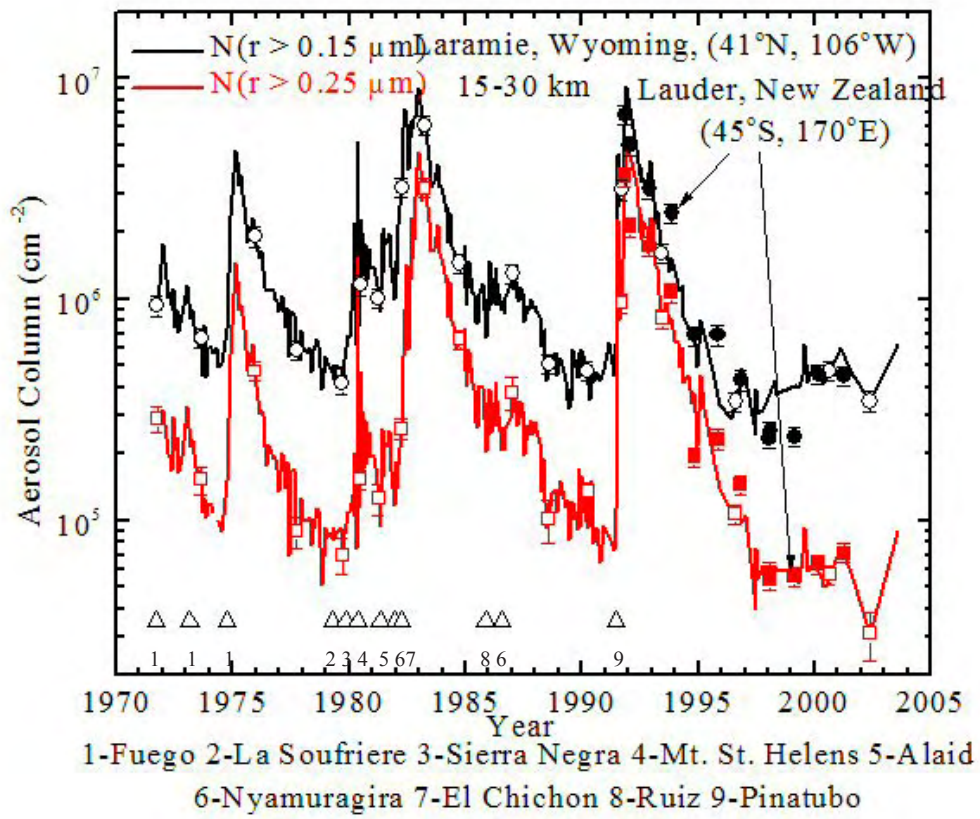

Figure 4.16. History of 15-30 km column integrals, above Laramie, Wyoming, of aerosol number for particles > 0.15 (black line) and 0.25 μm radius (red line). Example error bars are shown on the occasional data point. Twelve measurements from Lauder, New Zealand are included (filled symbols with error bars).

Formulation of a Lidar-Based Stratospheric Aerosol Climatology

Establishing a reliable stratospheric aerosol climatology from ground-based lidar observations is difficult because of the inhomogeneous geographical distribution of the lidar stations throughout the world, in latitude and longitude. Most lidar sites are located in industrial countries in the northern hemisphere, as shown in Figure 3.7, between 20°N and 50°N, and between 160°W and 15°E. Only three datasets are available in the southern hemisphere. Of these, two are polar and one is tropical so limited measurements are available from the southern mid-latitudes. Consequently, lidar observations do not give a complete picture of the zonal distribution of stratospheric aerosol properties.

Long-term time series of lidar aerosol measurements from selected sites are presented in Figure 4.17. They are presented as time evolution of the integrated backscatter coefficient. The various datasets are not readily compared due to the differences between experimental procedures, particularly operating wavelengths and processing methodologies used in each location, as well as different altitude ranges used for evaluation. Additionally, polar locations provide measurements only during winter, and their focus is polar stratospheric cloud observations. The dif-

ferences in aerosol content (background or volcanic) also induce a high variability of total uncertainties for each data set.

Ny-Alesund, Spitzbergen
78.92° N, 11.93° E
532 nm
trop+ 2 km → 30 km

Garmisch-Partenkirchen, Germany
47.48° N, 11.06° E
694 nm
trop + 1 km → 30 km

Hampton, U.S.A.
37.1° N, 76.3° W
694 nm
trop → 30 km

Mauna Loa, U.S.A
19.54° N, 155.58° W
694 nm
15.8 km → 33 km

Saõ José dos Campos, Brazil
23.2° S, 45.9° W
589 nm
17 km → 35 km

Dumont d'Urville, Antarctica
66.67° S, 140.01° E
532 nm
trop → 30 km

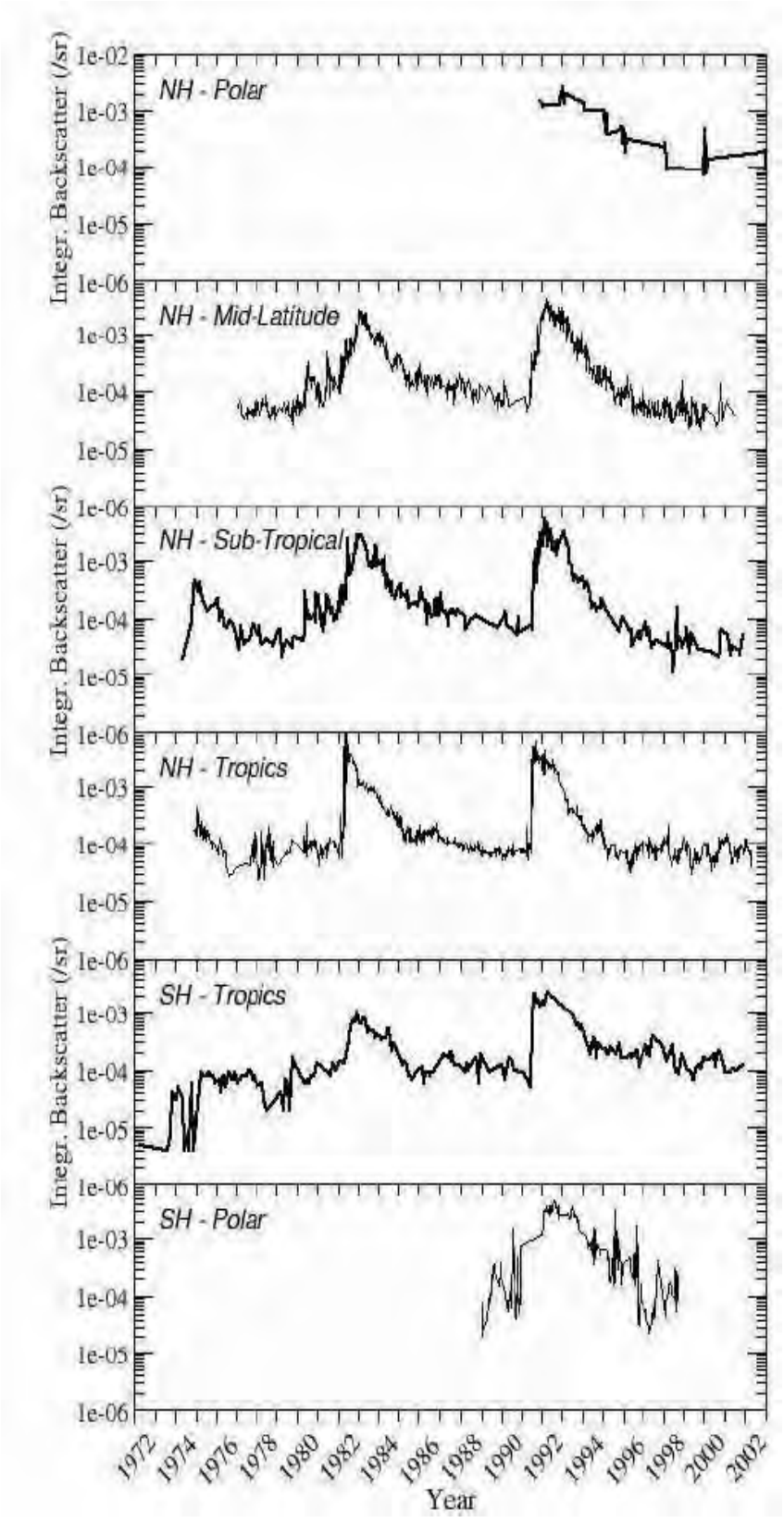

Figure 4.17: Time evolution of integrated backscatter coefficient from aerosol lidar measurements in different latitude bands, from north to south, between 1972 and 2003. The altitude integration interval is given for each station as last entry in the left column (trop. = tropopause height).

Polar Stratospheric Clouds are visible in the data sets from both Polar Regions. The impacts of various volcanic eruptions also appear, depending on the location of the eruption with respect to the measurement station. Most of the data sets clearly show the decay of the volcanic loading and an apparent return to background conditions.

4.2.4 Short Term Localized Measurements

NASA Langley Airborne Aerosol Lidar

Airborne lidars offer distinct advantages over ground-based systems in that they can characterize the horizontal as well as the vertical distribution of aerosol and can be deployed to locations of interest around the globe. They also offer advantages over satellite instruments in terms of far greater vertical and horizontal resolutions and the ability to focus the observations on a particular target at a specified time (e.g., a volcanic plume or the formation of PSCs in the Arctic cold pool). The disadvantage, of course, is that such systems are deployed only occasionally and do not provide wide geographic coverage. Nonetheless, occasional airborne lidar measurement campaigns have provided otherwise unobtainable information on the distribution of aerosols and insight into sampling issues associated with satellite instruments that rely on occultation or other geometries which have much lower horizontal and vertical resolution.

Below we present observations acquired by the NASA Langley Aerosol Lidar while deployed on the NASA DC-8 aircraft during the SOLVE-II/Vintersol campaign. This lidar is a piggyback instrument on the NASA Goddard Airborne Raman Ozone Temperature and Aerosol Lidar (AROTAL), which measures ozone and temperature profiles in a zenith viewing geometry.

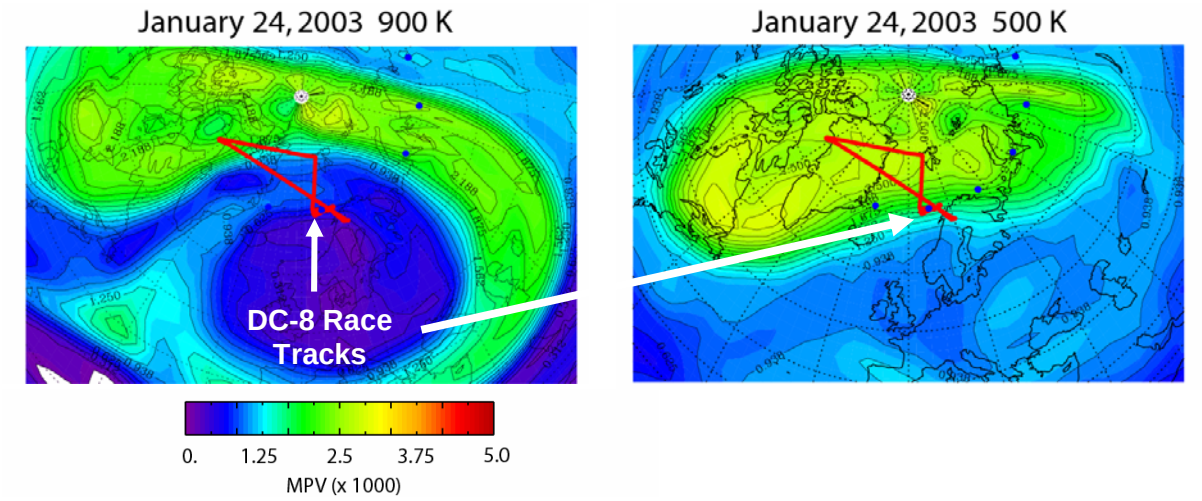

Figure 4.18. Potential vorticity contours for the 500K and 900K potential temperature surfaces and the flight track (red lines) of the NASA DC-8 for the 24 January 2003 flight of the SOLVE-II/Vintersol campaign.

On 24 January 2003, the polar vortex was transitioning from a two-lobe structure to an elongated elliptical circulation pattern. Figure 4.18 shows potential vorticity contours at the 500 K and 900 K levels and the flight track of the DC-8. As can be seen from the difference between the potential vorticity contours, the vortex boundary sloped to the northwest with altitude along the flight track of the DC-8. Figure 4.19 shows the lidar data and the contours of potential vorticity as a function of altitude and distance along the DC-8 flight track. The lidar profiles acquired along most of the flight track penetrated two regimes, with the lower altitude region being generally within the vortex and the higher region being generally outside the vortex. The

thin filamentary layers above 20 km are similar in structure to the potential vorticity contours. It is clear that these filaments were external to the polar vortex while the lower mass of stratospheric aerosol located toward the middle of the plot (~12:50 – 17:32 UT) was largely within the vortex. Seven-day back trajectories confirm that the filaments originated at lower latitudes.

From 10:30 to 12:00 UT, the DC-8 was flown in a series of nearly closed circuits at varying altitudes (racetrack pattern) in the vicinity of a SAGE III occultation point. Figure 4.20 presents a comparison between the SAGE III extinction profile and that computed from the lidar data acquired near the occultation point. The lidar backscatter data were converted to extinction using extinction-to-backscatter ratios derived from mid-latitude balloon-borne optical particle counter measurements of stratospheric aerosol size distributions [Jäger and Deshler, 2002]. The thin aerosol layers above 20 km appearing in the lidar data in Figures 4.19 and 4.20 are also apparent in the SAGE III data.

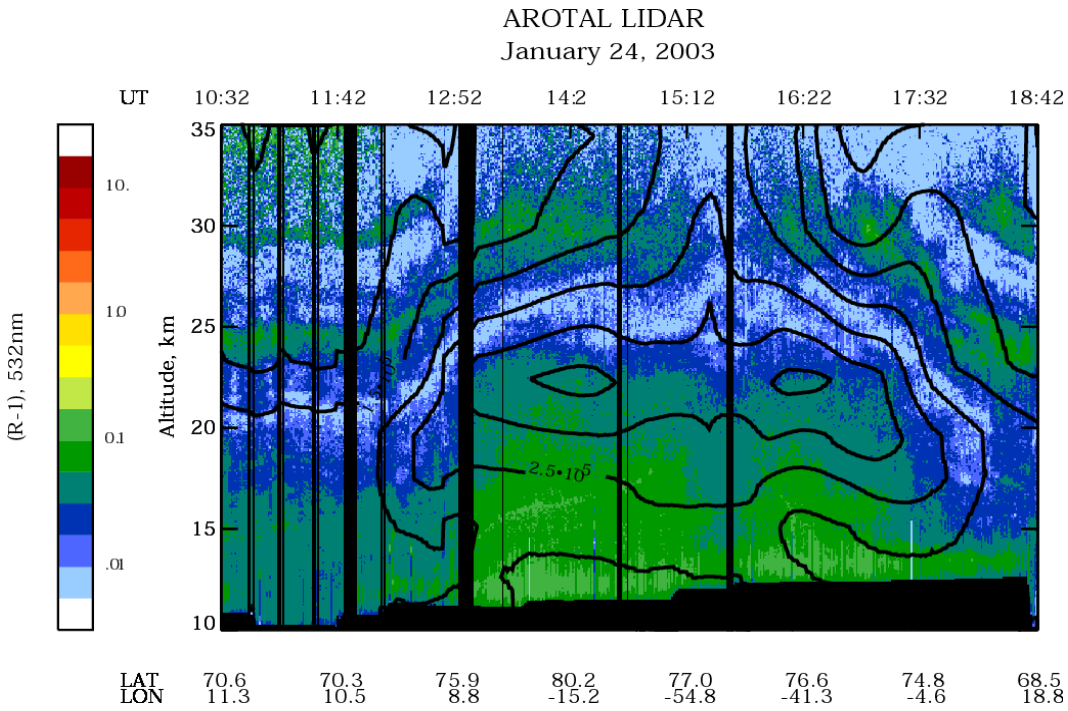

Figure 4.19. AROTAL/LaRC Aerosol Lidar data from the 24 January 2003 flight on SOLVE-II/Vintersol. The color contours show the 532 nm aerosol scattering ratio (ratio of aerosol backscatter to molecular backscatter) and the black lines show contours of potential vorticity.

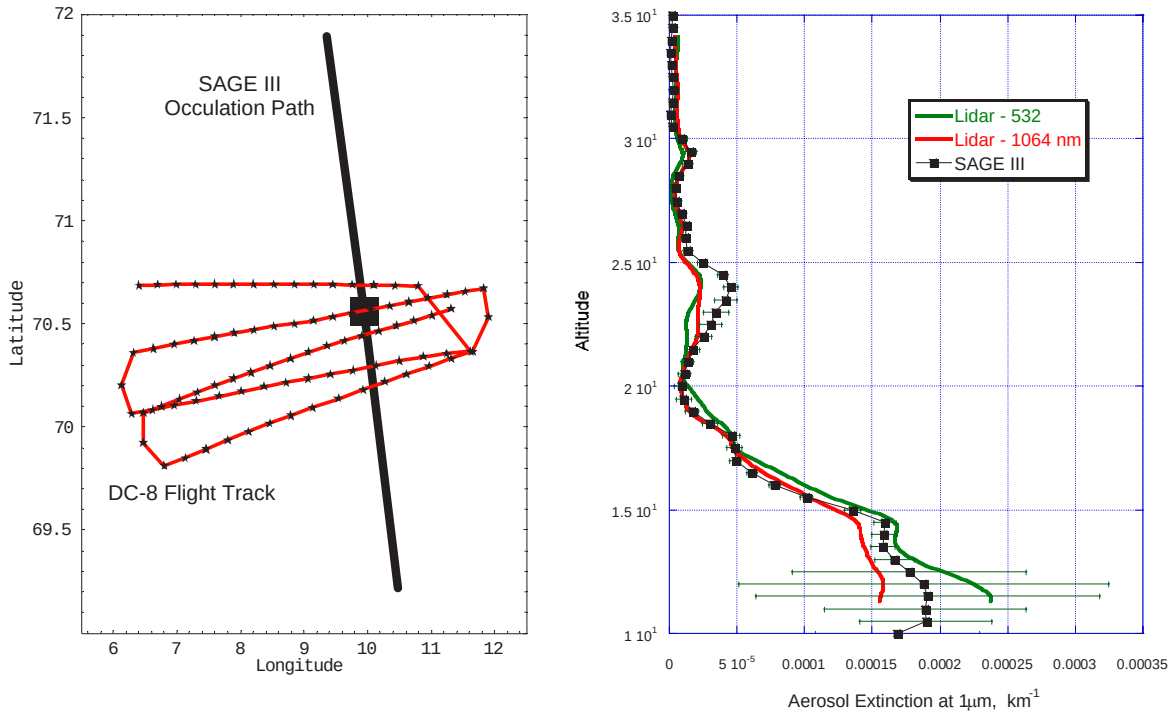

Figure 4.20. The left panel shows the DC-8 flight tracks and SAGE III occultation path for the 24 January 2003 validation coincidence from the SOLVE II mission. The DC-8 flight track is in red with locations of archived lidar profiles marked with stars. The SAGE III occultation path is shown in black. The right panel shows a comparison of SAGE III extinction at 1020 nm with extinction at 1064 nm computed from the lidar 532 nm (green) and 1064 nm (red) aerosol backscatter data averaged in the vicinity of the SAGE III ray path. The lidar aerosol backscatter data were scaled to extinction at 1064 nm using conversion parameters from Jäger and Deshler [2002].

The lidar data provide a useful validation of both SAGE III extinction values and altitude registration. The vertical structure observed in the SAGE III data is reproduced in the lidar data, and through much of the profile the lidar extinction values are nearly identical. Differences between the SAGE III and lidar extinction values (such as at 24 km in Figure 4.20) are likely due to several causes. First, the microphysical models used to convert aerosol backscatter to extinction were based on mid-latitude measurements of size distribution which can be quite different in the polar region. Second, the DC-8 did not fly its racetrack pattern along the direction of the SAGE III occultation path: the SAGE III occultation path was nearly perpendicular to the vortex boundary viewing across the largest gradients in aerosol distribution, while the DC-8 flight tracks were approximately parallel to the boundary. Third, differences may also be caused by subtle instrument nonlinearities (a very small nonlinearity can create a relatively large error in the aerosol retrieval when aerosol loading is very low, as it is for this case). Regardless of these differences, variation of the vertical and horizontal structure of the aerosol as shown by the lidar data in Figure 4.19 provides insight on sampling issues for satellite-based occultation instruments, in particular, the potential for vertical smearing of complex structures due to the long occultation path (e.g., ~175 km). For those situations where detailed information on the small scale vertical and horizontal structure of the aerosol distribution is required, airborne lidar remains the best technique currently available.

DLR Airborne Lidar

Figure 4.21 shows another example of a 2-D aerosol curtain as observed by an aircraft-borne lidar, the aerosol and ozone lidar (OLEX), onboard the DLR Falcon. The data were taken during a flight from Kiruna to Munich on 8 February 1999. This flight took place below the Arctic vortex, which was elongated towards central Europe and interleaved with layers of mid-latitude air. The air in the Arctic vortex is older than stratospheric air at mid-latitudes [Waugh and Hall, 2002] and is subjected to the general subsidence that takes place in the vortex. Therefore, the sulfate aerosol backscatter observed in the vortex differs from that observed outside the vortex, as is evident from Figure 4.21. Note that within the vortex, as outside it, the stratospheric aerosol is strongly stratified. During January 1999, there were intrusions of mid-latitude air into the vortex and a peeling of filaments from the vortex edge, followed by intensive stirring. The filament boundary layers typically extend over 100 m vertically and a few kilometers in the horizontal. Under typical stratospheric conditions, it takes about two weeks until 3-D turbulence takes over and effectively mixes air masses at these scales [Flentje and Kiemle, 2003].

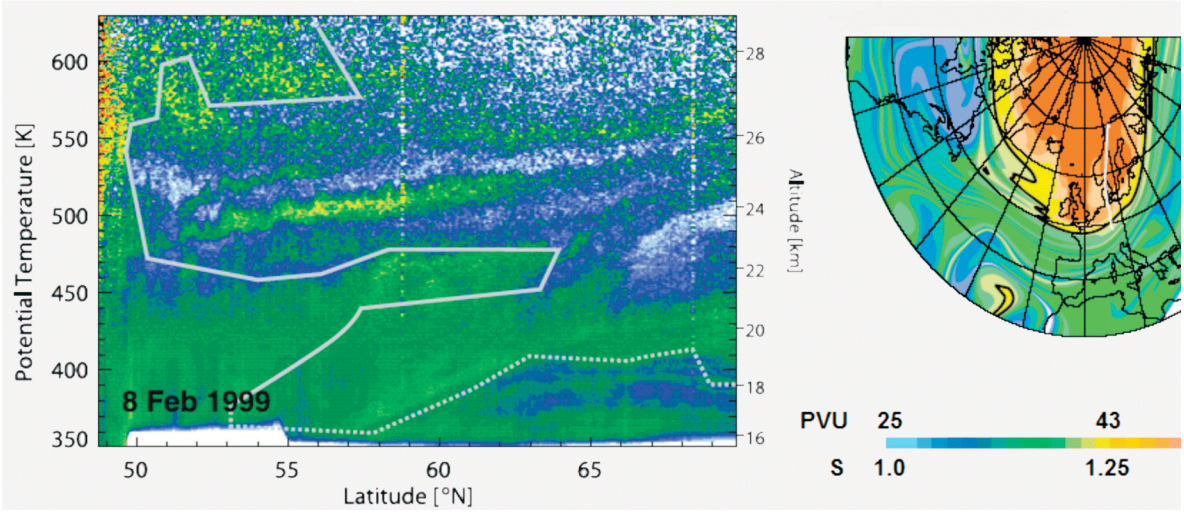

Figure 4.21: Left panel: Profile of aerosol backscatter ratio (S) at 1064 nm ranging between 1.0 and 1.5 along the aircraft flight path from Kiruna to Munich on 8 February 1999, not corrected for extinction. The altitude scale is accurate at the right border of the section. The superimposed bright contour marks the vortex edge derived from contour advection calculations; the dotted contour indicates the lower boundary of the vortex, which is not well defined. Right panel: Polar stereographic projection of the potential vorticity (PV) at 525 K calculated by contour advection. Colors correspond to PV-units (PVU) ranging from 26 to 61 □K m^2 kg^{-1} s^{-1}. The white line indicates the flight path. Adapted from Flentje and Kiemle [2003].

Airborne particle counters: FSSP-300 and MASP

FSSP-300 and MASP

The FSSP-300 (Forward Scattering Spectrometer Probe, Model 300) has been flown on the ER-2 aircraft since the late 1980s [Baumgardner et al., 1992] and on the Geophysica since the mid-1990s [Borrmann et al., 2000]. As discussed in Section 3.5.3, this instrument measures particles in the 0.2-20 μm radius range, i.e. the FSSP-300 sees only the large size tail of the distribution. Given this property, the instrument has been used for cloud measurements, in particular concerning PSCs and cirrus, whereas the instrument's capabilities to

completely depict stratospheric aerosol especially in volcanically quiescent times is limited. Nonetheless, the FSSP can provide valuable data about aerosol. For instance, Figure 4.22 depicts examples of particle size distributions in the 1996/97 winter from measurements inside (solid curve) and outside (dotted curve) of the polar vortex on similar levels of potential temperature, as well as close to the vortex boundary (dashed curve). These measurements were taken at a time when most of the Pinatubo aerosol had already disappeared from the stratosphere. The measurements corroborate the lidar observations presented in the previous section: Inside the vortex the smaller particles ($r \sim 0.2$ μm) are suppressed about a factor of 5 when compared to the out-of-vortex size distribution, whereas the larger particles ($r \sim 0.4$ μm) are suppressed about a factor of 40.

Figure 4.23 shows the measured particle number density for radii between 0.2 and 11.5 □m as function of flight time for flights conducted with the ER-2 and the Geophysica at various northern hemispheric latitudes [from Borrmann et al., 2000]. The time scale on the abscissa has been normalized with respect to the duration of the flight between takeoff and landing (usually between 4 and 8 h). On the left and right sides of the figure the concentration increases because these are the measurements from the takeoff and landing. The center region of the graph presents measurements by both aircraft at altitudes between 18 and 21 km pressure altitude. The uppermost line indicates the aerosol levels encountered by the ER-2 during flights between January and March 1992 [Borrmann et al., 1993]. The solid single thick line in the middle of the figure shows the levels measured by the ER-2 during a flight from Wallops Island, USA, to Stavanger, Norway, on 31 December 1988, mostly outside of the polar vortex. This flight took place in a period of relative volcanic quiescence and represents what were thought to be background conditions at that time. However, Thomason et al. [1997] pointed out that 1989 may not have been at true background level, due primarily to Nevado del Ruiz in 1985 and Nyamuragira in 1986. The group of 3 dotted lines underneath the ER-2 flight on 31 December 1988 are the measurements onboard the Geophysica during flights from Pratica di Mare (near Rome, Italy) in November and early December 1996. These represent outside vortex, mid-latitude data from similar latitudes as the ER-2 flight in late 1988. The lowermost 3 dashed lines are the Geophysica flights during the APE-POLECAT campaign [Stefanutti et al., 1999] from January 1997 from Rovaniemi, Finland, mostly inside the polar vortex. The lowermost solid curve shows another flight into the polar vortex from this campaign, however following a subtropical inversion, and showing distinctly less aged air with higher aerosol number densities.

This figure illustrates the atmospheric changes of the aerosol number densities from before until long after the Mount Pinatubo eruption. In particular, the decrease of the atmospheric particle concentrations in the winter 1996/97 compared to the previous apparent background aerosol of 31 December 1988 suggests that 1989 may not have been at true background level [Thomason et al., 1997]. However, questions of comparability must be asked in view of using separate flight series, separate aircraft, and especially different instruments. Particle number density for $r > 0.2$ μm is sensitive to the detector cutoff. As outlined in Section 3.5.3 the average uncertainty in sizing from the FSSP-300 is approximately 20 % over the range of this instrument. However, the question of comparability is a generic one applying basically to all measurements. While the 20-% uncertainty limits the accuracy of the FSSP-300 measurements, its precision and comparability may be expected to be better since the FSSP-300 underwent no changes in its design during the years of these measurements.

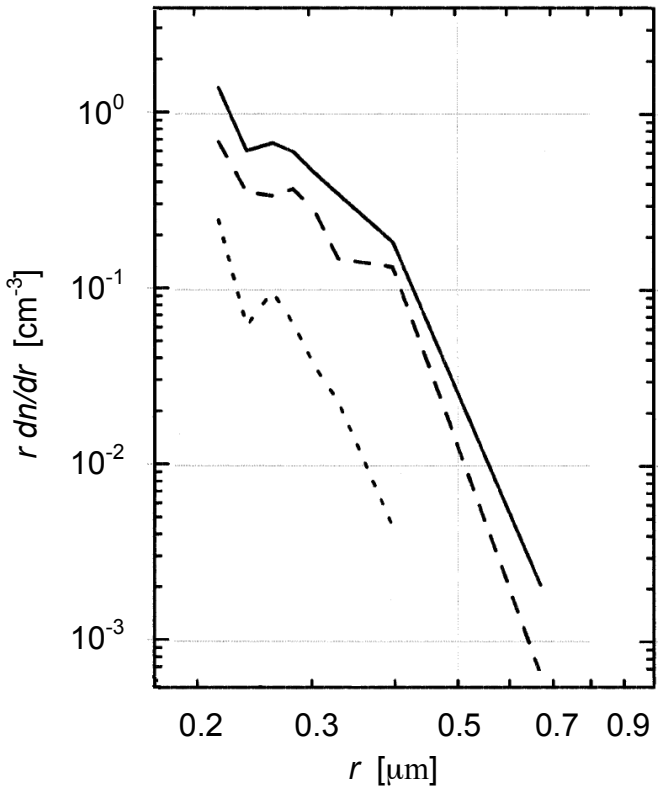

Figure 4.22: Size distribution measurements of the FSSP-300 system on Geophysica on the potential temperature surface ~ 480 K in December 1996. Solid curve: outside of the vortex (over Italy). Dashed curve: close to the edge of the polar vortex (over Scandinavia). Dotted curve: in the vortex (over Scandinavia). The averaging periods for these size distributions are between 300 and 1000 s of flight time depending on the counting statistics [adapted from Borrmann et al., 2000].

Whereas the FSSP-300 samples the light scattered by the particles in the near forward direction upon illumination, the MASP is a Multiangle Aerosol Spectrometer Probe which can obtain a higher size resolution and information on the index of refraction of the scattering particles. A summary of all quality-assured measurements made with the FSSP-300 and MASP, from December 28, 1988 to March 12, 2000, in the altitude range from 17 – 20 km is shown in Figure 4.24. Here the concentration has been averaged as a function of latitude, in 5° intervals (solid lines) and all encounters with possible cirrus clouds have been excluded from the analysis. The measurements in the southern hemisphere were only made from March to November, 1994. There is a distinct minimum at tropical latitudes, in contrast to the aerosol optical depths that are derived from various satellite products. This is because the aerosol particles at these latitudes are dominated by those with radii smaller than 0.2 μm and they are not detected by either the FSSP-300 or MASP whose size range is nominally 0.2 to 10 μm. The maxima occur at the mid-latitudes, more so in the northern than southern hemisphere. Most of the northern measurements at high latitudes were made in the winter months. This is most likely the reason for the rapid decrease in concentrations since the flights were mostly in the polar vortex where the majority of particles are smaller than the lower size thresholds of either spectrometer.

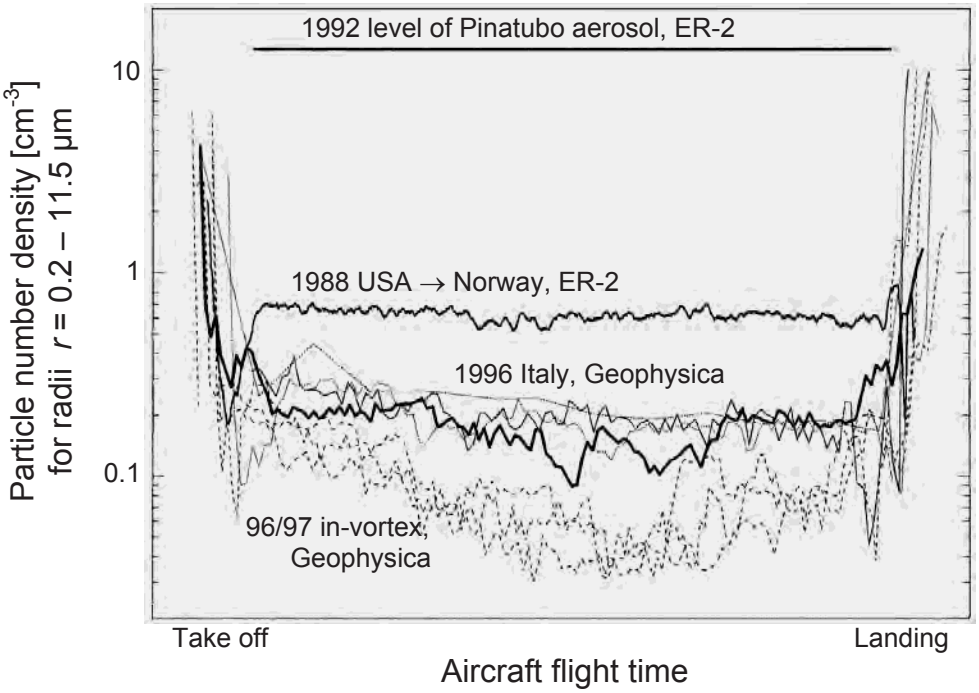

Figure 4.23: Particle number densities from FSSP-300 measurements on the ER-2 and Geophysica from northern hemispheric locations for the pre-Pinatubo background period, the Pinatubo volcanic aerosol period, and the 1996/97 winter, see text for details [Borrmann et al., 2000].

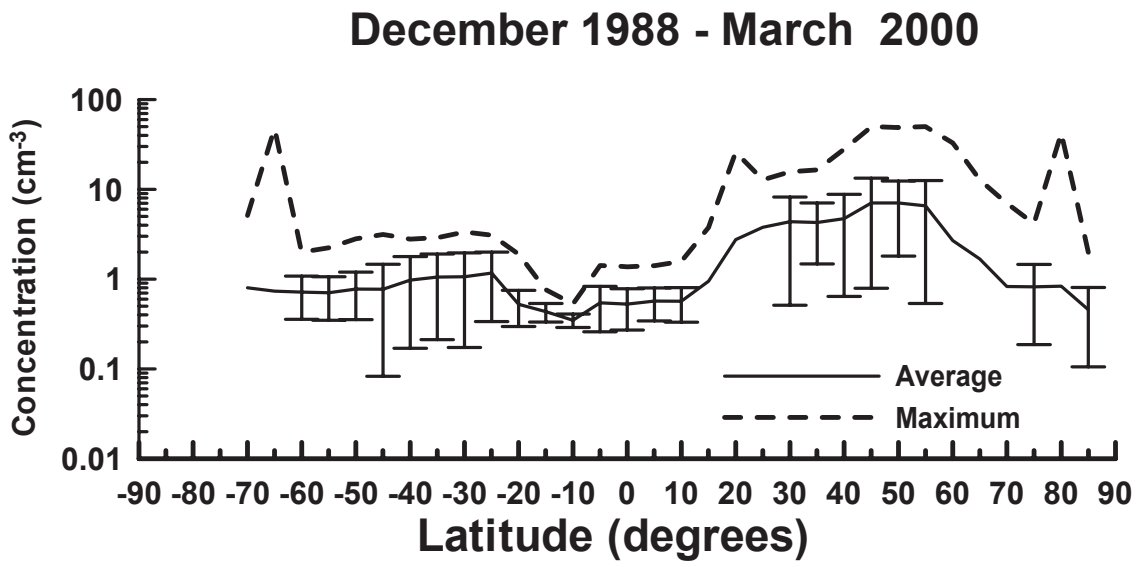

Figure 4.24: Particle number density measurements made with the FSSP-300 and MASP in the altitude range from 17 – 20 km averaged in 5° intervals of latitude. The vertical bars are standard deviations about the average (solid line) and the dashed lines are the maxima.

FCAS and N-Mass

The Focused Cavity Aerosol Spectrometer (FCAS), the Condensation Nucleus Counter (CNC), and the Nucleation-Mode Aerosol Sizing Spectrometer (N-MASS) measurements have been carried out in the upper troposphere and lower stratosphere during a number of recent missions, as shown in Table 4.1. The data set consists of 57,700, 30-second size dis-

tributions from 96 flights excluding the influence from 1991 Mt Pinatubo volcano eruption, rocket plumes and clouds.

Table 4.1 Mission Information (total flights: 96)

Mission	*Period*	*Latitudes*	*Pressure Altitudes (Km)*
STRAT	May, Oct 1995 & Jan, Feb Jun-Sep, Dec, 1996	2.2S - 60.2N	7.2 – 21.0
POLARIS	Apr – July 1997	3.4S – 89.9N	7.2 – 21.2
WAM	Apr, May 1998	9.5N – 45.9N	7.8 – 19.7
ACCENT	Apr, Sep, Oct 1999	5.0N – 39.2N	7.8 – 19.3
SOLVE	Jan – May 2000	42.4N – 89.1N	2.1 – 20.9

The FCAS heats particles to nearly 30 ºC prior to measurement and drives much of the water off of sulfuric acid-water particles. The dry aerosol volume is calculated from these measurements and expressed as mass mixing ratio of sulfate in air. Sulfate dominates the composition of particles (d>200 nm) at more than ~10 K (potential temperature) above the tropopause [Murphy et al., 1998]. The mass mixing ratio of sulfate increases with altitude above the tropopause. As air ascends in this region, sulfur precursor gases are converted to sulfuric acid that deposits on the preexisting aerosol. Values for sulfate mixing ratios range from 0.5 to 3 ppbm above (but near) the tropopause.

At high latitudes, two different particle sources were observed: new particles formed in the troposphere, and in aged, descending air. During the SOLVE mission, a few thousand particles/mg air were observed in the diameter range from 4-8 nm at 10-13 km altitude (Figure 4.25). This new particle formation may be due to the Hekla eruption that occurred during the mission and other pollution sources which enhanced background SO_2 concentrations. Also, during SOLVE, particles of similar size in the mid-latitude troposphere at higher number concentrations were observed (not shown).

Mixing ratios of particles having diameters less than 180 nm were clearly enhanced in descending air having low N_2O (Figure 4.26). (The air with the lowest N_2O mixing ratio is assumed to have descended from the highest altitude.) Previous CNC measurements in Antarctica during AAOE showed that descending air in the polar region is the source of particles. The present measurements show that by the time the air reached ER-2 altitudes (~20 km and below), most of the added particles were in the 30 to 180 nm diameter range (Figure 4.26).

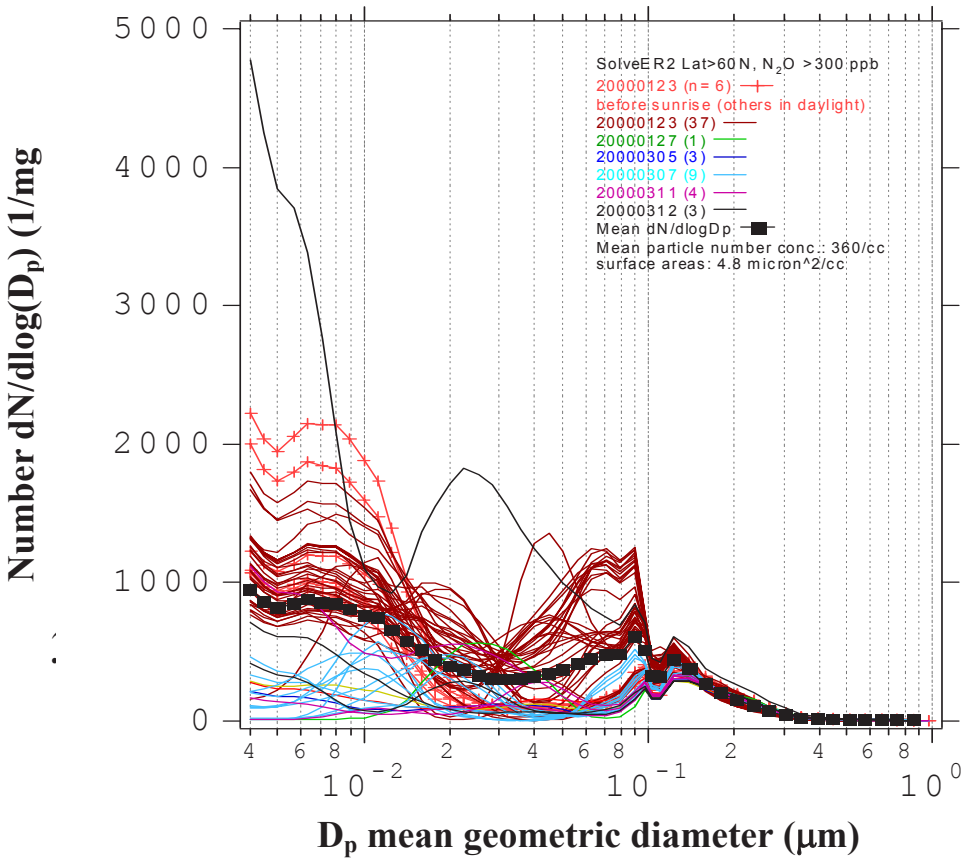

Figure 4.25 Number size distribution in the high latitude troposphere (N_2O > 0.3 ppmv). Fewer particles in diameter range from 4-8 nm were seen at high latitudes than at mid and low latitudes. The new particle formation might have been promoted by the Hekla volcanic plume or other pollution sources.

4.3 Retrieved Products

In this section we present some retrieved (or derived) products from the various measurements described above. These are generally the products of interest to modelers, namely, number density, surface area and effective radius of the aerosol particles.

4.3.1 Retrieved Products from Global Long-term Measurements

Retrieved products from SAM II, SAGE, and SAGE II

Routinely retrieved aerosol products for the SAGE series of instruments are limited in scope. Currently, no products beyond aerosol extinction are stored in the SAM II or SAGE data files. Operational SAGE II products report estimates of aerosol surface area density (SAD) and effective radius ($r_{eff,}$ defined as three times the ratio of volume density to surface area density). The calculation of r_{eff} was first based on the method of Thomason et al. [1997b], using principal component analysis to derive SAD and total aerosol volume density from a linear combination of the four aerosol extinction measurements where the coefficients are selected to move the weight of the retrieval to the more reliable long wavelength channels. This relationship for SAD has been simplified for implementation in the operational software using an empirical fit based on the 525 to 1020-nm extinction ratio, r,

and the absolute 1020-nm aerosol extinction that captures approximately 90% of the variance of the original. It is given as

$$SAD = k_{1020}\left(\frac{1854.97 + 90.137 * r + 66.97 * r * r}{1. - 0.1745 * r + 0.00858 * r * r}\right) \qquad (4.1)$$

This has the advantage of being a considerably faster calculation and avoids the use of the shortest wavelength channels that are much noisier than the two channels retained in the calculation.

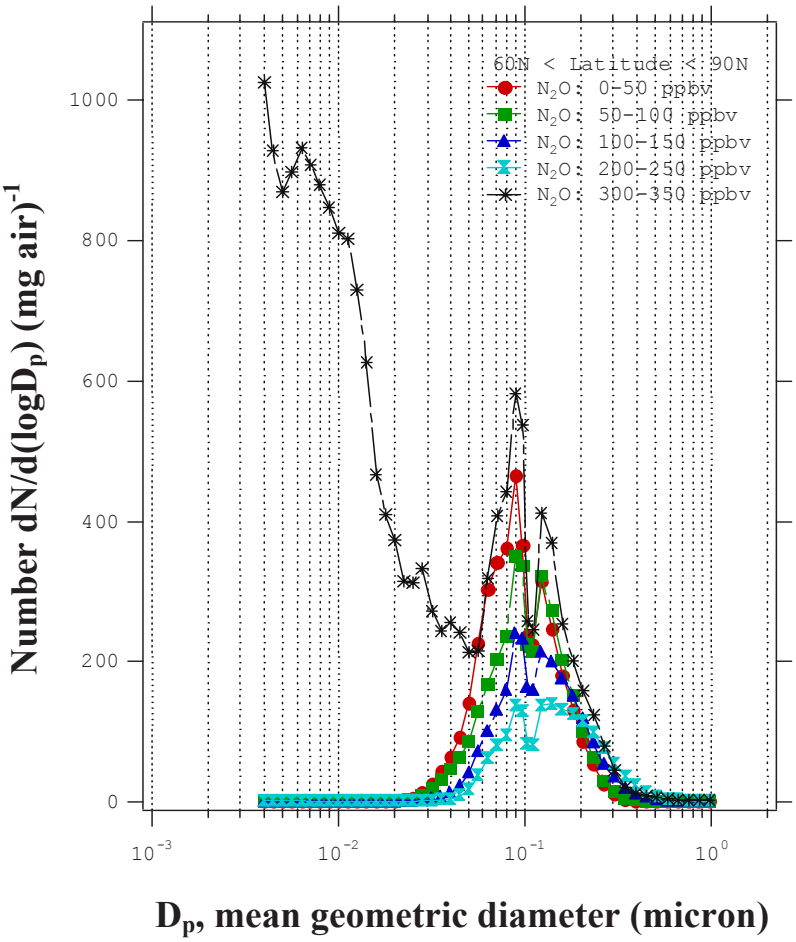

Figure 4.26 Particle number distribution at high latitude as a function of N_2O mixing ratios. The smallest particles (<0.01 μm) are seen in the tropospheric measurements. The air with lowest N_2O has descended most and has the most added particles amongst the stratospheric air parcels. They appear in the 0.03 to 0.18 μm diameter range.

The SAGE II SAD data product for January 1994 is shown in Figure 4.27. A number of techniques including fitting to model size distributions like the log-normal, constrained linear inversion, and linear error minimization have been employed to infer either the aerosol size distribution or aerosol bulk properties [e.g., Wang et al., 1989; Lin et al., 1992; Steele and Turco, 1997; Yue, 1999]. While these techniques can be quite different in mathematical expression, they tend to yield values for higher moments (such as SAD) that are within realistic uncertainty bounds of the retrievals (15-30%).

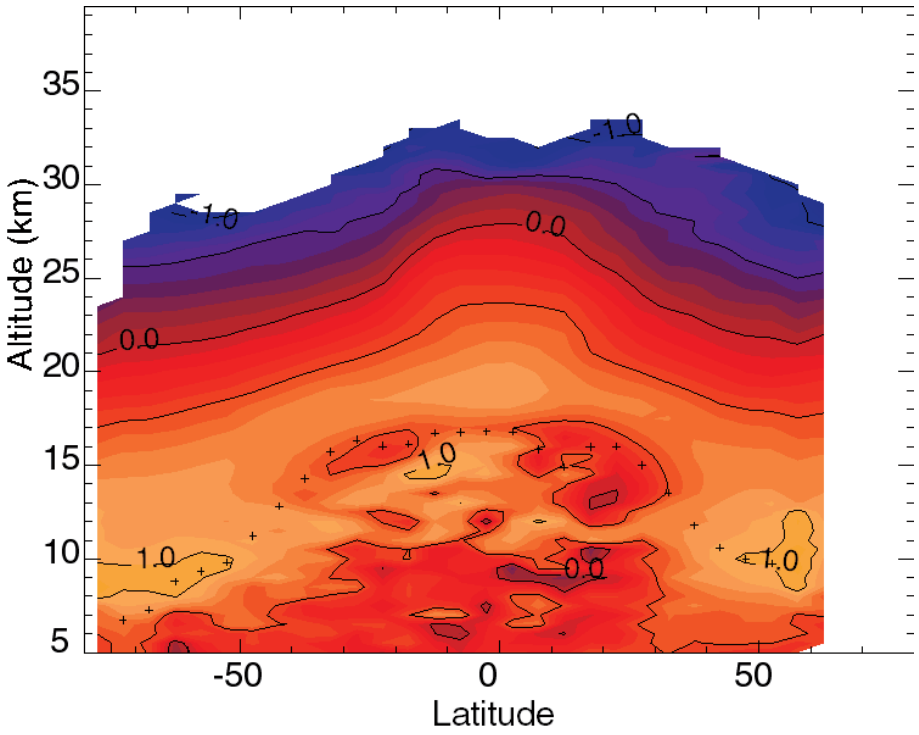

Figure 4.27: Aerosol surface area density in units of $\mu m^2 cm^{-3}$ (shown as $\log_{10}$ SAD) estimated from SAGE II aerosol extinction measurements for January 1994. Crosses indicate the average tropopause.

The efficacy of any technique for retrieving aerosol attributes is limited by the kernels of the integral equation from which extinction is derived. The Mie expression for the computation of the extinction by a distribution of spherical aerosol particles is given by

$$k_\lambda = \int \frac{3Q_\lambda(r)}{4r} \frac{d\upsilon(r)}{dr} dr \qquad (4.2)$$

where λ is wavelength, r is radius, $Q_\lambda(r)$ is the Mie extinction efficiency factor at this wavelength, and $d\upsilon(r)/dr$ is the differential volume density of aerosol between r and $r + dr$. For SAGE II, these kernels are shown in Figure 4.28. The refractive indices used were from Palmer and Williams [1975]. The plots demonstrate several important features of any effort to extract either the underlying aerosol distribution or bulk properties thereof. The four channels provide some coarse size discrimination capabilities for aerosol between 0.1 and 0.6 μm, but little sensitivity to aerosol below 0.05 μm and little size discrimination for aerosol larger than 0.8 μm. As a result, for properties such as total particle number or mean radius that are highly dependent on the number of small particles, retrievals are very sensitive to the model used in the retrieval algorithm. Even higher order moments like surface area density or volume density (or mass) can be significantly dependent on model assumptions regarding effectively invisible small aerosol particles during low aerosol loading periods (when the aerosol particles are fewer and also typically smaller than during higher loading periods). Since the operational retrieval model puts little material in this 'blind spot', it is possible that values reported in these conditions significantly underestimate SAD, slightly underestimate the volume density, and concomitantly overestimate the value of r_{eff}. The scope of the problem remains unclear. Because of the difficulty in deriving physically

meaningful values for low order moments, aerosol number density and mean radius are not a part of the SAGE II operational product. These quantities have, however, been estimated by other investigators, including Bingen et al. [2004a, 2004b] and Bauman et al. [2003a, 2003b].

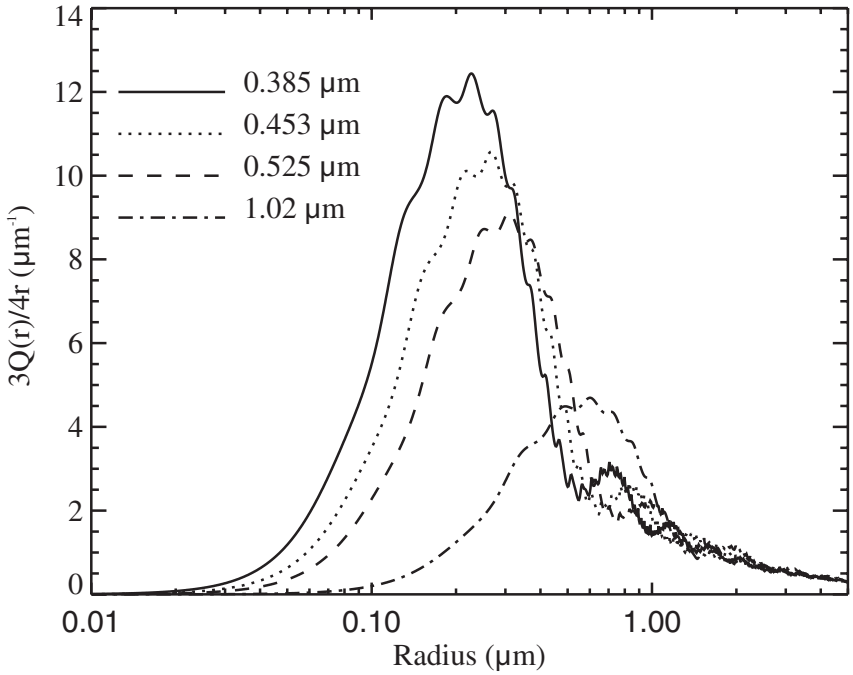

Figure 4.28: Mie scattering kernels for the four SAGE II aerosol extinction channels.

Since SAM II is a single channel instrument at 1000 nm and SAGE has its most reliable aerosol channel also at 1000 nm, no operational version of SAD or r_{eff} is routinely produced from either data set. However, Thomason et al. [1997b] presented a simple relationship for converting from 1000-nm aerosol extinction to SAD. The standard deviation of SAD using this relationship relative to the four channel method (applied to SAGE) is about 30% for extinctions larger than 10^{-4} km^{-1}. Solomon et al. [1996] found good agreement between this relationship and SAD from the University of Wyoming Optical Particle Counter. The technique is based on a regression between the two parameters that is allowed under most circumstances by the well-behaved relationship between SAGE II 1020-nm aerosol extinction and the SAD derived using four channels. This relationship is expressed as

$$SAD = s = \begin{cases} 425 \times k^{0.68} & k < 4 \times 10^{-3} \\ 1223 \times k^{0.875} & 4 \times 10^{-3} < k < 2 \times 10^{-2} \\ 2000 \times k & 2 \times 10^{-2} < k \end{cases} \quad (4.3)$$

where k is the 1000-nm aerosol extinction in units of km^{-1} and surface area density is produced in units of μm^{2}cm^{-3}. This relationship is based upon the observation that under most circumstances the wavelength dependence of aerosol extinction (as expressed in the 525 to 1020-nm aerosol extinction ratio) is nearly constant for a given aerosol extinction [Thomason and Osborn, 1992]. The only significant deviation from a tidy relationship was ob-

served in the lower stratosphere in the northern hemisphere in the first few months following the eruption of Mt. Pinatubo in 1991. This deviation was the result of injection of large amounts of small aerosol that created an unusual situation where large extinction occurred in conjunction with small aerosol size. As a result, it is possible that the use of this model during similar periods (e.g., Mt. St. Helens or El Chichón) may result in a similar transient period with large errors in the estimation of SAD.

For the purposes of this assessment and the creation of the most complete possible long-term aerosol climatology, an additional function has been derived for the computation of aerosol effective radius from 1000-nm aerosol extinction using the same procedure used to derive Equation 4.2. Four-channel retrieved values for r_{eff} versus 1020-nm aerosol extinction are shown in Figure 4.29 for January 1994 to June 1994. As with SAD, this relationship varies little with time and can be expressed in analytic form as

$$r_{eff} = \begin{cases} 0.0303 \times [\ln(k) + 11.513] + 0.16 & 1 \times 10^{-5} < k < 3.0 \times 10^{-4} \\ 0.15 \times \exp\left(0.04916 \times [\ln(k) + 11.513]^2\right) & 3.0 \times 10^{-4} < k < 1.8 \times 10^{-3} \\ 0.55 & 1.8 \times 10^{-3} < k \end{cases} \quad (4.4)$$

where k is the 1000-nm aerosol extinction in units of km^{-1} and the effective radius is produced in units of μm. The standard deviation from this relationship is about 0.05 μm but, unlike SAD, there are substantial outliers during all periods and, as a result, this relationship should be viewed and applied cautiously. The use of these equations with the SAM II and SAGE data sets yields estimates of SAD and r_{eff} that are generally consistent with those data sets, but they also inherit the limitations associated with the data.

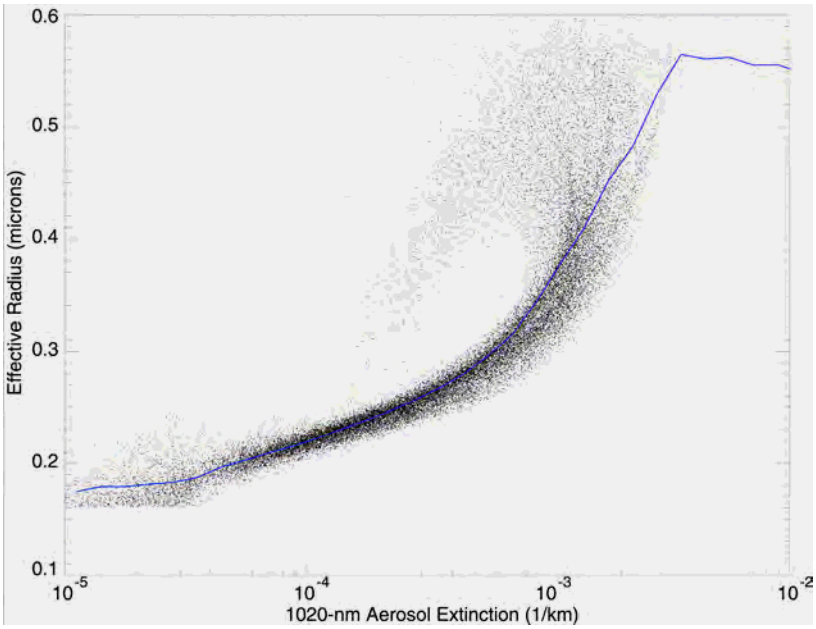

Figure 4.29: A depiction of the correlation of SAGE II 1020-nm aerosol extinction and aerosol effective radius derived from the multi-wavelength aerosol extinction measurements. The blue line shows the median fit through these data.

Figure 4.29 demonstrates that in general there is a good correlation between the two parameters but that there is also a substantial spread in the relationship. The median is used

rather than the mean because the mean or average value can be biased towards outliers (that is, the clouds). The median filter used is applied in steps of $1/10^{th}$ of a log cycle and eliminates the effects of clouds missed by the cloud filter.

Cloud Clearing with SAGE data. Clouds are a ubiquitous feature of SAGE and solar occultation data. They are observed most often in the troposphere where they often are responsible for terminating an occultation measurement, but are also seen in the stratosphere both as polar stratospheric clouds (PSCs) and possibly as thin cirrus clouds occurring near the tropopause. Clouds can simply terminate a specific observational event (extinction going off scale) or appear in the data as non-opaque features with cloud-like spectral features. These clouds are sometimes referred to as sub-visual clouds with the expectation that they are thin sheet-like cirrus clouds invisible to nadir-viewing instruments. However, this interpretation has not been rigorously tested and the geometry of occultation measurements is sufficiently complex that this interpretation is arguable [Kent et al., 1997b]. For the purposes of this aerosol assessment in which cloud contaminated data were removed, clouds in the SAGE II data set were identified using the technique developed by Kent et al. [1997a] in which aerosols and clouds are distinguished by the ratio of extinction at 525 and 1020 nm. Under most circumstances, the 525 to 1020-nm aerosol extinction ratio for aerosols is greater than two, indicating that stratospheric aerosol extinction is dominated by particles less then 0.3 or 0.4 μm. Cloud particles, with the exception of Type I PSCs, are considerably larger and exhibit an extinction ratio close to one. Thus, the technique identifies clouds based on the magnitude of extinction and the extinction ratio. An example of the partitioning between cloud and aerosol is shown in Figure 4.30 for March through May 1999. For most of the record, this technique works well and there is little obvious leakage of clouds into the aerosol data set. However, during the few years following the Pinatubo eruption, aerosol extinction ratios were close to one and cloud identification is not possible between June 1991 and the end of 1993. Toward the end of this period there is evidence that some cloud events (seen as enhanced extinction) remain in the aerosol data set. These events are relatively rare and their impact was to a great extent mitigated by the use of median filters in the creation of the ASAP SAGE data files. Figure 4.31 shows the frequency of clouds within 3 km below the tropopause between 1985 and 1989. Not surprisingly this figure is very similar to Figure 3.2 (penetration frequency) with a noteworthy maximum in the tropics and minima in the subtropics. Generally, there is no strong longitudinal dependency in cloud occurrences except in the tropics where there is a maximum over the Indonesian warm pool. It is probably worth noting that the zonal parameters in the SAGE data files are, as a result, weighted to longitudes away from this region.

Base Data Files and Filling Data Gaps. While the SAGE series of instruments have produced almost 300,000 solar occultation events over the previous 25 years, there are substantial and climatically important periods in which the data are either incomplete (due to saturation by volcanic aerosols) or missing entirely. Unfortunately a major volcanic event (El Chichón) occurred during the SAGE-SAGE II gap, and a gap in data occurred following the second major volcanic event (Pinatubo). To facilitate long-term climate modeling, we have produced a complete, nearly gap free, data set using SAM II data and a variety of lidar data sets to fill gaps in the El Chichón period (1982-1984) and post-Pinatubo period (1991-1993). Discrepancies of up to 4% resulting from wavelength differences between SAM II (1000 nm) and SAGE II (1020 nm) extinctions are ignored. The sources of data used to fill the Mt. Pinatubo and El Chichón data gaps are presented in Table 4.2.

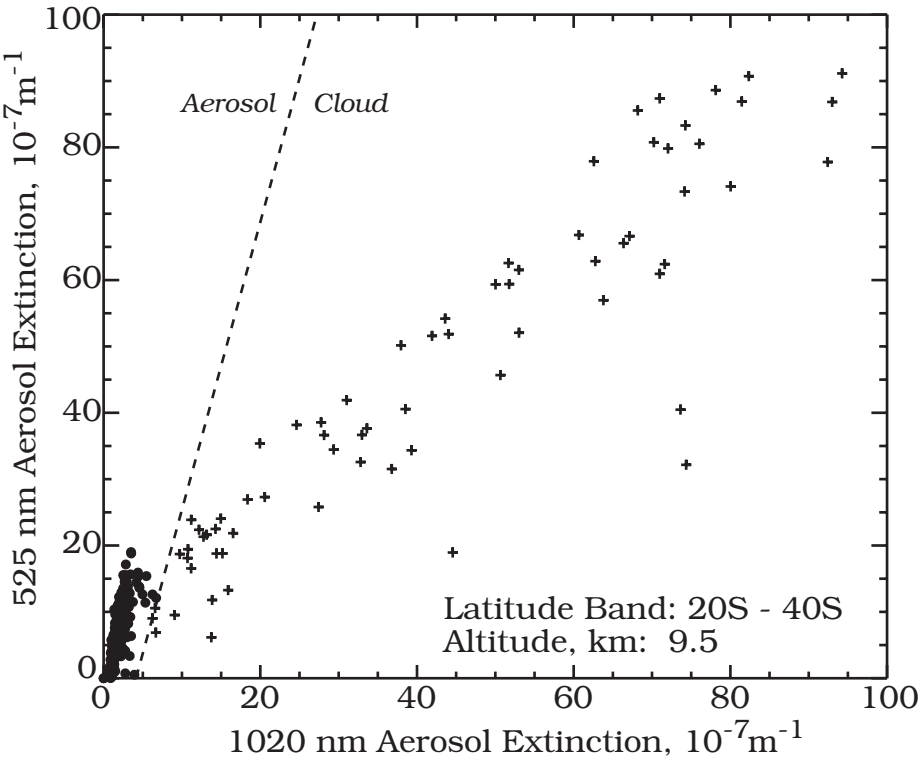

Figure 4.30: A demonstration of the two-wavelength cloud identification method of Kent et al. **[1997b]. High extinction but small extinction ratio pairs (right of the dashed line) are considered cloud and, for this application, excluded from the analysis.**

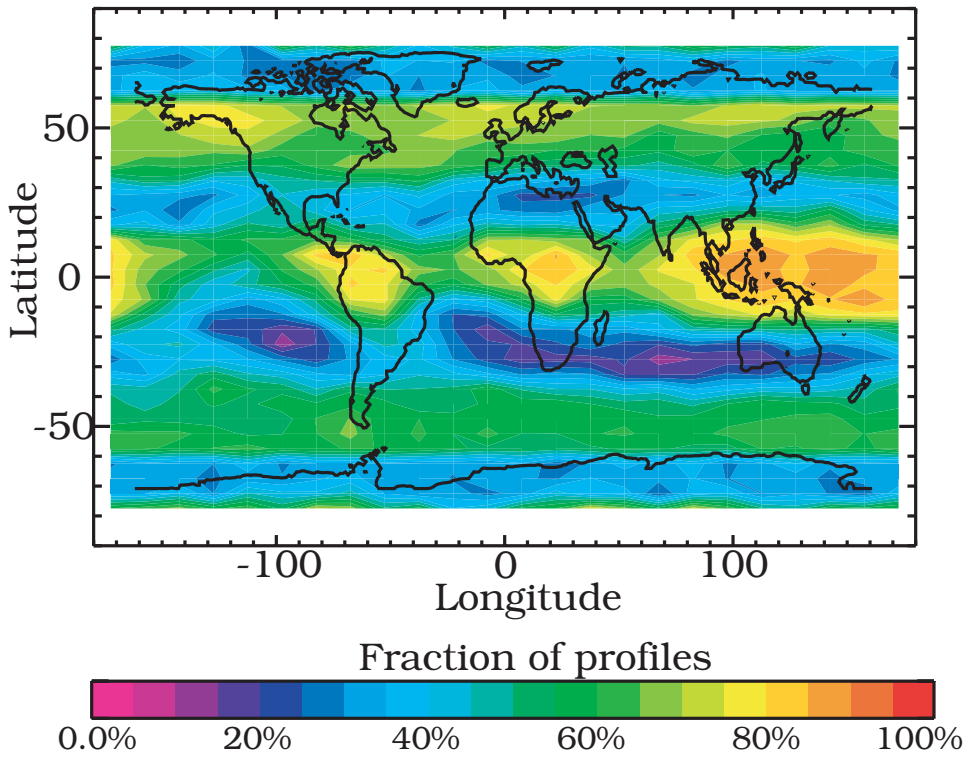

Figure 4.31: The fraction of events for which a cloud has been identified at or above the tropopause – 3km for 1985 through 1989.

Table 4.2: Sources of data used to fill the El Chichón and Mt. Pinatubo data gaps.

Time Period	*Zone*	*Fill Source*
1982-1984	North polar	SAM II
	North mid-latitudes	Langley 48-inch lidar
	Tropics	NASA airborne lidar
	South mid-latitudes	SAM II
	South high latitudes	SAM II
1991-1994	North mid and high latitudes	Langley 48-inch lidar
	Tropics	Composite of the Mauna Loa and Camaguey lidars
	South mid and high latitudes	Backscatter sondes (Lauder, New Zealand)

The data analyses produces the aerosol extinction at one or more wavelengths, as well as SAD and r_{eff} in 0.5 km (SAGE II) or 1-km (SAGE) monthly 5-degree latitude bins. Since the latitude for SAM II observations changes slowly with time, SAM II is reported at a mean latitude for each event type (sunrise and sunset) in 1-km, monthly bins. The base data files, referred to as non-interpolated, contained values only in months in which observations occur. These files are most suitable for comparing with other data sets such as the HALOE data. Individual values are not true monthly medians but rather are median values for observations occurring within that month. The observations may occur over several days anytime within the month including non-contiguous periods. The mean day of observations is included in the data files.

Due to the sampling characteristic of solar occultation, for any given month many latitudes are not sampled during the month. To fill these ubiquitous data gaps, a second set of files is created where the sampling window has been increased to 10 degrees of latitude (still reported every 5 degrees) and fit temporally with a spline (but not in altitude or latitude). The resulting fit is used to fill missing values whenever observations occur within 1.5 months. This eliminates almost all sampling related gaps except at high latitudes in winter, during the mechanical downtime episode (July-December 2000), at low altitudes during post Pinatubo saturation, and in the gap between SAGE and SAGE II (1982-1984). Interpolated values in these files are denoted with uncertainties of -1.

Pinatubo Gap Filling. Between the June 1991 eruption of Mount Pinatubo and the end of 1993 substantial parts of the SAGE II interpolated files are missing due to the saturation effect. Aerosol backscatter profile measurements from lidar sites at Camaguey (Cuba), Mauna Loa, Hawaii (USA), and Hampton, Virginia (USA) and backscatter sonde measurements from Lauder, New Zealand were used to fill the missing values. The most critical area to fill is the tropics between 15ºS and 15ºN. Unfortunately, only a few scattered lidar observations are available in these latitudes. The stations in Cuba and Hawaii, while close to the tropics, are best considered sub-tropical stations and their individual records show that they periodically underlie both the tropical pipe (where the Pinatubo aerosol was concentrated) and air more typical of the mid-latitudes. To synthesize a tropical record from these two data sets, a 3-month window was used from which the maximum value at each altitude was selected assuming that the largest values were most representative of the aerosol within the tropical pipe. The backscatter was converted to 1020-nm aerosol extinction using the method of Antuña et al. [2003]. A comparison of this composite data file with SAGE II observations between 0 and 5ºN is shown in Figure 4.32. In regions where the

two records overlap, the comparison, while not perfect, is generally favorable and gives at least modest confidence that the composite lidar record can be used to fill missing tropical SAGE II data.

For northern latitudes, the NASA Langley 48-inch lidar record converted to 1020 nm aerosol extinction was used (as in Antuña et al. [2003]). The comparison of SAGE II and this record is shown in Figure 4.33 and is also favorable though perhaps not as good as the tropical comparison. Particularly after the eruption, the mid-latitudes are not zonally homogeneous and it is not surprising that this comparison is less robust. It is possible that averaging data from a number of sites would improve this model. In southern latitudes, the backscatter sonde data from Lauder, New Zealand was used after conversion to 1020 nm aerosol extinction following the method recommended by the instrument principal investigator (James Rosen, personal communication). Like the northern hemisphere, the comparison of the data (not shown) is broadly favorable though with a broader scatter than is found for the tropical data record.

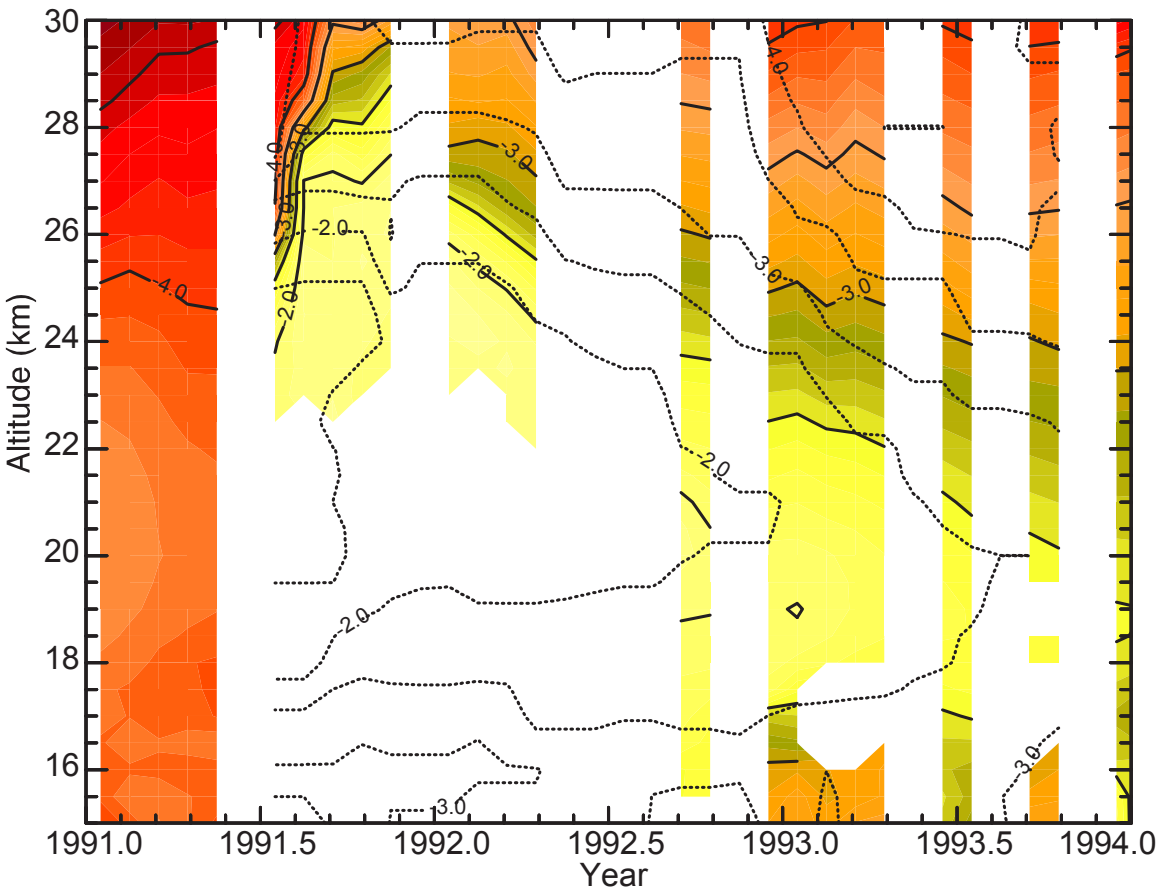

Figure 4.32: A comparison of the SAGE II aerosol extinction between 0 and 5ºN (color contours and solid lines) and the composite Camaguey/Mauna Loa lidar based record (dotted lines), which has been used for filling the observational gaps in the SAGE II record in the tropics. Contour labels give $\log_{10}$ extinction (in km^{-1}).

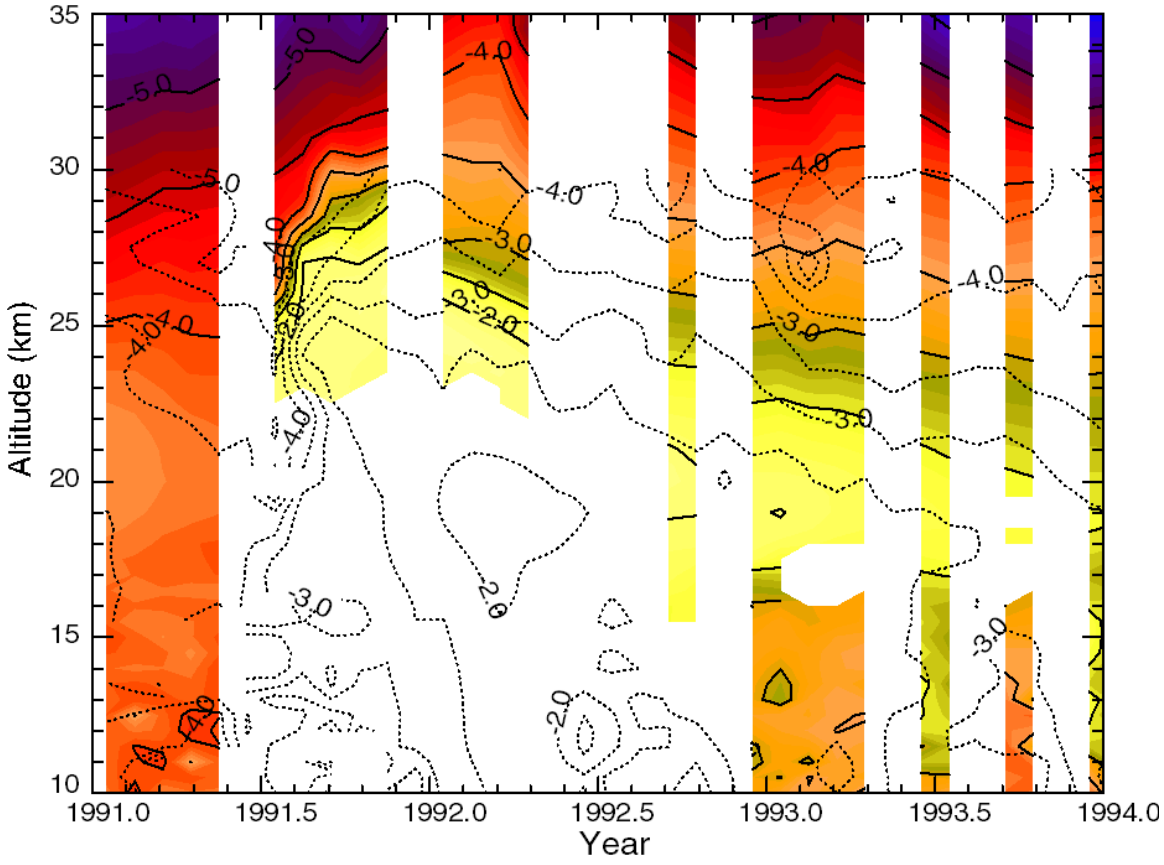

Figure 4.33: A comparison of the SAGE II aerosol extinction between 35 and 40ºN (color contours and solid lines) and the NASA Langley 48-inch lidar based record (dotted lines) which has been used for filling the observational gaps in the SAGE II record in the northern mid-latitudes.

These three temporal records are used to fill missing values in the SAGE II interpolated record for 1020-nm aerosol extinction, the tropical record for latitudes between 15ºS and 15ºN, the northern record for 25ºN to 80ºN, and the southern record for 25ºS to 80ºS. The subtropics are filled using a linear interpolation of the mid-latitude and tropical records. The mid-latitude records are shifted in altitude as a function of latitude following zonally-averaged potential temperature surfaces. Estimates for SAD and r_{eff} are produced using Equations 4.3 and 4.4. In the archived 'filled' versions of these data files interpolated and filled values are denoted by the use of -1 in the measurement uncertainty values.

El Chichón Gap Filling. Between November 1981 and October 1984, global space-based aerosol extinction profile measurements were not available. This period encompassed the El Chichón eruption and the onset of the Antarctic ozone hole and is, therefore, of particular interest. The last full month of SAGE data (November 1981) was used for December through March 1982. Beginning in April 1982 and through the beginning of SAGE II observations in 1984, a composite of data consisting of SAM II, the NASA Langley 48-inch lidar system, and lidar data from the NASA Langley Airborne Lidar System was used to produce a complete 1-km by 5-degree by month grid. The NASA Langley Airborne Lidar System made five flights between July 1982 and January 1984 of which three flights entered the tropics and two extended into the southern hemisphere; a description is given in Chapter 3 (The NASA Langley Airborne Lidar System). In this case, only SAM II events that have been tagged as outside the polar vortices using the method developed by M. Fromm were used [e.g., Bevilacqua et al., 2002].

In the northern hemisphere, the 1000-nm extinction record is filled with SAM II data between 80ºN and 65ºN. From 65ºN to 40ºN, a linear interpolation in latitude of the logarithm of extinction between the SAM II data and 1000-nm aerosol extinction derived from the NASA Langley 48-inch lidar system were used. From 40ºN to 25ºN, the 48-inch lidar is used. From 25ºS to 80ºS, the entire record is filled (by hemisphere) using SAM II data shifted in altitude as a function of latitude following zonally averaged potential temperature surfaces. From April 1982 to September 1984, a composite of profiles is used to create an effective tropical El Chichón record. For April through July, the southernmost (13ºN) airborne lidar profile July 1982 was used . Following that period a linear interpolation in time of the logarithm of 1000-nm aerosol extinction estimated from lidar profiles (using a ruby backscatter to 1000-nm extinction ratio of 30) in July 1982 (4.1ºS) and May 1983 (0º) and the SAGE II tropical data in October 1984 was used. This synthetic record is shown in Figure 4.34. As with the Pinatubo gap filling process, the subtropics (25 to 15º) are filled using a linear interpolation of the mid-latitude and tropical records. Estimates for SAD and r_{eff} are produced using Equations 4.3 and 4.4.

As an example of the end result of the gap-filling process, Figure 4.35 depicts the 1000-nm stratospheric aerosol optical depth (shown unfilled in Figure 4.4) in which the procedures described above have been used to produce a gapless record. In generating Figures 4.34 and 4.35 no correction was applied for differences between 1020 nm and 1000 nm extinctions.

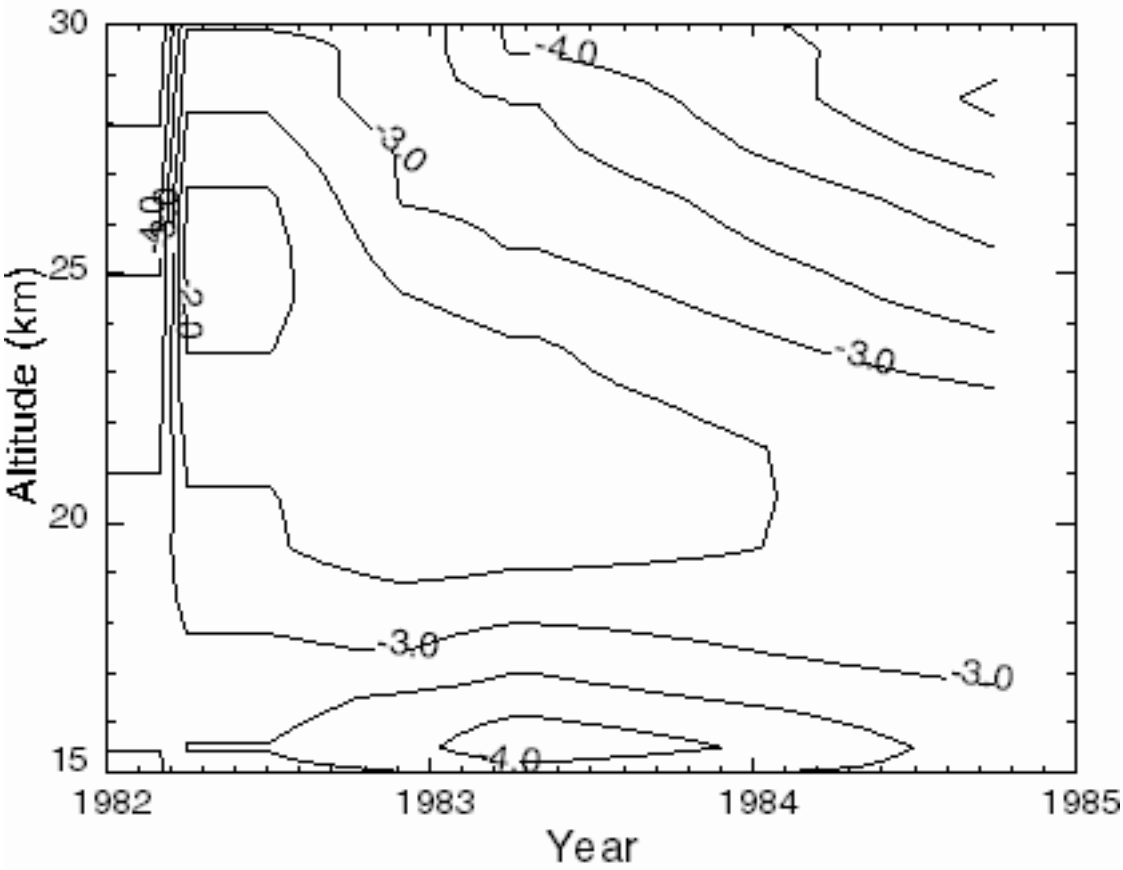

Figure 4.34: Tropical 1000-nm aerosol extinction (shown as $\log_{10}$ of aerosol extinction) spanning the SAGE/SAGE II gap. It includes data from SAGE, SAGE II, and three flights by the NASA Langley Airborne Lidar System (July 1982, November 1982, and May 1983).

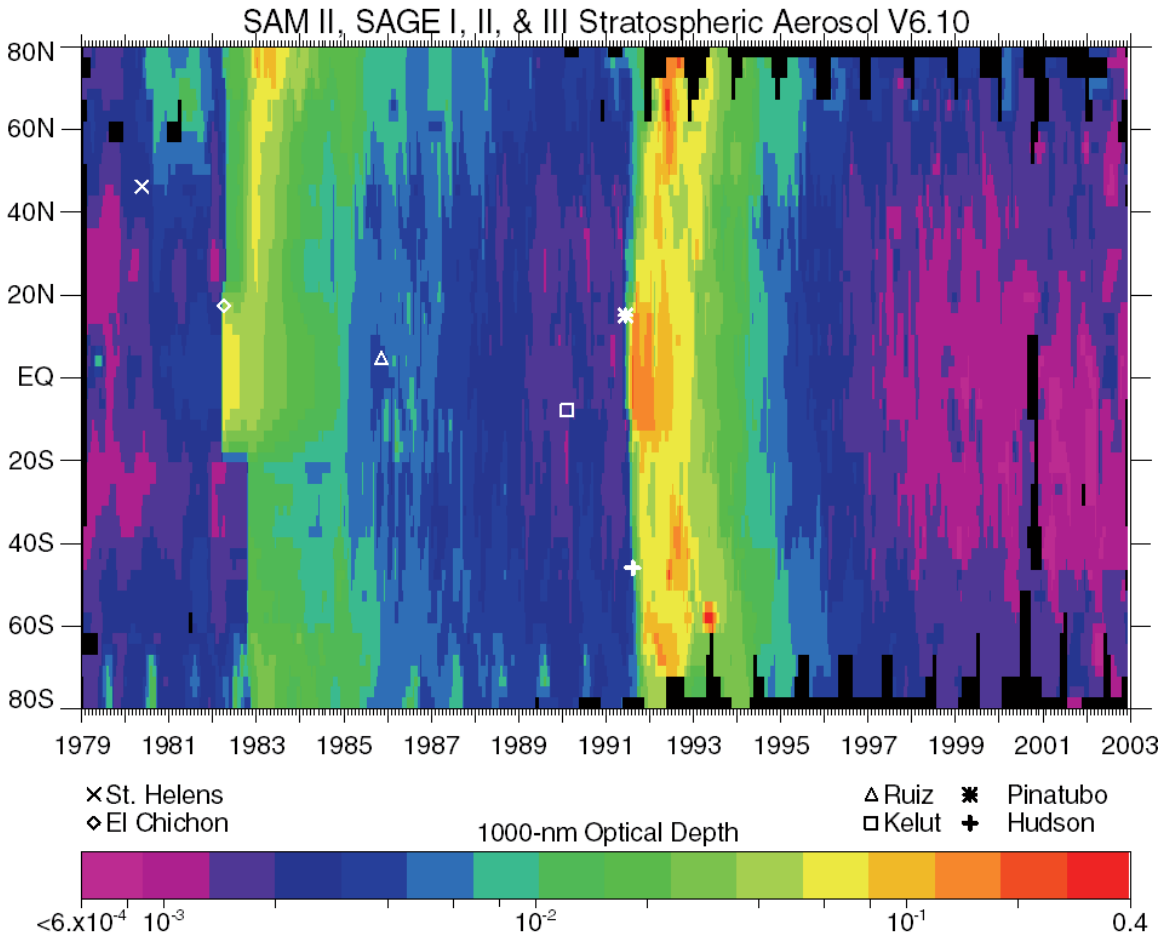

Figure 4.35: A 1000-nm aerosol optical depth record for 1979 through 2002 in which data gaps have been filled (see text).

The work described here has not exhausted available data sources. A more complete use of the airborne lidar data, particularly in the southern hemisphere would be helpful. Other data sets for northern mid-latitudes are also available and could be used to make at least the northern hemisphere depiction more realistic. In addition, the Solar Mesospheric Explorer (SME) used limb scattering to measure ozone, NO_2 and other species and has also produced aerosol measurements that span this period. That data is undergoing a significant revision at this time (Cora Randall, personal communication) and has not been used in this data set.

Extinction Presented in Terms of Equivalent Latitude and Potential Temperature

One frequently presents the SAGE extinction in the usual format of extinction at a given altitude as a function of latitude. This section illustrates a different format for presenting the data which can be considered an aspect of data gap filling since it increases the coverage at high latitudes.

For long-lived atmospheric constituents, the calculation of zonal means can blur steep meridional gradients in constituent concentrations across transport barriers, e.g. the polar vortex edge. This problem becomes particularly acute when the concentration field is far from zonally symmetric. One approach to avoiding this problem is to regrid the data from the native latitude, longitude, altitude and time coordinate system to an equivalent latitude (ϕ_{eq}) [Nash et al., 1996], potential temperature (θ), and time (t) coordinate system before calcu-

lating zonal means. The equivalent latitude is a vortex-aligned coordinate system where 90° latitude is at the center of the vortex, that is, the highest absolute potential vorticity value in that hemisphere. Randel and Wu [1995] and Bodeker et al. [2001] have shown some of the advantages of regridding atmospheric constituent measurements to a (ϕ_{eq},θ, t) coordinate system.

In Bodeker et al. [2001], version 6.1 SAGE II data (including O_3, NO_2, H_2O, aerosol extinction at 386, 452, 525 and 1020 nm, and their respective errors) were analyzed to this coordinate system for isentropic levels of 300, 315, 330, 350, 400, 450, 550 and 650 K, for the period October 1984 to June 2001. Individual solar occultation events (profiles) were extracted from the version 6.1 SAGE II data base. For each of the 8 isentropic levels listed above, the altitude was calculated by linear interpolation within a θ vs. altitude profile. The θ vs. altitude profile for a given occultation event consists of 140 pairs of altitude and θ values. The altitude was read directly from the SAGE II data record and θ was calculated from $T\times(1000./P)^{0.285572}$, where T and P are the NMC temperature and pressure, respectively, provided in the SAGE II data files. For a profile latitude, longitude and potential temperature, the associated PV value was extracted from NCEP/NCAR reanalyses PV fields using bilinear spatial interpolation and linear interpolation in time. The NCEP/NCAR reanalyses are available every 6 hours at 2.5°×2.5° resolution on each of the 8 isentropic surfaces used here. The equivalent latitude associated with this PV value is calculated from linear interpolation within an equivalent latitude vs. PV profile which in turn was calculated using the method described in Nash et al. [1996]. The equivalent latitude vs. PV profiles were calculated for every 6 hours and the profile closest in time was used. Concentrations for the constituents listed above were then calculated using linear interpolation within a constituent vs. potential temperature profile, which in turn was calculated in a manner identical to the altitude vs. potential temperature profile. An additional constraint that at least one of the levels used in this interpolation was within 10 K of the present isentropic level was imposed.

For ASAP, a similar procedure has been used to produce a complete analysis of SAGE aerosol data products on potential temperature surfaces from 375 to 1300 K in 25 K increments and are available on the ASAP web site. For this analysis, the potential temperature and equivalent latitude information came from auxiliary data files associated with version 6.2 SAGE II data files that were produced by Gloria Manney, JPL. In Figure 4.36a, the results of an analysis of 1020-nm extinction at 550 K is shown while a comparable altitude/latitude analysis (at 22 km) is shown in 4.36b,There are clearly discernable differences between panels (a) and (b), viz.: the data plotted by equivalent latitude extend to higher equivalent latitudes than the data plotted by true latitude, particularly in the Arctic; the data plotted by equivalent latitude show more clearly the exclusion of aerosols from the Antarctic vortex during the winter and spring; further the data plotted by equivalent latitude more clearly show the very low extinctions in the Arctic vortex each winter/spring.

It should be noted however that the transformation into the (ϕ_{eq},θ, t) coordinate system is not mass conserving and no scaling of the data to conserve total aerosol mass has been made. Care should also be taken in the interpretation of these results at low latitudes. At low latitudes the potential vorticity does not act reliably as a tracer of isentropic transport and it is therefore less likely that contours of long-lived aerosols will be well aligned with those of potential vorticity. For these reasons the regridding to equivalent latitude is most advantageous poleward of ~50°.

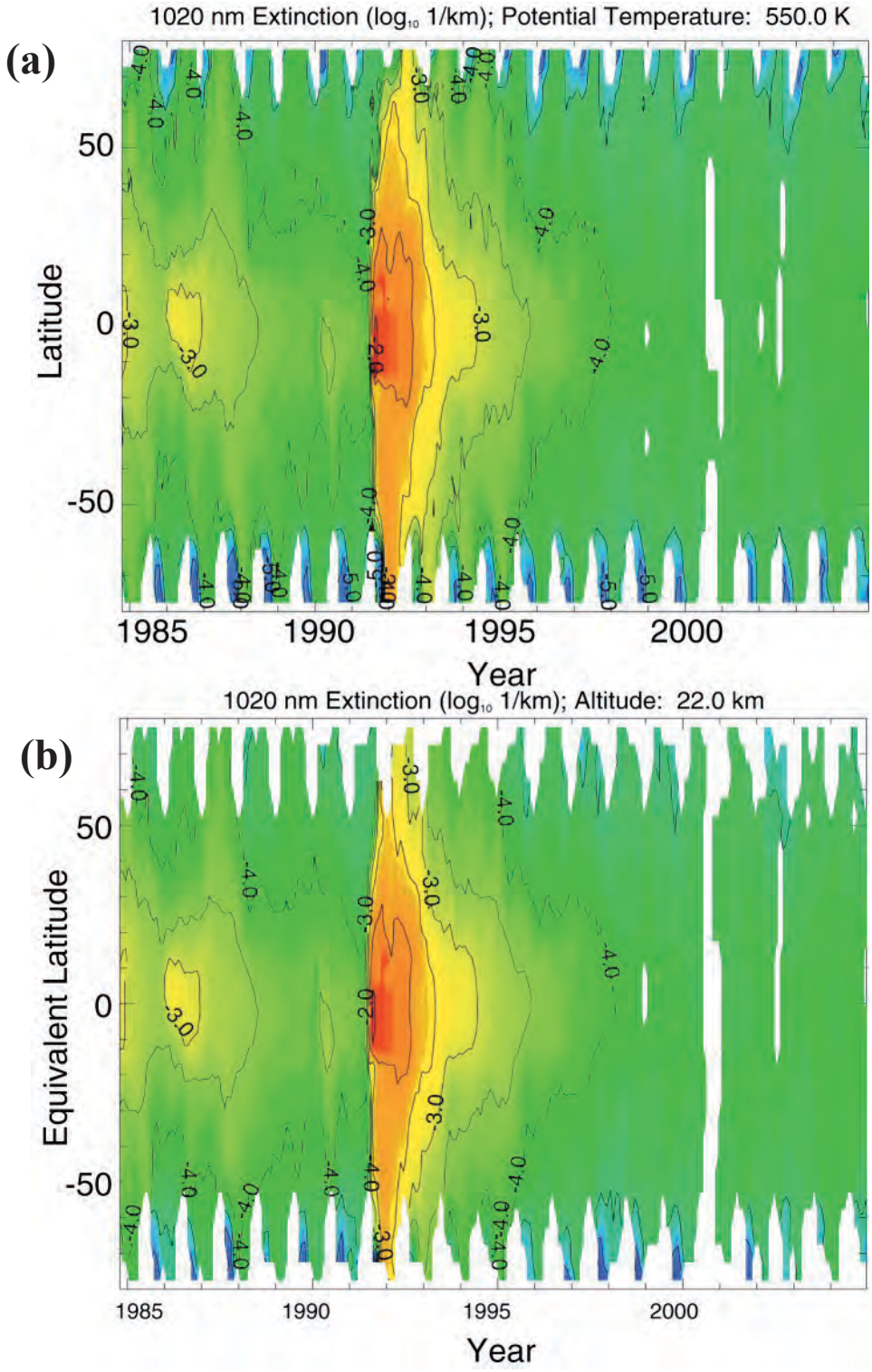

Figure 4.36: SAGE II aerosol extinction at 1020 nm, (a) on the 550 K potential temperature surface as a function of equivalent latitude and (b) at 22 km as a function of latitude.

Retrieved products from HALOE

HALOE measurements of stratospheric sulfate aerosols have been used to retrieve unimodal lognormal size distributions, as described in detail by Hervig *et a*l. [1998]. The unimo-

dal lognormal size distribution describes concentration versus radius as a function of the total number concentration (N), distribution width (σ), and median radius ($\bar{r}$). Although the HALOE extinction spectrum alone cannot be used to reliably infer the aerosol size distribution (except when the aerosol population contains particles larger than about 0.5 μm), the inverse problem is well-defined when the effective radius is known. Using theoretical relationships derived from *in situ* aerosol measurements, effective radii can be determined from the HALOE 2.45 μm extinctions with uncertainties of about ± 15%. Using extinction ratios with the effective radii determined from the HALOE extinctions, unimodal lognormal size distributions are retrieved from HALOE measurements. The HALOE size distributions are generally unbiased with respect to coincident *in situ* aerosol measurements. Error analysis reveals that uncertainties in the inferred surface areas and volumes are less than 30% and 15%, respectively.

Refractive indices of aqueous sulfuric acid solutions are fundamental to the size distribution retrievals, and the results reported in Hervig et al. [1998] were based on room temperature (300 K) indices [Palmer and Williams, 1975] adjusted to stratospheric temperatures according to the Lorentz-Lorenz relationship using sulfate densities from Luo et al. [1996]. Sulfate indices measured at a lower temperature (215 K) more relevant to the stratosphere were published by Tisdale et al. [1998]. A comparison of the Tisdale et al. indices to the Palmer and Williams room temperature indices, adjusted to 215 K, shows notable differences. Thus, the Tisdale et al. indices were used to recalculate the HALOE aerosol size distributions for this work. Hervig et al. [1998] compared profiles of HALOE unimodal size distributions and surface areas to OPCs over Laramie for 17 coincidences during 1991 to 1996. That work used HALOE size distributions based on the Palmer and Williams [1975] sulfate refractive indices, and showed that the HALOE surface areas were from 10 to 30% higher than the OPC values. HALOE size distributions based on cold temperature refractive indices [Tisdale et al., 1998] result in ~ 25% less surface area than the previous results. Note that HALOE aerosol size distributions currently available on the HALOE web site are based on the Palmer and Williams refractive indices adjusted to stratospheric temperatures. Aerosol size distributions were only retrieved in the absence of clouds. Cloud identification in HALOE data is described in Section 3.2.2.

The complete record of HALOE aerosol size distributions is available on the internet: http://gwest.gats-inc.com/haloe_aerosols/HALOE_size_distribution_data.html. This archive reports retrievals based on the Tisdale et al. [1998] refractive indices and HALOE V19 extinctions. Examples of aerosol size distribution parameters (concentration, median radius, and distribution width) and size distribution moments (surface area, volume, and effective radius) retrieved from HALOE are shown in Figure 4.37 as time – height cross sections near the equator. The aerosol size distribution is noticeably perturbed when Pinatubo aerosols are present, showing larger median radii and narrower distribution widths. This pattern gives way to broader distributions of smaller particles as time progresses. The aerosol concentration remains fairly stable throughout the time period, at roughly 10 cm^{-3} at altitudes above 19 km. These characteristics are consistent with *in situ* aerosol size distribution measurements from the University of Wyoming. The aerosol surface area and volume are dramatically higher during the Pinatubo period compared to the late 1990s, and suggest that a near steady state was reached after 1997. A complete set of such plots can found on the web site.

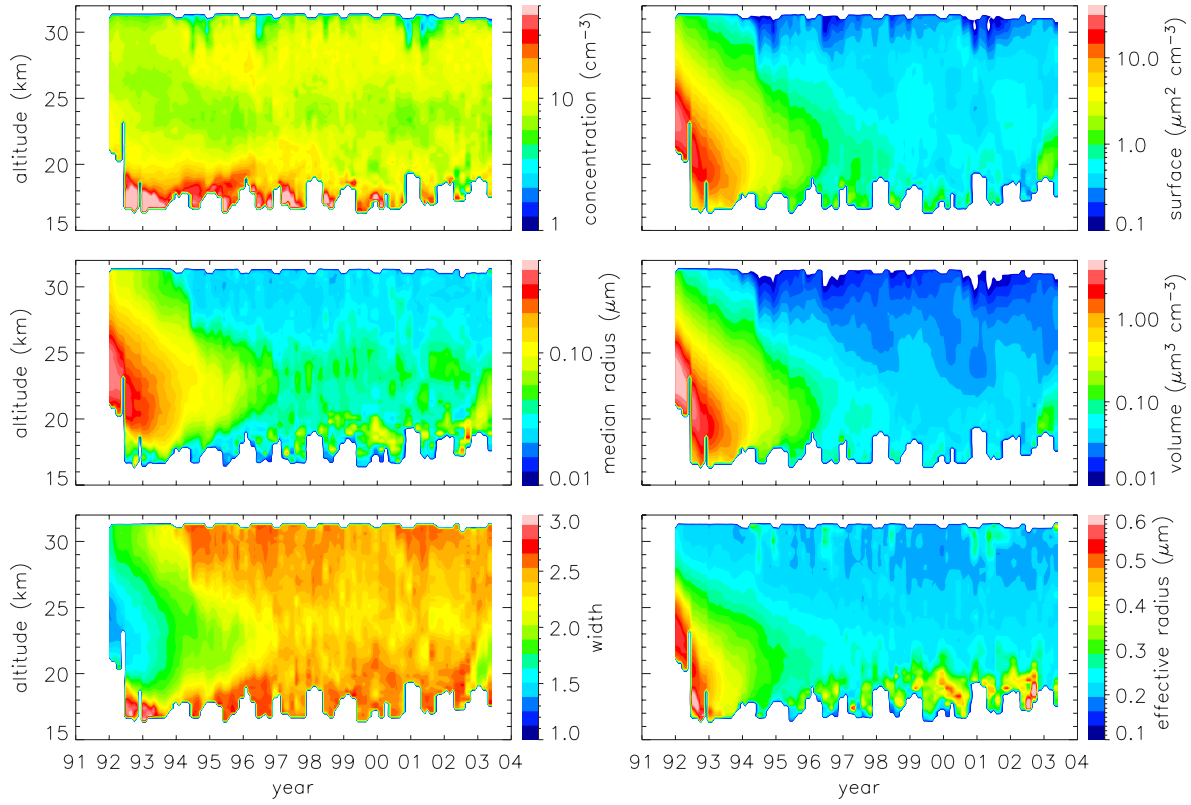

Figure 4.37: Time – height cross sections of aerosol size distribution parameters and size distribution moments retrieved from HALOE. The data are averages for 0°–5°N latitude and are presented at the native vertical sampling interval of 0.3 km. Data identified as cirrus were removed.

Retrieved products from POAM II, POAM III

Aerosol surface area and volume densities have been calculated (Figures 4.38 and 4.39), from both POAM II and POAM III retrieved aerosol extinction using the principal component analysis (PCA) technique [Steele et al., 1999]. In this approach the aerosol surface area and volume are parameterized as a linear combination of the aerosol extinction in the five POAM aerosol channels. The PCA coefficients, which multiply the aerosol extinction values, are wavelength dependent, but time invariant. The random error in the POAM surface area and volume density retrievals is about 8-15% in the stratosphere for background aerosol conditions [Steele et al., 2003]. To evaluate the bias in the POAM PCA surface area and volume retrievals (as well as that obtained using the same technique with the SAGE II aerosol extinction measurements), Steele et al. [1999] used measurement simulations performed with realistic background aerosol size distributions. The results suggest that POAM surface area and volume retrievals are biased low relative to the true values. The measured aerosol extinction at POAM wavelengths, which is assumed to be due entirely to scattering (not absorption), has low sensitivity to particles with radius $\lesssim 0.1$ μm, although particles in this size range may make a significant contribution especially to the surface area [Randall et al., 2001, Deshler et al., 2003]. The amount of the underestimate is dependent upon the specific size distribution parameters. Average biases were predicted to be around –10% and –5% for surface area and volume densities respectively, with values approaching –40% and –30% for extreme size distributions with the smallest width and mean radius.

Figure 4.38 shows the change in the POAM II aerosol area and volume density from 1994 to 1997 during the decay of the Mt. Pinatubo aerosol. Figure 4.39 shows the seasonal variation of the POAM III area and volume density during the period of 1998-2004, when there was little inter-annual variation.

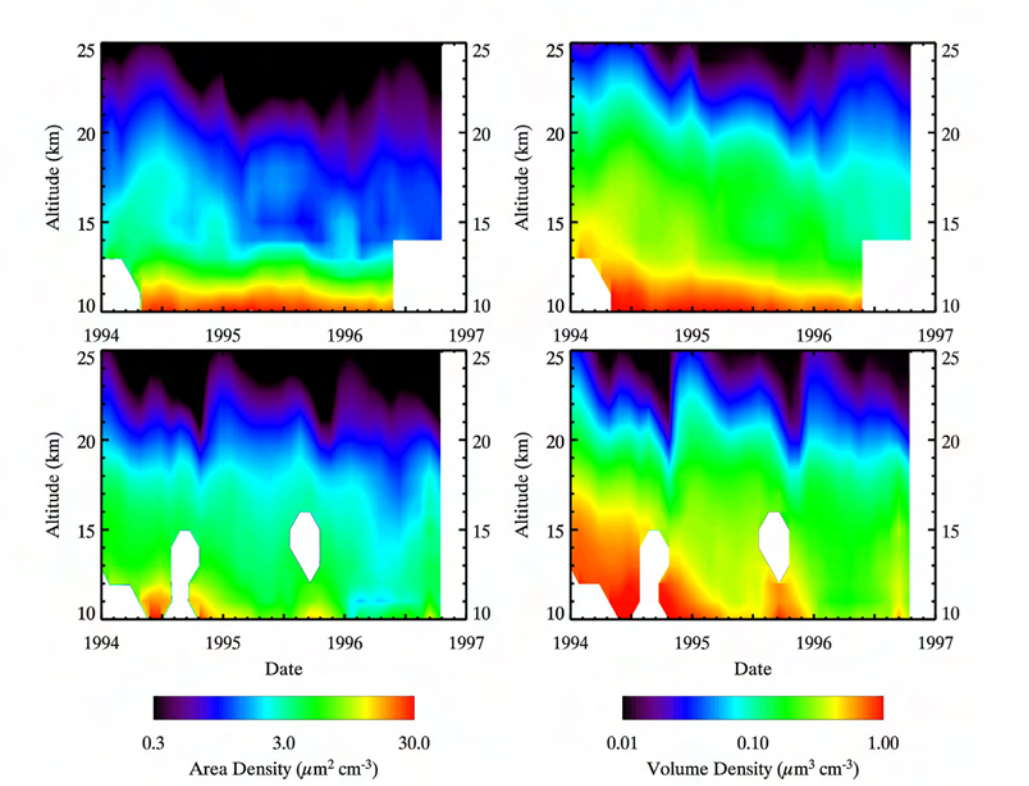

Figure 4.38: Aerosol area and volume density obtained from POAM II measurements at 54-71 N (top row) and at 63-85 S (bottom row) during the period 1994 to 1997.

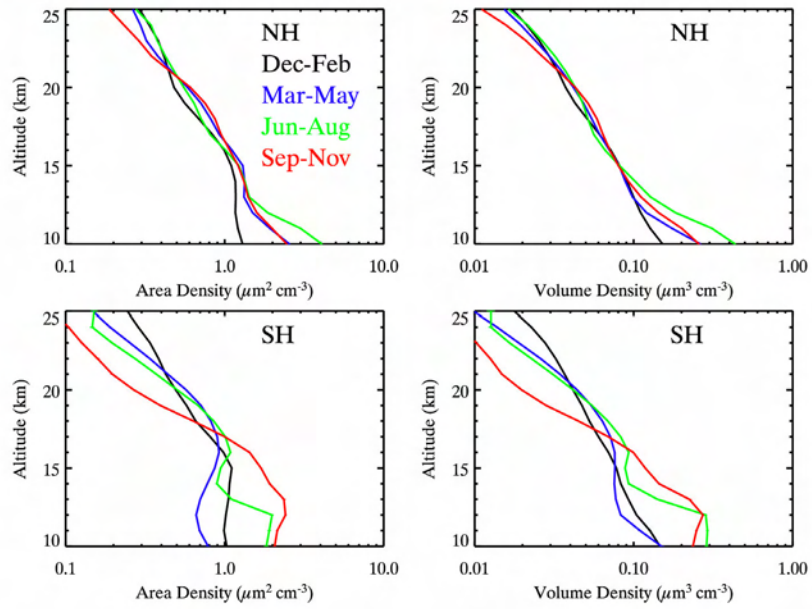

Figure 4.39: Seasonally averaged aerosol area and volume density obtained from the POAM III measurements during 1998 to 2004. Top row shows northern hemisphere results (54-71 N) and bottom row shows southern hemisphere results (63-88 S).

4.3.2 Retrieved Products from Localized Long-term Measurements

Retrieved products from the OPC

To provide functional size distributions representing the cumulative concentration measurements, data are fit with either unimodal or bimodal lognormal size distributions [Jäger and Hofmann, 1991; Hofmann and Deshler, 1991; Deshler et al., 2003]. Thus each measurement of particle concentration at several discrete size bins is fit with a function of the form,

$$N(>r) = \sum_i \int_r^\infty \frac{N_i}{\sqrt{2\pi}\ln\sigma_i} \exp\left(\frac{-\ln^2[a/r_i]}{2\ln^2\sigma_i}\right) d\ln a\,, \qquad (4.5)$$

where the summation is over either one or two modes of the size distribution. For each mode of the distribution, N_i is total number concentration, r_i median radius, and σ_i distribution width. N ($>r$) represents the concentration of all particles larger than the lower integration limit, r, and is the quantity measured by the OPCs. The fitting method consists of minimizing the root mean square error = $\Sigma_k \log^2 [N_m(>r_k) / N(>r_k)]$. The summation is over all measured size channels, r_k. $N_m(>r_k)$, the measured concentration of all particles with $r > r_k$, $N(>r_k)$, is defined by (4.5). The method consists of trying all combinations of measured concentrations to find the set of 5 discrete sizes plus CN concentration giving size distribution parameters which minimize the root mean square difference when all measurements are compared to estimates from the fitted size distribution. Lognormal size distributions are used because: (1) they represent the data well in most cases, (2) they are easy to use - three parameters specify the complete size distribution for each mode included, (3) there are analytical expressions for the distribution moments, and (4) there is some experimental basis to expect aerosol populations to evolve into lognormal size distributions [Granqvist and Buhrman, 1976]. To obtain bimodal distributions requires six estimates of size resolved number concentration. In practice a minimum of five independent measurements are sufficient since the sixth measurement can be inferred to be a low concentration at some size larger than the largest size for which there are measurements. For less than five measurements a unimodal distribution is used.

Monte Carlo simulations were used to assess the impact of measurement uncertainty, due to counting statistics and precision for concentration measurements, and due to pulse width broadening for sizing uncertainties [Deshler et al., 2003]. Results of 750 simulations on four example measurements lead to the conclusion that for lognormal size distributions fitted to the *in situ* measurements, surface areas, volumes and effective radii have uncertainties of ± 40%, median radii ± 30%, and distribution widths ± 20%. The greatest uncertainties were in determining N_2 in periods of low aerosol loading. In these cases standard deviations were over 100%. In contrast, under high aerosol loading N_2 is determined to within 10%. The uncertainty in N_1 is always less than 10%.

Figure 4.40 presents the column integrals of aerosol surface area and volume which can be derived from the size distribution measurements presented in Figure 4.16.

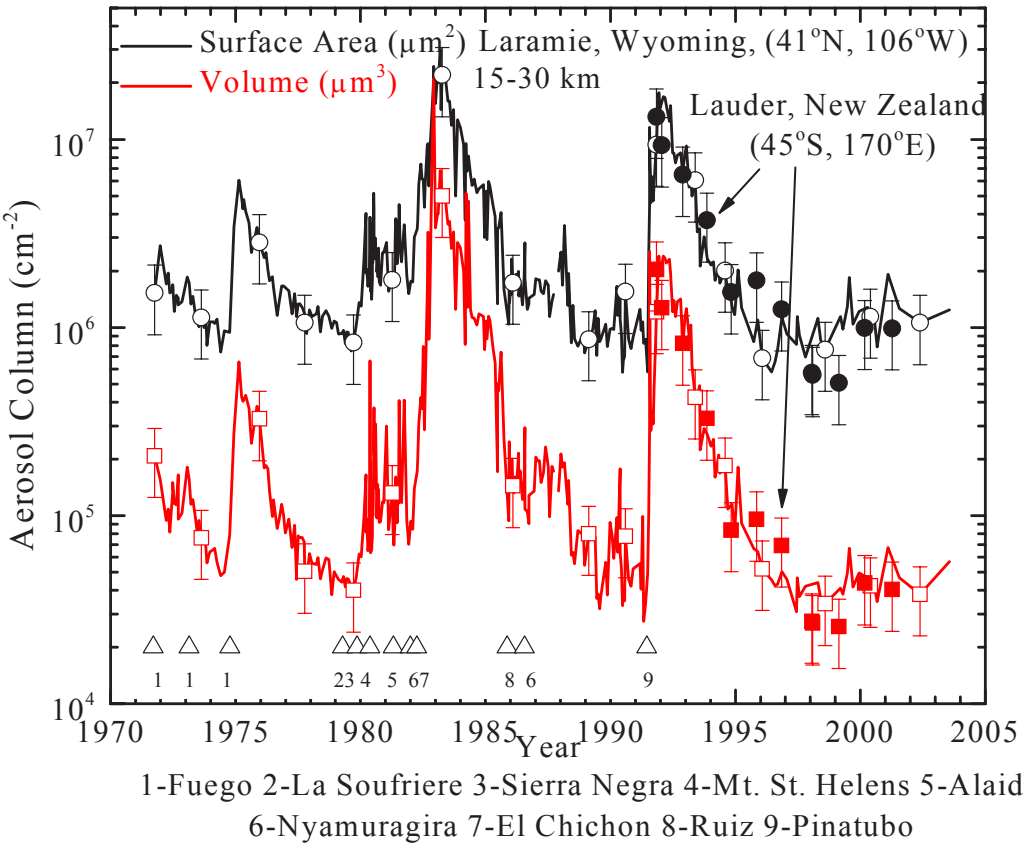

Figure 4.40. History of 15-30 km column integrals, above Laramie, Wyoming, of aerosol surface area (full line) and volume (dotted line). Example error bars are shown on occasional data points. The aerosol surface area and volume are derived from size distributions fit to the in situ measurements. Error bars represent the ± 40% error determined for surface area and volume estimates from in situ size distributions. Also included are 12 measurements from Lauder, New Zealand (filled symbols, with error bars) using the same instrumentation. The Laramie measurements represent about 340 individual profiles. Eruption times for the nine stratospherically important volcanic eruptions occurring during the period are indicated.

Retrieved Products from the FSSP-300 and MASP

Figure 4.41 presents the derived quantities obtained from measurements made by the FSSP-300 and MASP as a function of latitude, from December 28, 1988 to March 12, 2000. The top panel shows the effective radius, calculated as the ratio of the third moment of the size distribution to the second moment. The middle panel is the volume density (particle volume per unit volume of air) and the bottom panel is the surface area density. The dashed lines are the maximum values measured in each interval and the vertical bars are the standard deviations about the averages. As in the case of the number concentration, there is a distinct minimum at tropical latitudes with maxima at mid-latitudes, particularly in the north-

ern hemisphere. The decrease in concentration, area and volume in tropical and polar latitudes are a reflection of the shift to smaller particles that are below the detectable size (0.2 μm) of either the FSSP or the MASP. In the tropical latitudes, published studies have shown that the large increase in particles less than 0.1 μm is a result of new particle formation. In the Arctic regions the shift to smaller particles is a result of the descending air in the Polar vortex.

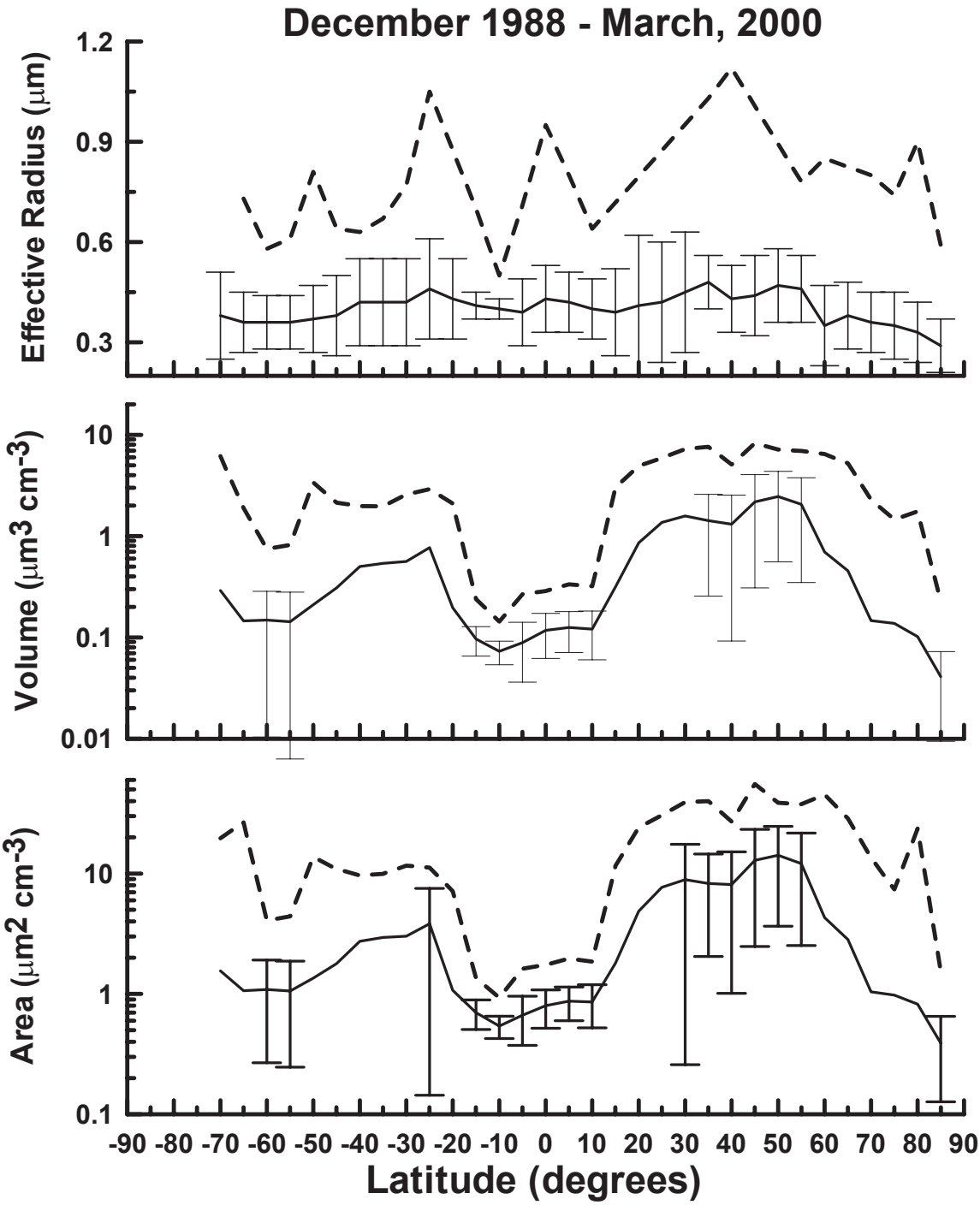

Figure 4.41: Effective radius, volume density and surface area density derived from measurements made with the FSSP-300 and MASP in the altitude range from 17–20 km averaged in 5° intervals of latitude from December, 1988 to March, 2000. The vertical bars are standard deviations about the average (solid line) and the dashed lines are the maxima.

4.4 Relevant Cross-Comparisons Of Averages Or For Coincidences

4.4.1 SAGE/HALOE/OPC Comparisons

Extinction Comparisons

Since aerosol extinction is a strong function of wavelength, comparing measurements made at different wavelengths poses a challenge. Some investigators have dealt with this problem by applying a constant scaling factor to adjust extinctions from visible to IR wavelengths [e.g., Massie et al., 1996; Lu et al., 1997]. While this approach can be valid within the infrared region, bridging the gap between visible and infrared wavelengths is less straightforward. Complications arise because the relationship between visible and infrared extinction is highly dependent on the size distribution and aerosol composition (e.g. sulfuric acid concentration given as wt% H_2SO_4), which determines the refractive index. Since both quantities vary notably with height and time in the stratosphere, a constant scaling factor is generally inadequate. Here aerosol size distributions from the OPCs and from HALOE were used to calculate extinction at the SAGE II wavelengths. For HALOE-SAGE II comparisons this is a robust approach for resolving inherent differences due to measurement wavelength. While the HALOE measurements were manipulated many times (from IR extinctions to size distributions and then to visible extinctions), the SAGE II data set was left in its original state.

Aerosol extinctions at the SAGE II wavelengths were computed from Mie theory using the HALOE and OPC size distributions with refractive indices from Palmer and Williams [1975], which are adequate for visible wavelengths. The refractive index is a function of aerosol composition, and aerosol compositions were determined as a function of temperature, pressure, and water vapor mixing ratio [e.g., Steele and Hamill, 1981]. HALOE water vapor measurements were used for this purpose. Visible sulfate indices are a weak function of composition and potential errors in calculated extinction due to errors in estimated composition are less than 1%. Uncertainties in the calculated extinctions are principally due to uncertainties in the size distributions. Test calculations show that the size distribution errors propagate into extinction uncertainties on the order of 30 to 40%, for HALOE and OPC size distributions.

Time Series Comparisons. Time series were constructed over Laramie (41°N) from the HALOE, SAGE II, and OPC data sets, and over the equator from the HALOE and SAGE II data sets. The time series comparisons did not require coincidence of the respective measurements, and all measurements near a desired location were used. Each data set samples a chosen latitude frequently enough that the average magnitude and trend of extinction should be well represented. The effect of meteorological variability on the aerosol distribution is a factor in comparing non-coincident measurements. However, for the long duration of these comparisons small scale variations become less important than the overall magnitude and trend. An alternative to this approach would be to require time and space coincidence of the measurements. While this approach can work for comparisons of two data sets, three-way coincidences are rare. Additionally, there are no direct coincidences between HALOE and SAGE II at equatorial latitudes.

In Figures 4.42 and 4.43, time series are shown at three representative altitudes over each location for all SAGE II wavelengths. Average tropopause heights are roughly 12 km at middle latitudes and 16 km in the tropics, and the lowest levels chosen were above these

heights to minimize data loss from cloud filtering. SAGE II, HALOE, and OPC measurements over Laramie are compared in Figure 4.42. The appearance and decay of volcanic aerosols are well represented by the three instruments. Aerosol loading due to the eruptions of El Chichón (1982) and Mt. Pinatubo (1991) resulted in similar extinction enhancements during the post-eruption years. These extinctions were observed to decay by roughly two orders of magnitude during a six year period following each eruption. A summary of the comparison differences over Laramie is presented in Table 4.3.

The Laramie comparisons show generally good agreement among the three data sets prior to 1997 at 16 and 22 km, with greater variability and poorer agreement at 28 km at all times. Greater variability at 28 km may be a result of lower aerosol concentrations and smaller sizes at these altitudes. Under these conditions, the extinction measurements are approaching their noise levels, and greater uncertainties are expected for SAGE II and HALOE. Concerning the OPCs, low particle concentrations increase the statistical uncertainty of the measurements due to Poisson counting errors and thus create greater proportionate variability in calculated extinction. The comparisons can be roughly divided into volcanic and background periods, where some clear differences emerge. Volcanic periods were characterized by generally good agreement among the three data sets at all SAGE II wavelengths. During both background periods at 16 and 22 km OPC extinction estimates are lower than the SAGE II extinctions at all wavelengths, with the greatest differences for the 1.02 μm comparison. For example, at 16 km after 1996, the OPC 1.02 μm extinctions are on average a factor of 4 lower than SAGE II, while the 0.386 μm OPC extinctions are a factor of two lower than SAGE II. The SAGE II 1.02 μm measurements should generally have the lowest uncertainties, on the order of 10%, and are roughly 100 times above the detection limit even during background periods. In addition, HALOE extinctions tend to agree with SAGE II values after 1997, except in 1999 when HALOE values can be very low. The extinction differences at the longest SAGE II wavelengths after 1996 indicate problems in deriving longer wavelength extinctions from the OPC measurements in low aerosol loading. This problem is not as severe at the shorter wavelengths during background periods. This difference may arise because of sample volume differences between the OPC and SAGE II. The much larger sample volume of SAGE II would be sensitive to low concentrations of larger particles, which dominate the 1.02 μm Mie kernel (Figure 4.28), while these concentrations may be below the detection limit of the OPC. The shorter wavelength Mie kernels are dominated by smaller more abundant particles. At shorter wavelengths in background periods HALOE extinction estimates are lower than SAGE II extinctions and are closer to OPC estimates.

HALOE and SAGE II measurements were compared over the equator at longitudes from 180°E to 270°E where the occurrence of cirrus is a minimum [e.g., Wang et al., 1996]. These comparisons (Figure 4.43) show less variability at 30 km than over Laramie at 28 km (Figure 4.42). At 25 km HALOE and SAGE II 1.02 μm extinctions are within 25% of each other during the entire comparison period. At shorter wavelengths HALOE and SAGE II agree until the aerosol approaches its background state near 1997. After that time HALOE systematically underestimates SAGE II extinctions for wavelengths < 1.02 μm. The shorter wavelength comparisons at 20 km are similar to those at 25 km. The equatorial differences are similar in direction, if not magnitude, to the HALOE - SAGE II comparisons over Laramie.

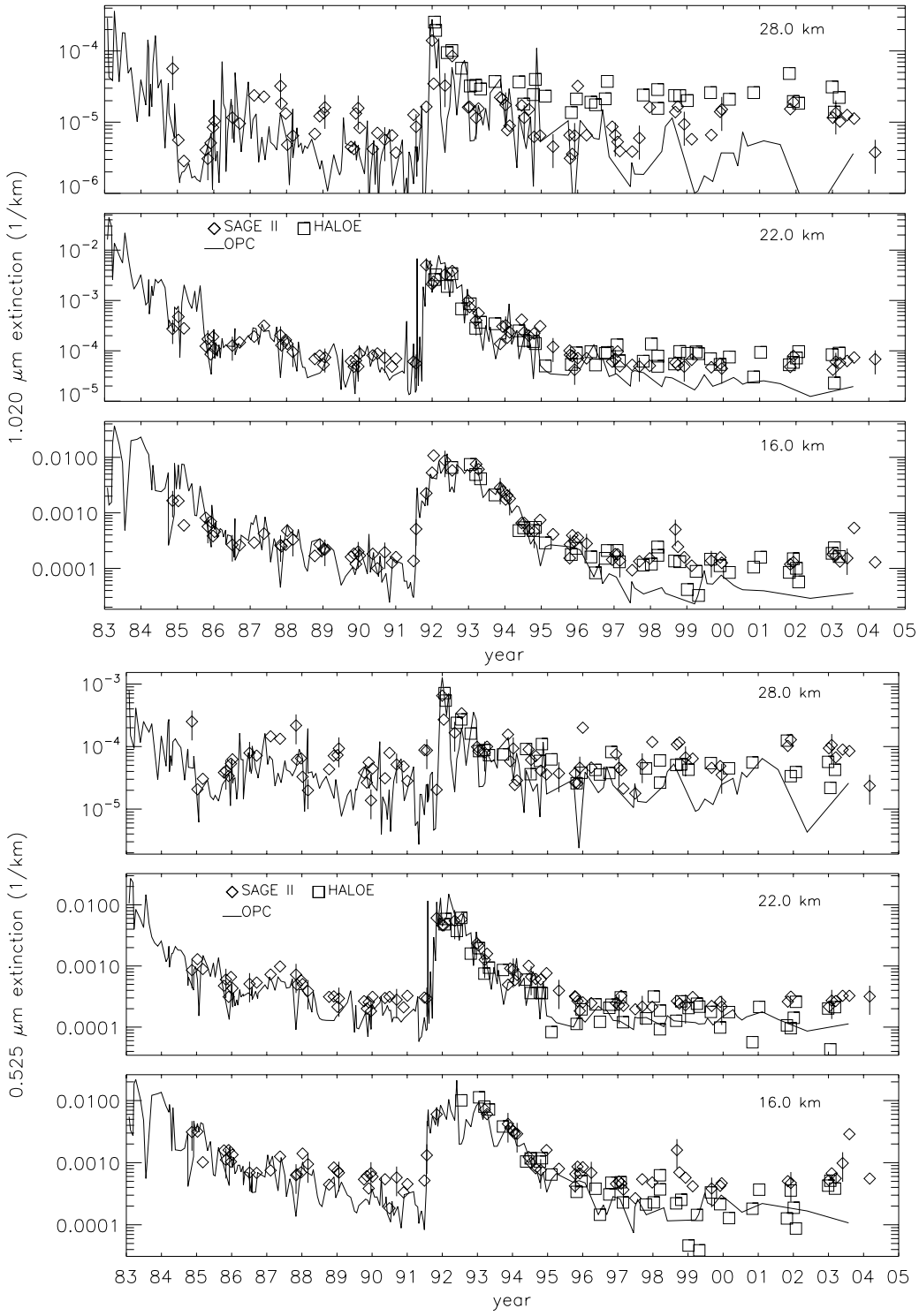

Figure 4.42: Time series at three altitudes over Laramie of aerosol extinction at four SAGE II wavelengths. SAGE II (◊) measurements are compared to extinctions calculated from OPC (—) and HALOE (□) size distributions. HALOE and SAGE II measurements between 41°N and 42°N latitude and 245°E and 265°E longitude were used. Vertical bars on the occasional SAGE II measurement indicate ± 50%. The SAGE II uncertainties are less than this, and these bars serve only to add perspective. This time series is composed of 81 SAGE II, 202 OPC, and 43 HALOE measurements.

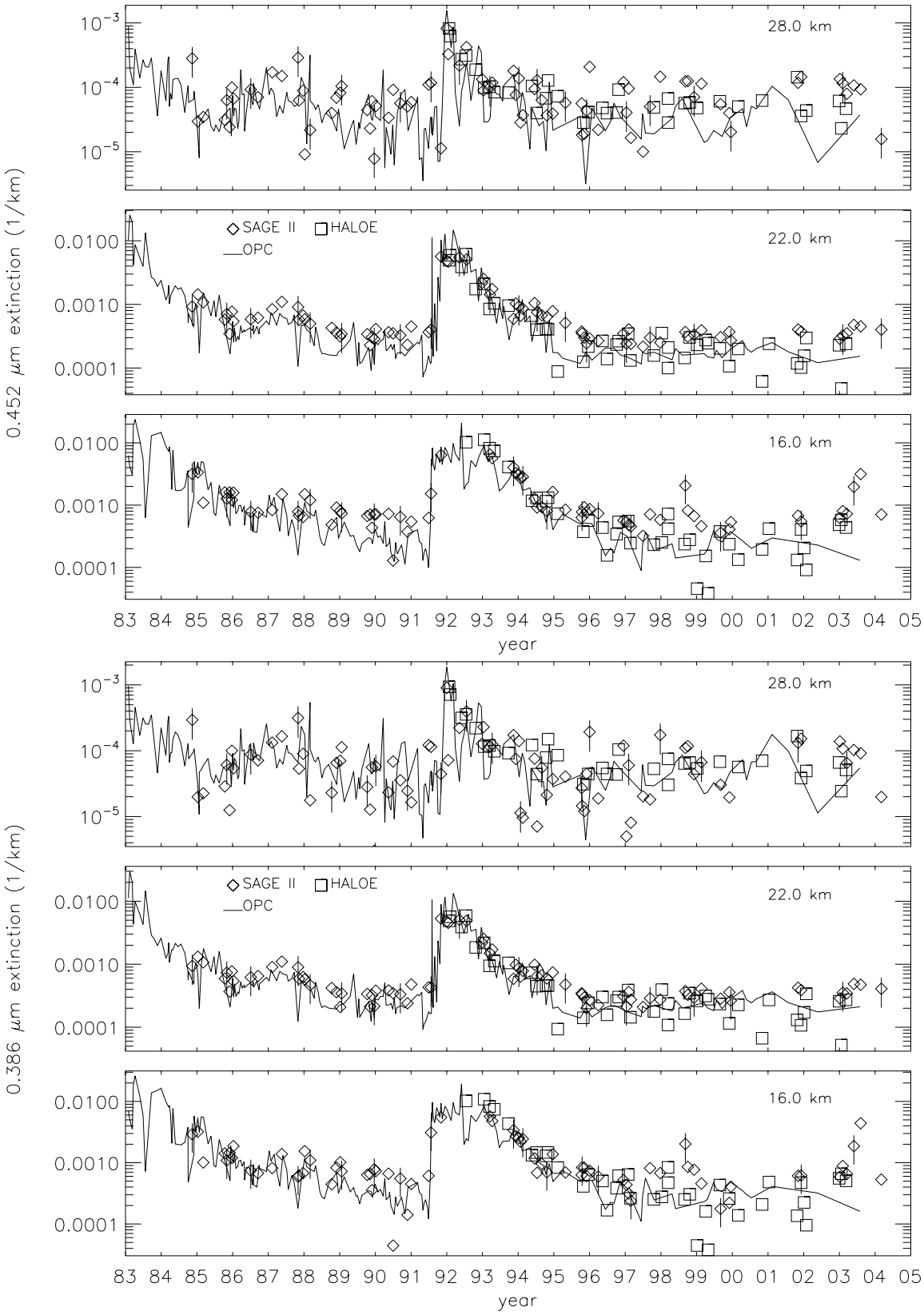

Figure 4.42: Continued.

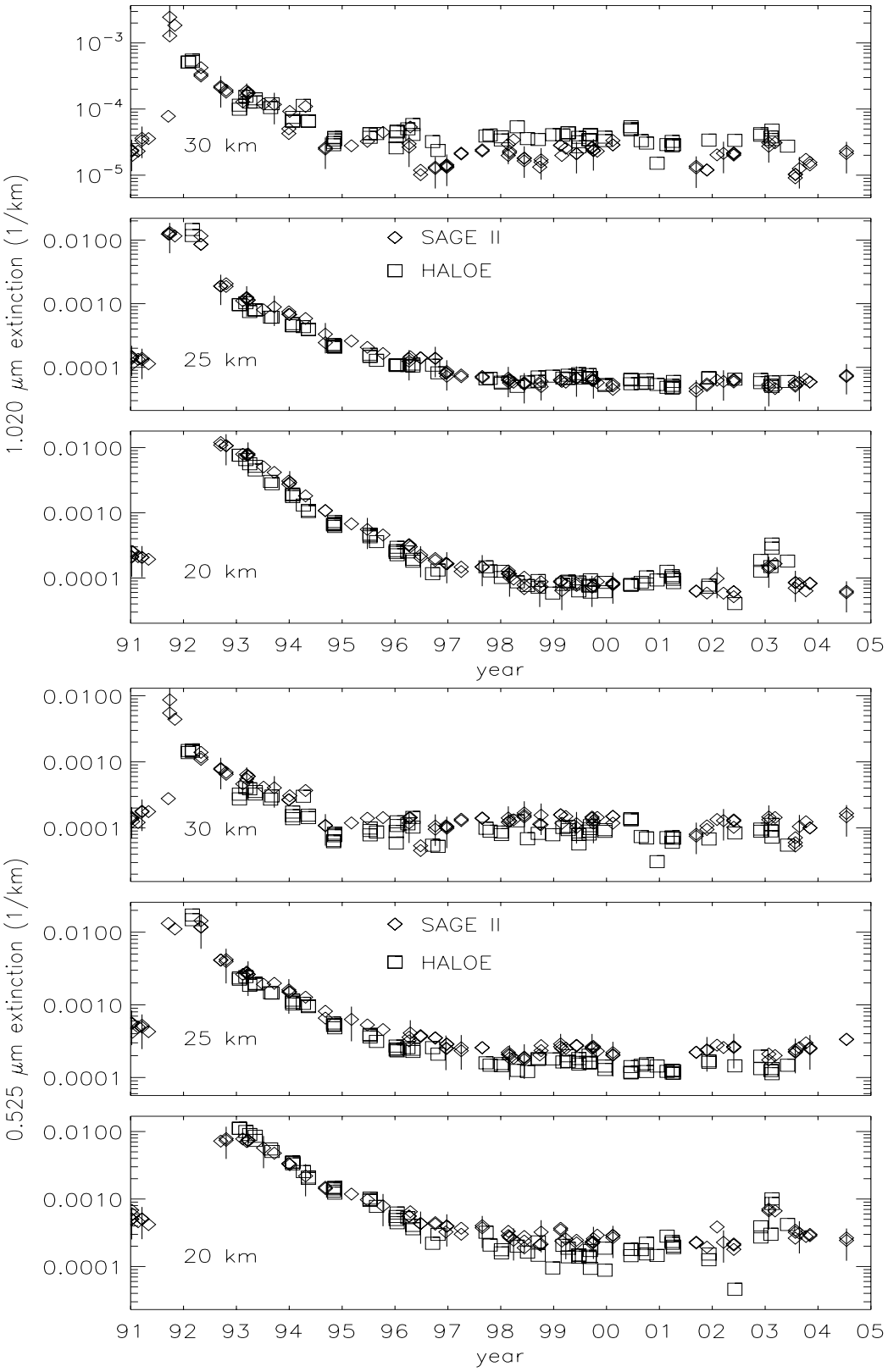

Figure 4.43: Time series at three altitudes of aerosol extinction at four SAGE II wavelengths, from HALOE (□) and SAGE II (◊). Measurements used were between the equator and 1°S latitude and 180°E and 270°E longitude. Vertical bars on the occasional SAGE II measurement indicate ± 50%. The SAGE II uncertainties are less than this, and these bars serve only to add perspective. This time series is composed of 96 SAGE II and 78 HALOE measurements.

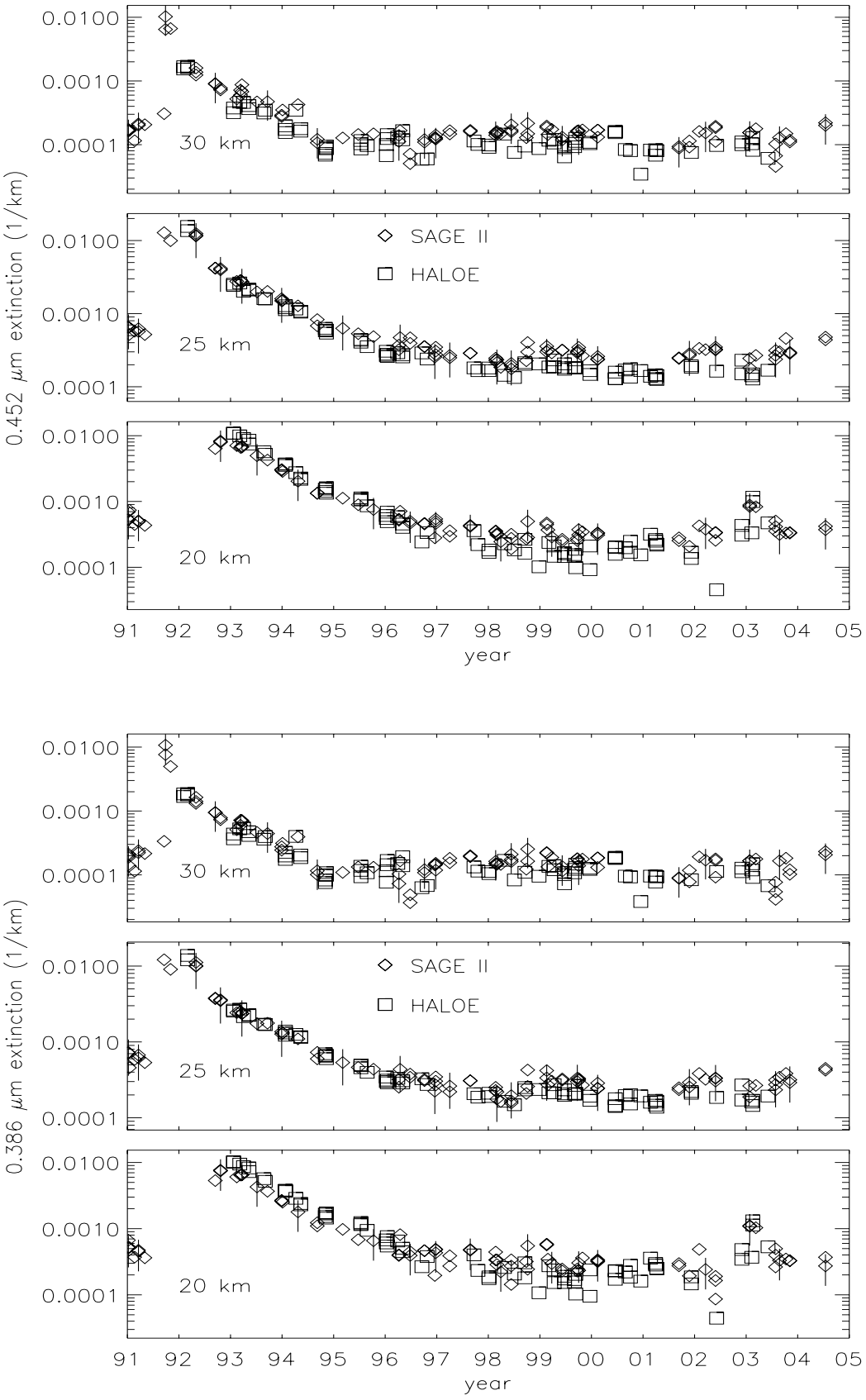

Figure 4.43: Continued

Profile Comparisons. Vertical profiles for coincident measurements between SAGE II and HALOE and SAGE II and the OPCs were compared over the time periods sampled by the instrument pairs. For this purpose, coincident measurements were identified using maximum separations of 24 hours, 2° latitude, and 20° longitude. This led to 353 HALOE-SAGE II comparisons near 41°N and 30 OPC-SAGE II comparisons over Laramie. Coincident profiles were compared for the duration of the data sets and comparison statistics were generated. These are presented as mean profiles, mean differences, and difference standard deviations (random differences). At each altitude, the mean relative difference in percent between SAGE II (S) and the other (O) measurements was computed as

$$\overline{\Delta} = \frac{1}{N} \times \sum_{i=1}^{N} \Delta_i \,,$$

where N is the number of coincident measurements and $\Delta_i = 200 \times (O_i - S_i)/(O_i + S_i)$. Standard deviation of the mean relative difference was computed as

$$\sigma_{\overline{\Delta}} = \left(\sum_{i=1}^{N} (\Delta_i - \overline{\Delta})^2 / (N-1)\right)^{1/2}.$$

Separating each comparison into individual years can show varying agreement among the three data sets; however, presenting this analysis is difficult. A hint of such comparisons can be obtained by referring to Figures 4.42 and 4.43 as the composite profile statistics are presented.

Comparison results for coincident HALOE and SAGE II measurements between 38°N and 44°N (± 3° latitude of Laramie) are shown in Figure 4.44. These comparisons show a generally constant bias for all wavelengths and altitudes, with HALOE roughly 30% less than SAGE II. The most notable exceptions to this pattern are at 1.02 μm wavelength above 22 km and for the other wavelengths above roughly 30 km. Uncertainties in the mean differences, ($\sigma_{\overline{\Delta}}/N^{1/2}$), are generally less than 5%, indicating that these biases are statistically significant. Comparison statistics for coincident SAGE II and HALOE profiles at southern middle latitudes (not shown) are very similar to comparisons in the northern hemisphere shown in Figure 4.44. There are no direct HALOE-SAGE II coincidences in the tropics and Figure 4.43 serves to document HALOE-SAGE II agreement there.

Comparison results for coincident SAGE II and OPC measurements over Laramie are shown in Figure 4.45. These results indicate clear systematic differences, with the OPC extinctions roughly 30% less than SAGE II at most altitudes and wavelengths. The most notable exception to that statement is at 1.02 μm where differences are larger above 20 km and close to zero below 20 km. While uncertainties in the mean differences can be large (5 to 20%) the reported biases are typically greater than the uncertainties and therefore statistically significant. Larger uncertainties in the OPC-SAGE II mean differences are due to the lower number of coincidences. The results in Figures 4.44 and 4.45 are generally consistent with Figure 4.42, showing greater variability (random differences) at the highest altitudes, and systematic differences that can change with altitude. Because the profile statistics include measurements during volcanic and background periods, certain features in Figures 4.42 and 4.43 are not visible in Figures 4.44 and 4.45.

While the extinction comparisons required manipulation of the HALOE and OPC measurements, the SAGE II measurements were untouched. Thus, these comparisons establish agreement among the instruments at perhaps the most fundamental level possible. While the overall agreement is encouraging, it is clear that the differences change with wavelength, latitude, altitude, and time. As these data sets continue to be used to infer various optical and physical aerosol properties, the extinction comparisons provide a useful

standard to assess the validity of the inferred properties.

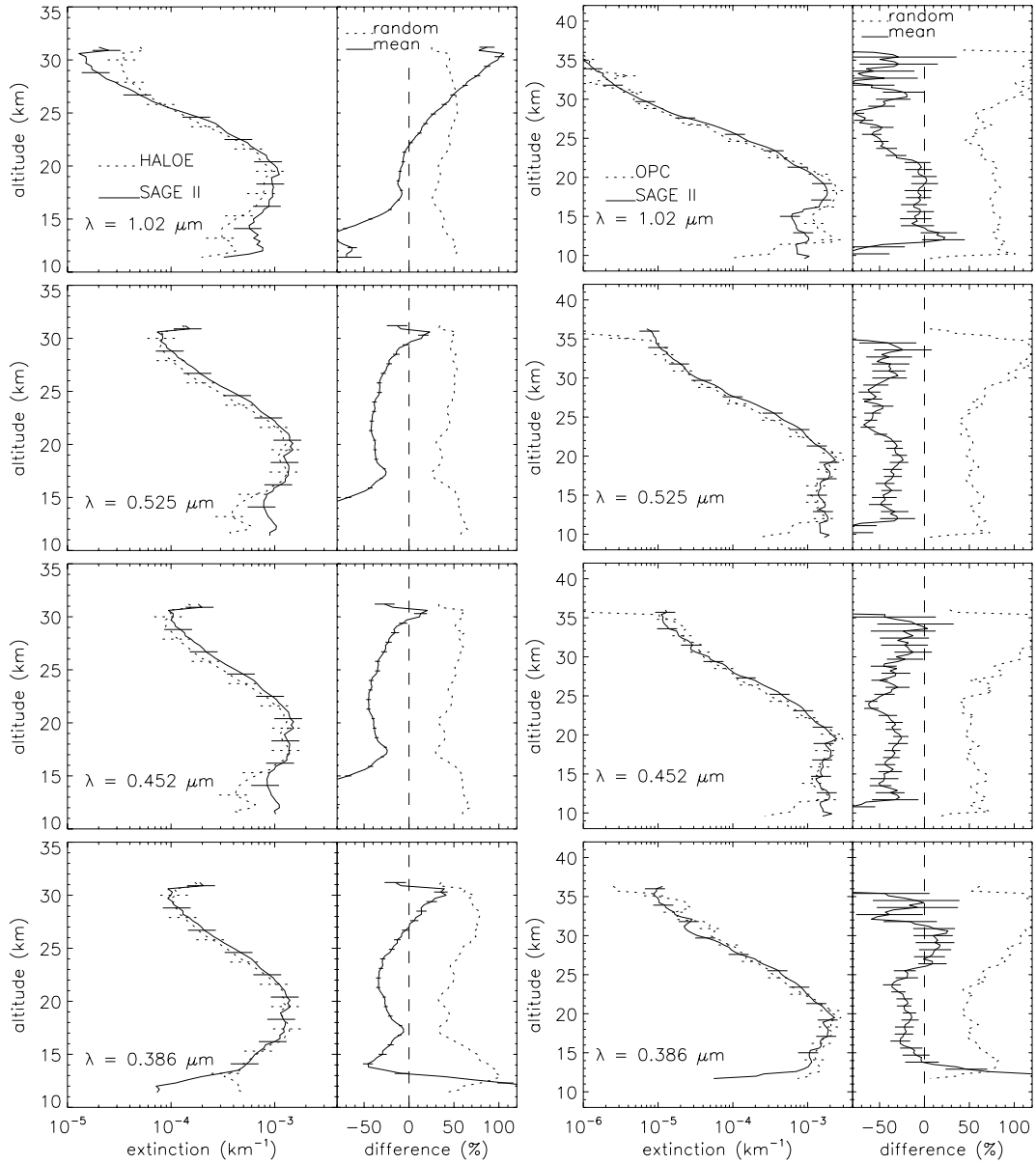

Figure 4.44 (left column): Comparison statistics for 353 coincident HALOE and SAGE II profiles between 38°N and 44°N latitude, from 1991 through 2002. The average profile separations were 11.6 hours, 0.8° latitude, and 7.6° longitude. Statistics are shown as mean profiles, mean differences (HALOE - SAGE II), and difference standard deviations (random differences). See text for details. Error bars on the mean profiles indicate the reported measurement uncertainties, and error bars on the mean differences indicate uncertainties in the mean differences ($\sigma_{\bar{\Delta}}/N^{1/2}$).

Figure 4.45 (right column): Comparison statistics for 30 coincident OPC and SAGE II profiles over Laramie, from 1984 through 1999. The average profile separations were 12.2 hours, 0.9° latitude, and 6.8° longitude. Statistics are as described in Figure 4.44, except the differences are OPC - SAGE II.

Surface Area Comparisons

This section evaluates aerosol surface area densities (SAD) determined from SAGE II, HALOE, and the OPCs. Thomason et al. [1997b] compared SAGE II aerosol surface areas (derived from V5.96) to the OPCs over Laramie for four years after the Pinatubo eruption. That work showed good agreement for surface areas less than about 15 $\mu m^2\ cm^{-3}$, and systematic differences (SAGE II > OPC) under higher aerosol loading conditions. Hervig et al. [1998] compared HALOE surface areas based on room temperature refractive indices from Palmer and Williams [1975], to OPC results over Laramie. While that work showed that HALOE surface areas were from 10 to 30% higher than the OPC values, the current HALOE surface areas which are based on cold temperature refractive indices from Tisdale et al. [1998] are ~ 25% lower than the previous results. For the comparisons presented here, SAGE II surface areas were taken from the version 6.2 SAGE II data files. A description of SAGE II SADs is available in section 4.2.1 of this document and in Thomason and Osborn [1992].

Time series of surface area at three altitudes from HALOE, SAGE II, and the OPCs are compared over Laramie in Figure 4.46. A summary of the measurement differences is offered in Table 4.3. SAGE II and the OPCs are in generally good agreement during the entire comparison period at 16 and 22 km. HALOE tends to agree with SAGE II and the OPCs at 16 and 22 km prior to 1998, but is generally lower than SAGE II and the OPCs after 1998. Significant differences exist nearly all the time at 28 km, where SAGE II surface areas are generally lower than HALOE and the OPCs, and at all altitudes after 1998. Steele et al. [1999] noted that surface areas derived from SAGE II using the PCA technique can be biased low when particles are small, which occurs during low aerosol loading, such as at high altitudes or in background periods. This bias can be partly understood from the Mie kernels shown in Figure 4.28. The median radii of these extinction kernels decrease from 0.6 to 0.2 μm for wavelengths from 1.02 to 0.386 μm. In contrast surface area distributions during low aerosol loading have median radii near 0.1 μm. Deshler et al. (2003) present example surface area and extinction distributions illustrating this difference. Thus, during low aerosol loading extinction measurements are not sensitive to a majority of the particles which control surface area. In this case the observed differences in 1.02 μm extinction between the OPCs and SAGE II may be unimportant when comparing surface area density. In general, agreement between SAGE II and the OPC SAD most closely matches the shorter wavelength extinction comparisons. The factor of four bias in the OPC-SAGE II 1.02 μm extinction comparison (Figure 4.42) is not evident in the SAD comparisons shown in Figure 4.46. It might be noted that the quantity plotted in Figure 4.28 is $3Q/4r=dk/dV$. The effect discussed here is more properly related to $dk/dA=3Q/8$ which falls off more steeply than dk/dV for small r.

Time series of aerosol surface area over the equator from HALOE and SAGE II are compared in Figure 4.47. The HALOE-SAGE II surface area comparisons are similar to the equatorial extinction comparisons (Figure 4.43), suggesting that the variability shown is primarily related to the measurements and to atmospheric variability, rather than errors in the conversion to SAD. The HALOE and SAGE II comparisons of extinction and surface area maintain a consistent relationship throughout the comparisons. The OPC and SAGE II comparisons show opposite biases for extinction and surface area (*cf.* Figures 4.42 and 4.46). Although the SAD agreement is fairly reasonable, the OPC extinction is significantly less than SAGE II at all wavelengths, but most notably at 1.02 μm after 1999.

Profile statistics for HALOE-SAGE II surface area comparisons over Laramie are shown in Figure 4.48. These results show that HALOE and SAGE II surface areas match to within the respective error bars, although HALOE is roughly 20% less than SAGE II at altitudes from 19 to 26 km. HALOE-SAGE II surface area comparisons in the southern hemisphere (not shown) are very similar to the northern hemisphere comparisons. Profile statistics for OPC-SAGE II surface area comparisons over Laramie are shown in Figure 4.49. This comparison shows statistically insignificant differences for altitudes from roughly 16 to 25 km, generally covering the peak in aerosol surface area. Below 16 and above 25 km SAGE II underestimates SAD by 30-60% compared with OPC estimates.

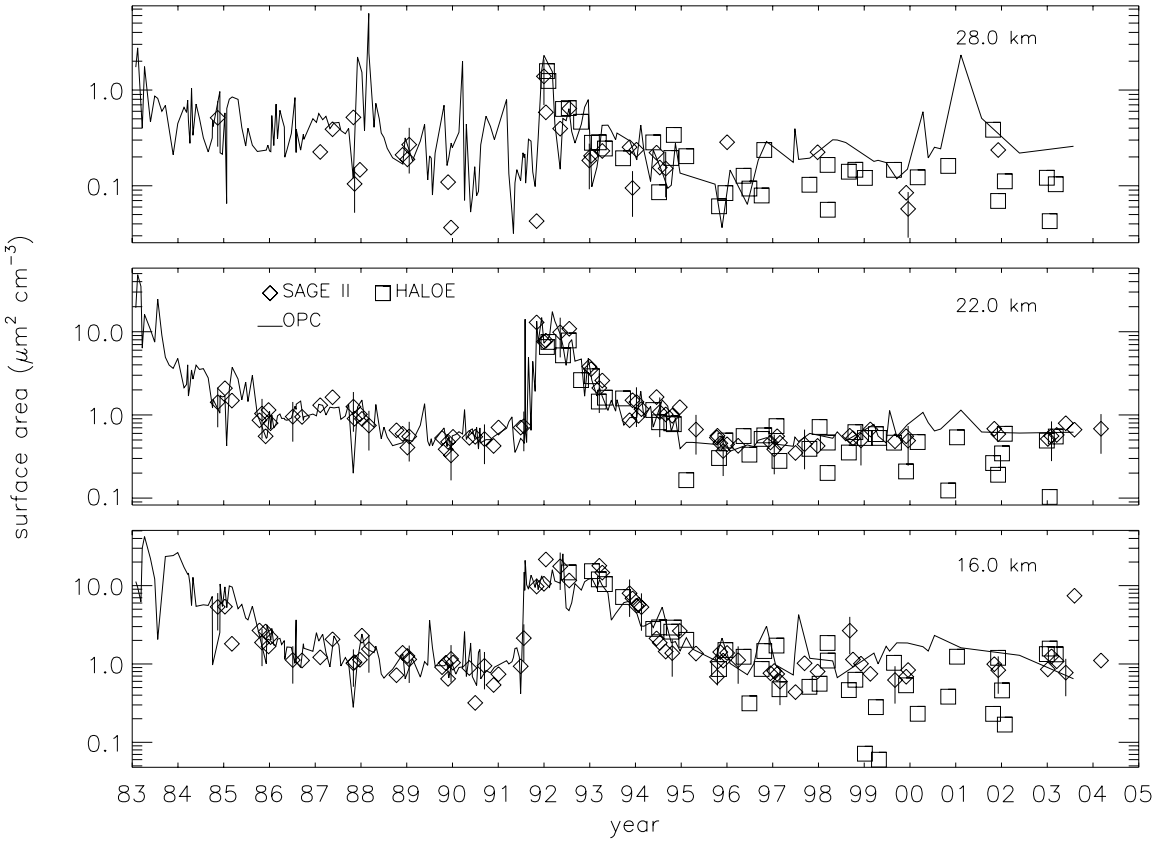

Figure 4.46: Time series of HALOE, OPC, and SAGE II measurements over Laramie as in Figure 4.42, except that aerosol surface area densities are compared.

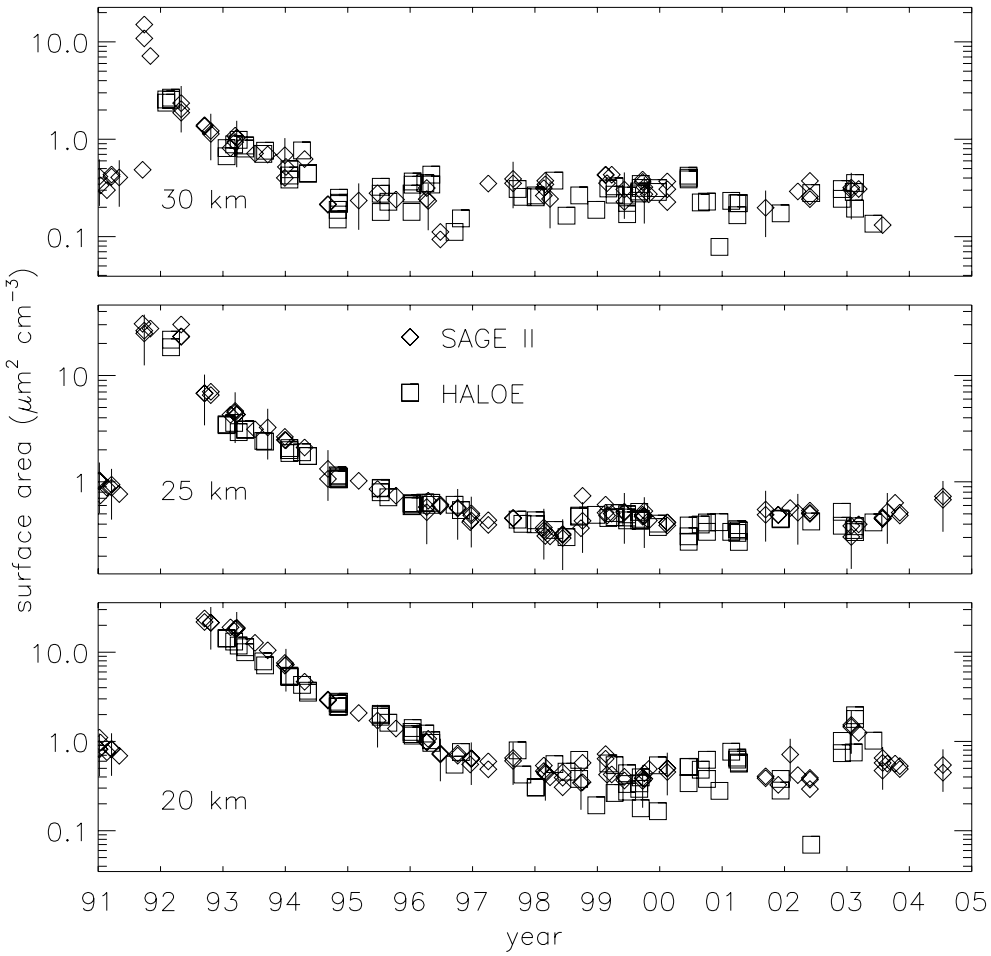

Figure 4.47: Time series of equatorial SAGE II and HALOE measurements as in Figure 4.43, except aerosol surface area densities are compared.

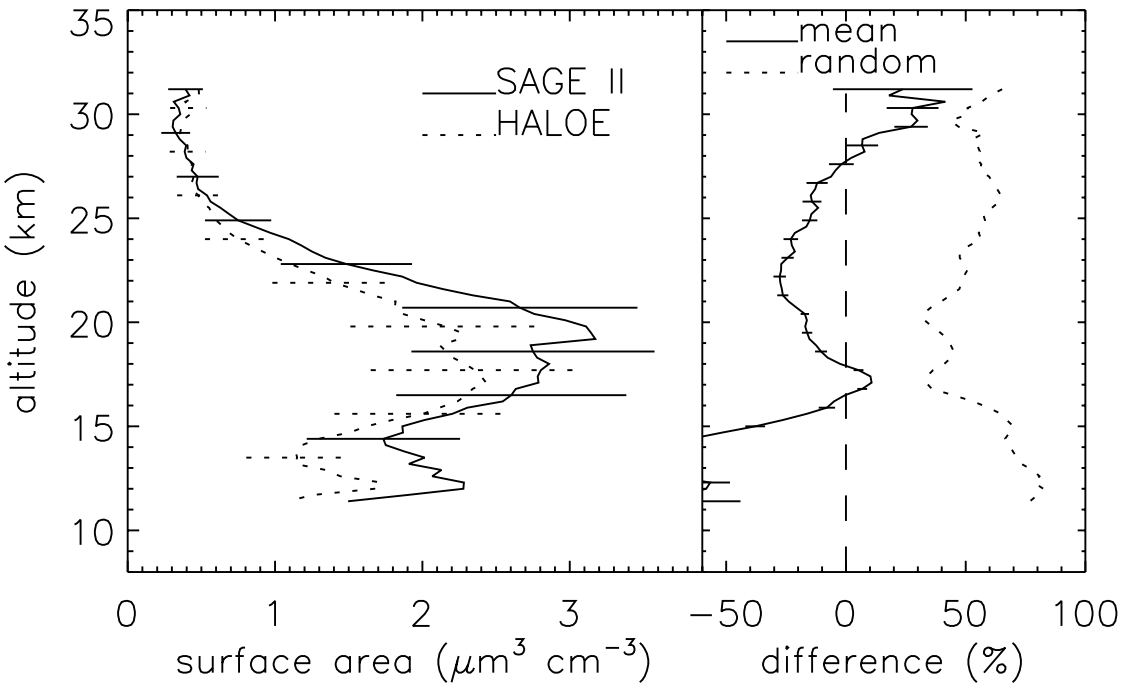

Figure 4.48: Comparison of HALOE and SAGE II measurements over Laramie, as in Figure 4.44 except the results are for surface area density.

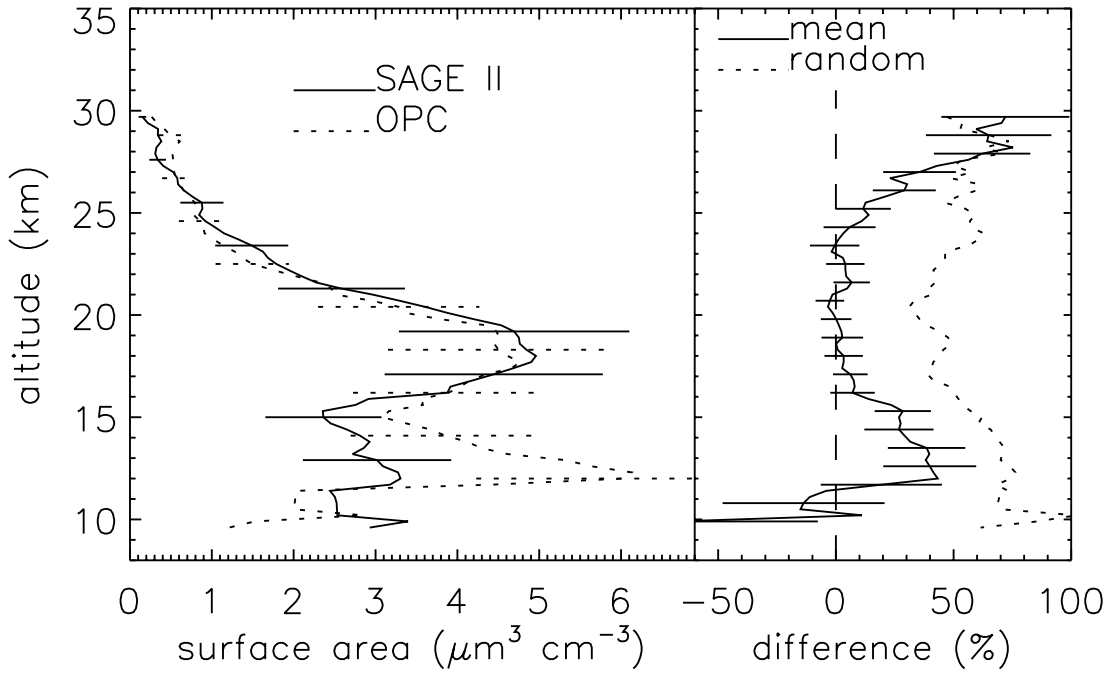

Figure 4.49: Comparison of SAGE II and OPC measurements over Laramie, as in Figure 4.45 except the results are for surface area density.

Summary

Stratospheric aerosol measurements from SAGE II, HALOE, and balloonborne OPCs were compared. These instruments measure different quantities, and a common basis was required to compare the data sets. For this purpose, extinctions at the SAGE II wavelengths were computed from the HALOE and OPC aerosol size distributions for comparison to SAGE II. Aerosol surface areas derived from each data set were compared as well. While the overall impression from these comparisons is encouraging, the agreement can change with latitude, altitude, time, and parameter. The best agreement was generally found when the aerosol extinctions and surface areas were large. For example, the three data sets were in excellent agreement for 1.02 μm extinctions greater than roughly 2×10^{-4} km^{-1}. Notable differences can emerge when the aerosol amounts are low, such as background periods at all altitudes, and at altitudes above about 25 km during most years.

Table 4.3 summarizes some of the observed differences near 41°N latitude for a variety of times, altitudes, and parameters. The SAGE II – OPC comparisons are somewhat inconsistent under low aerosol loading when comparing differences for the 1.02 and 0.386 μm extinctions and for SAD. The extreme example shown here is the comparison for 1999 – 2000 at 16 km which indicates SAGE II 1.02 μm extinctions nearly three times larger than OPC estimates, while SAGE II SADs are 60% lower than the OPC estimates. These inconsistencies persist at higher altitudes, but diminish when shorter wavelength extinctions are compared and when aerosol loading is higher. It should be noted that there were only 3 coincidences during this time period. The inability of the OPCs to properly estimate 1.02 μm extinction probably has minimal impact on the SAD comparisons, since the 1.02 μm measurements are insensitive to the small particles that control surface area under low aerosol loading. That is, the particle sizes that control the OPC calculation of the 1.02 μm extinction and SAD are sufficiently disjoint that the discrepancy in the calculations of 1.02 μm

extinction does not carry over into the calculation of SAD. Considering the operational algorithm to calculate SAD it is clear that if, say, the OPC underestimates the SAGE II extinctions by roughly the same amount at 1020 and 525 nm, then SAD estimates would agree even if extinction estimates did not. As might be expected, the numerical values presented in the table are altered somewhat when one uses a different set of latitude-longitude-time windows to define coincidences. The small number of coincidences between SAGE II and the OPC make it difficult to put a high degree of confidence in these results. It might also be noted that under very low aerosol loadings the influence of non-sulfate particles will be more significant than under high aerosol loadings. Furthermore, some of the problems associated with the low aerosol loading comparisons are due to the difficulty in identifying the aerosol signal in the measurements.

The SAGE II – HALOE comparisons tend to be internally consistent, with the extinction and SAD comparisons showing similar differences at most times and altitudes. It is not clear that better agreement could be expected, considering the various assumptions made, including the assumptions that the size distribution is log normal and the index of refraction is that for sulfuric acid solutions.

Table 4.3. Summary of HALOE/SAGE II/OPC extinction and surface area density (SAD) differences. Results were divided into three time periods and three altitudes. Differences are indicated as the average ratios of quantities for various instrument combinations. The results are based on coincident measurements near Laramie and the number of coincidences in each time period is indicated. Coincident measurements were identified using maximum separations of 24 hours, 2^o latitude and 20^o longitude.

Measurement Ratio	*Altitude*	*Quantity*	*Period* 1987-1990	1992-1994	1999-2000
SAGE II / OPC	Number of coincidences		8	5	3
	16 km	1.02 μm ext.	1.3 ± 0.8	1.9 ± 1.6	2.6 ± 1.5
		0.386 μm ext.	2.0 ± 1.0	1.3 ± 0.5	1.2 ± 0.1
		SAD	1.1 ± 0.3	1.2 ± 0.4	0.4 ± 0.1
	22 km	1.02 μm ext.	2.1 ± 0.5	2.0 ± 1.4	2.7 ± 1.4
		0.386 μm ext.	1.7 ± 0.6	1.4 ± 0.5	1.8 ± 0.3
		SAD	1.1 ± 0.3	1.6 ± 0.5	0.9 ± 0.1
	28 km	1.02 μm ext.	2.2 ± 0.9	3.1 ± 2.0	3.6 ± 1.4
		0.386 μm ext.	1.4 ± 2.3	1.8 ± 1.7	1.5 ± 1.0
		SAD	0.2 ± 0.1	1.4 ± 0.5	N/A
SAGE II / HALOE	Number of coincidences		N/A	99	53
	16 km	1.02 μm ext.		1.4 ± 0.3	1.3 ± 0.7
		0.386 μm ext.	N/A	0.9 ± 0.3	3.0 ± 3.5
		SAD		1.0 ± 0.3	2.7 ± 3.4
	22 km	1.02 μm ext.		1.4 ± 0.7	0.9 ± 0.5
		0.386 μm ext.	N/A	1.5 ± 1.5	2.4 ± 3.4
		SAD		1.6 ± 1.5	2.1 ± 3.0
	28 km	1.02 μm ext.		0.7 ± 0.6	0.5 ± 0.2
		0.386 μm ext.	N/A	1.3 ± 1.1	1.6 ± 1.1
		SAD		1.1 ± 0.8	1.2 ± 0.6

4.4.2 SAGE/POAM Comparisons

Since the POAM II-III and SAGE III measurements are taken at very nearly the same wavelengths, they produce aerosol extinction coefficients that can be easily compared. For POAM II and SAGE II the wavelengths are 0.448-0.452 μm and 1.06-1.02 μm, for POAM III and SAGE II they are 0.442-0.452 μm and 1.02-1.02 μm. Coincidence measurements are selected with a distance smaller than 500 km (350 km on average in both hemispheres) and a time interval smaller than 2 hours (20 min on average in NH, 45 min in SH).

For the whole period covering POAM II and for that covering POAM III, the mean of the relative difference (that enables us to show any possible bias) $\overline{\Delta} = N^{-1}\sum_{i=1,N}\Delta_i$ was computed as well as the root mean square difference of the relative differences (which enables us to estimate the mean agreement) rmsd = $(\sum_{i=1,N}\Delta_i^2/(N\text{-}1))^{1/2}$. Here N is the number of coincident events and $\Delta_i = 200\times(P_i - S_i)/(P_i + S_i)$ where P stands for POAM and S for SAGE. Results for both hemispheres are shown in Figure 4.50 for POAM II and in Figure 4.51 for POAM III. Below about 12 km and above about 30 km the rmsd is always very large.

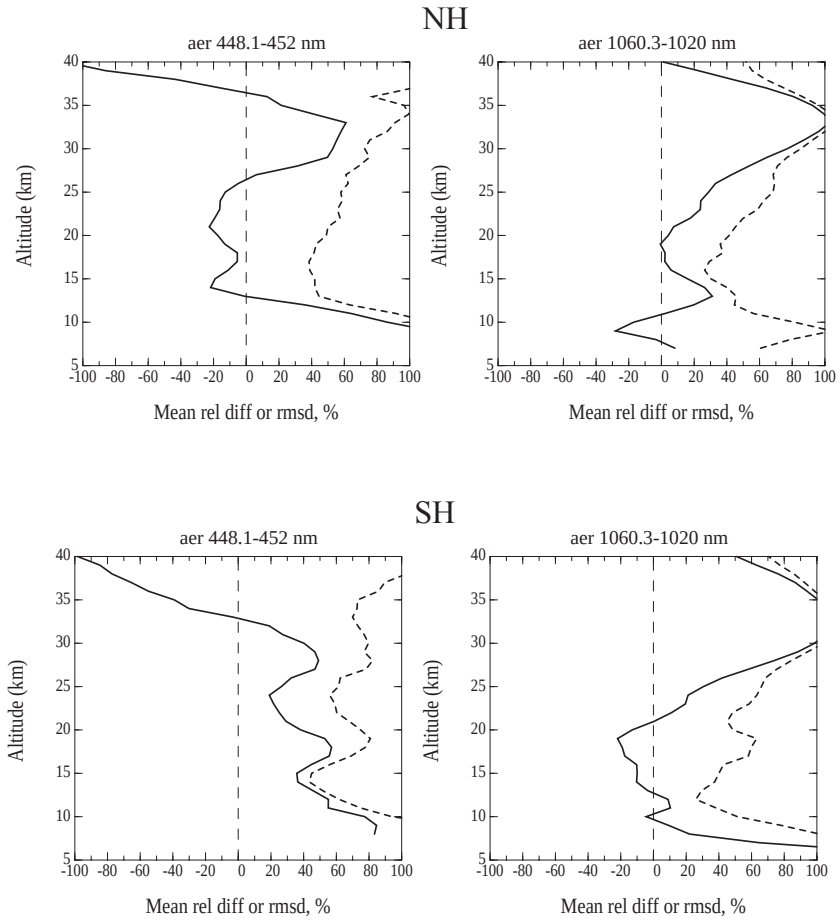

Figure 4.50: Mean relative difference of the extinctions (full line) and root mean square difference (dashed line) for POAM II / SAGE II coincidences. In the northern hemisphere 291 coincidences were identified, and 340 in the southern hemisphere.

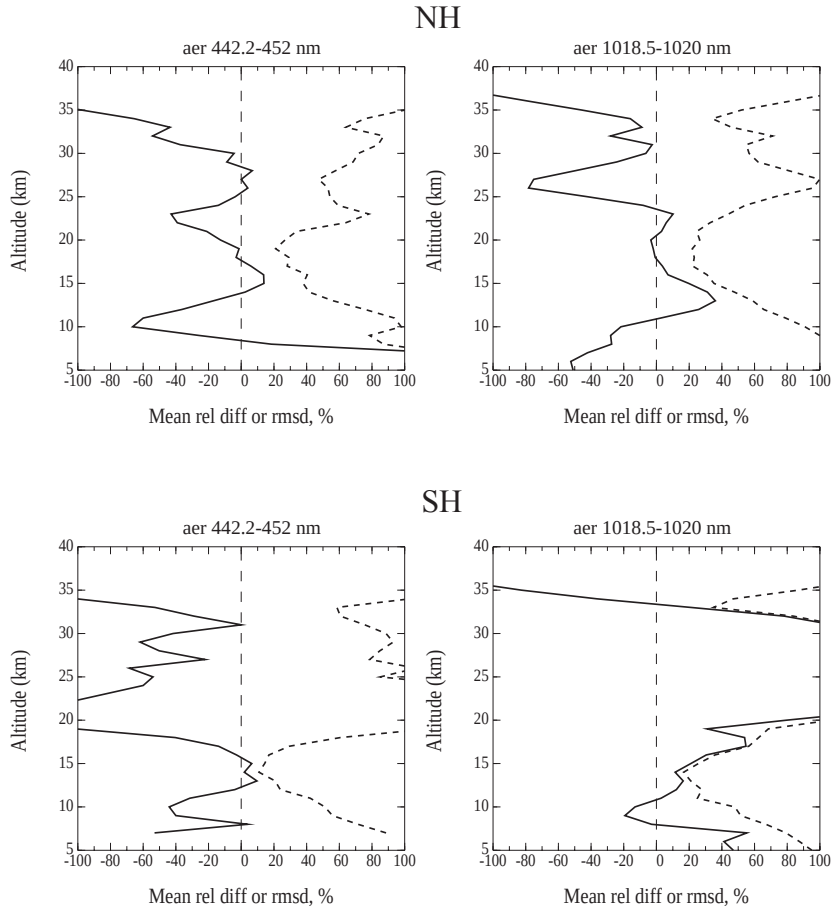

Figure 4.51: Mean relative difference of the extinctions (full line) and root mean square difference (dashed line) for POAM III / SAGE II coincidences. In the northern hemisphere 236 coincidences were identified, and 285 in the southern hemisphere.

For POAM II measurements, the comparison at 448-452 nm shows a small negative bias (POAM<SAGE) in the NH and a large positive bias (POAM>SAGE) in the SH. The mean agreement (rmsd) is worse than 40% in both hemispheres. At 1060-1020 nm there is a positive bias in the 10-15 km range in the NH and a weak bias in the SH. The mean agreement is worse than 30% in both hemispheres. The comparison for POAM III at 442-452 nm exhibits a large negative bias in both hemispheres around 20 km. The mean agreement is worse than 20% in both hemispheres, that is, better than for POAM II. At 1018-1020 nm in the NH there is no bias in the 15-23 km range and a positive bias above 12 km in the SH. The mean agreement is worse than 20% in both hemispheres which is also better than for POAM II.

4.4.3 SAGE/ORA Comparison

A comparison between SAGE and ORA extinction profiles has been carried out previously [Fussen et al., 1998; 2001], making use of 25 coincident events. Figure 4.52 shows a comparison of the 1013 nm ORA channel with the SAGE II 1020 nm from these 25 events. The error bars have been determined as a combination of the experimental error and the statistical variance of the event population. It can be seen that both profiles fit within the error bars.

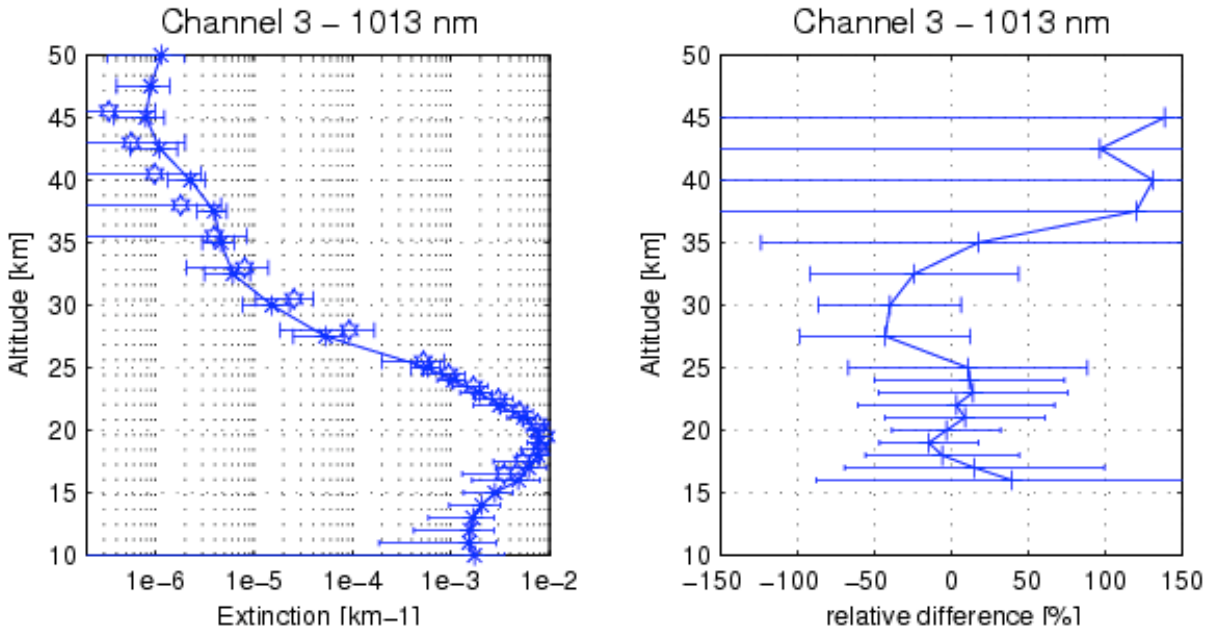

Figure 4.52 (left): Comparison of ORA (asterisks) and SAGE (six-pointed stars) aerosol extinctions at the 1013 nm ORA channel. From Fussen et al. [2001].
Figure 4.53 (right): Relative difference between ORA and SAGE aerosol extinction profiles for the 1013 nm ORA channel. From Fussen et al. [2001].

The relative difference between SAGE II and ORA, calculated as 100 × (ORA-SAGE) / SAGE, is reported in Figure 4.53. The difference is found to be lower than 50%, at least for altitudes lower than 35 km. Concerning the other ORA spectral channels, a comparison using data interpolated in altitude and wavelength from available SAGE II extinctions result in relative differences between both data sets which do not exceed 50% in most cases. A detailed description of the comparison can be found in the cited references.

It is worth noting that extinction data are available to ground level in the case of ORA, which constitutes a main advantage of the ORA data set.

4.4.4 Comparisons of SAGE Extinctions with Lidar Backscatter

The use of lidar for validation of the SAGE instruments has been conducted mainly at mid-latitudes and under background aerosol conditions [Russell and McCormick, 1989, Ackerman et al, 1989, Osborn et al., 1989; Oberbeck et al., 1989, Yue et al., 1995, Lu et al., 1997; Lu et al., 2000, Thomason and Osborn, 1992].

Few comparisons between SAGE instruments and lidar aerosol extinction/backscatter profiles measured in the tropics have been reported. Six SAGE I aerosol/molecular extinction ratio profiles at 1.0 μm [McCormick et al., 1979] measured on April 9, 1979 were compared with six lidar aerosol scattering ratio profiles obtained on November 25-26, 1978, measured at 0.694 μm by the Mark II lidar system located at the University of West Indies (18°N, 76.8°W), Kingston, Jamaica [Kent et al., 1971]. The comparison conducted under background conditions showed, on average, lidar aerosol scattering ratios with higher values than SAGE I in the altitude range of 20-25 km [Kent et al., 1982].

Only two comparisons of stratospheric aerosol measurements from SAGE II with a lidar have been reported in the tropics, both qualitative. One of them has been done under stratospheric aerosol background conditions using data from Trivandrum, India (8.6°N, 77°E) for the first months of 1987 [Parameswaran et al., 1991]. The other comparison was conducted at Ahmedabad (23°N, 72.5°E) in April 1992 [Jayaraman et al., 1995], shortly after the Mount Pinatubo eruption.

The comparisons conducted in the tropics, as well as those conducted at midlatitudes, have some common features. They are characterized, in general, by only a few pairs of lidar-SAGE II selected profiles. They are conducted only at one wavelength, mostly under stratospheric aerosol background conditions or only for very few lidar-backscattering profiles measured during at least one and half year after the Mt. Pinatubo eruption. Estimates of the magnitude of the relative percent differences are provided together with visual estimates of the magnitude of the extinction or backscattering differences, obtained from the plots of coincident profiles. However, they lack statistics on the magnitude of such differences. In general all focused on the instrument comparability.

So far, the most extensive post-Pinatubo comparison between SAGE II and lidar aerosol extinction profiles used SAGE II aerosol extinction profiles at 0.525, and 1.020 μm from version 6.0 of the SAGE II data set, provided by the Langley Research Center [Zawodny et al., 2000]. The lidar dataset consists of the vertical profiles of lidar backscattering coefficients at 0.694 or 0.532 μm from five lidar stations (Table 4.4). Two sets of extinction-to-backscattering conversion coefficients were used for converting lidar backscatter profiles at 0.532 and 0.694 μm to SAGE II extinction profiles at 0.525 and 1.020 μm [Thomason and Osborn, 1992] or to the nearby wavelengths at 0.532 μm and 1.064 μm [Jäger and Deshler, 2002]. Absolute and percent differences between SAGE II - measured and lidar - derived aerosol extinction profiles were calculated for the set of coincident profiles at each lidar station. In addition the magnitude of the aerosol extinction variability was determined using both SAGE II sunset/sunrise coincident aerosol extinction profiles as well as lidar derived aerosol extinction profiles from consecutive days. Also the capability of using lidar derived aerosol extinction profiles for filling SAGE II measured aerosol extinction profiles gaps was demonstrated [Antuña et al., 2002; 2003].

Table 4.4: Lidar stations, with wavelength and vertical resolution of lidars, as well as number of coincident profiles.

Station	*Latitude*	*Longitude*	*λ in μm*	*Resolution*	*Coincident Profiles*
Mauna Loa	19.5°N	155.6°W	0.694	300 m	49
Camagüey	21.4°N	77.9°W	0.532	300 m	20
Hefei	31.3°N	117.2°E	0.532	600 m	55
Hampton	37.1ºN	76.3°W	0.694	150 m	76
Haute Provence	43.9°N	5.7°E	0.532	300 m	178

Figures 4.54 and 4.55 show some SAGE II and lidar coincident profiles for Hampton and Mauna Loa during the first seven months after the Pinatubo eruption. Gaps in SAGE II

(blue profiles) are evident in several panels. Qualitatively, good agreement is obtained if one takes into account the great differences between the principles of measurement and sampling geometry of the two instruments. The preliminary analysis of the differences confirmed the existence of two periods after the eruption, according to the magnitude of the aerosols extinction variability [Chazette et al., 1995]. The quantitative analysis of the differences was conducted for each of those periods separately.

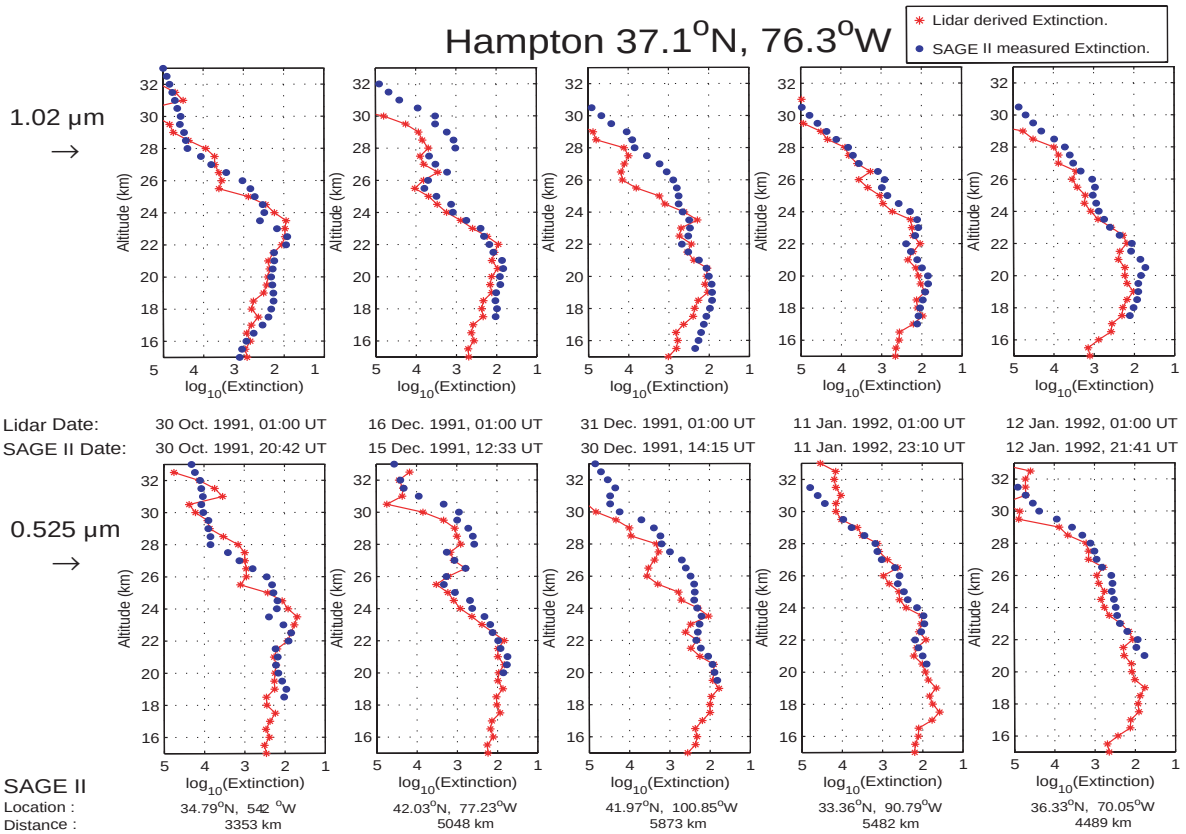

Figure 4.54: SAGE II (blue filled circles) and lidar (red stars) coincident profiles for Hampton during the first seven month after the Pinatubo eruption. Upper panel: 1.020 µm wavelength. Lower panel: 0.525 µm. Coefficients used for converting lidar backscatter profiles at 0.532 and 0.694 µm to SAGE II extinction profiles at 0.525 and 1.020 µm are from Thomason and Osborn [1992].

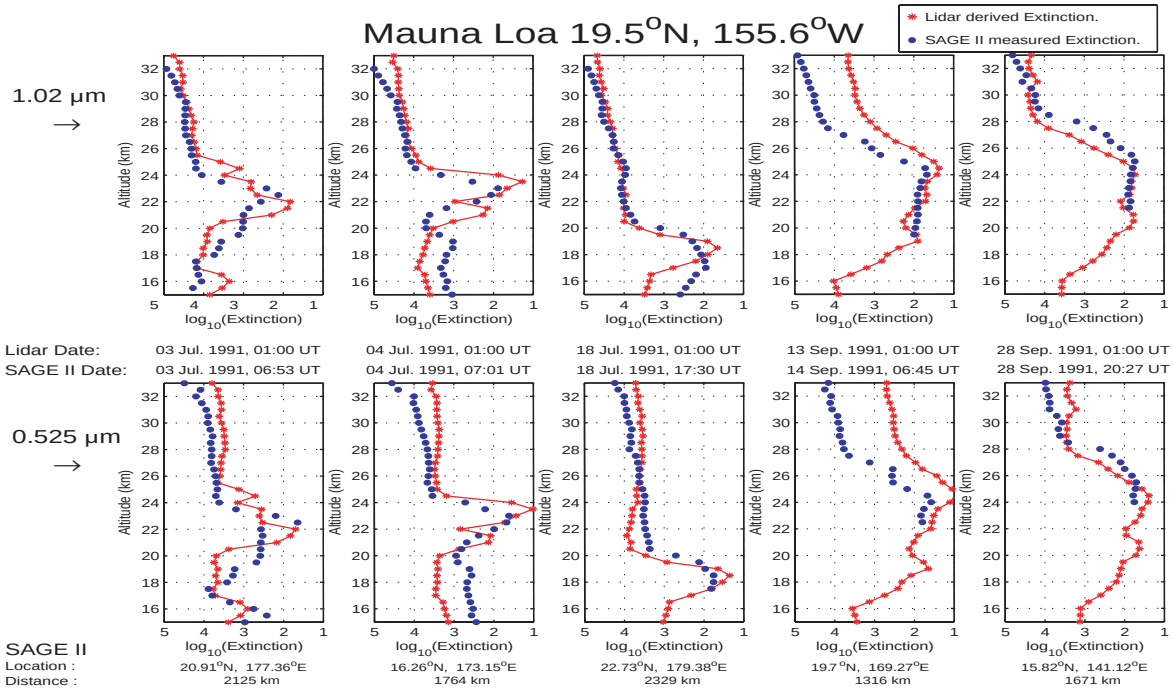

Figure 4.55: SAGE II (blue filled circles) and lidar (red stars) coincident profiles for Mauna Loa during the first seven months after the Pinatubo eruption. Upper panel: 1.020 µm wavelength. Lower panel: 0.525 µm. Coefficients used for converting lidar backscatter profiles at 0.532 and 0.694 µm to SAGE II extinction profiles at 0.525 and 1.020 µm are from Thomason and Osborn [1992].

Magnitudes of the absolute percent extinction differences are shown in Figure 4.56. The first period (Jul 1991 – Jan 1992) is characterized by larger mean percent differences, but they are lower in magnitude at Hampton than at Mauna Loa, because the cloud did not arrive at Hampton until 3 August 1991 [Osborn et al., 1995]. By that time, the initially highly non-homogeneous cloud had become more homogeneous after the settling of the volcanic ash and the mixing effect produced by wind transport. The mean percentage extinction differences do not show a peak in the lower part of the profiles. The vertically averaged mean percentage differences show a decrease of around 15% in the whole column from the first to second period. The second period coincides with significantly smaller peak scattering ratios, with smoother and less layered profiles [Osborn et al., 1995]. The differences are larger at Mauna Loa than at Hampton, because of the higher variability of the stratospheric cloud during its initial stage in low latitudes. As discussed in Antuña et al. [2002], the lidar-derived extinction is higher in general than that measured by SAGE II, except around 20 km. The maximum positive and negative differences are located around 20 and 23 km respectively. From 24 km to around 33 km and between 21 and 22 km the extinction derived from lidar is higher, but the opposite is true below 21 km.

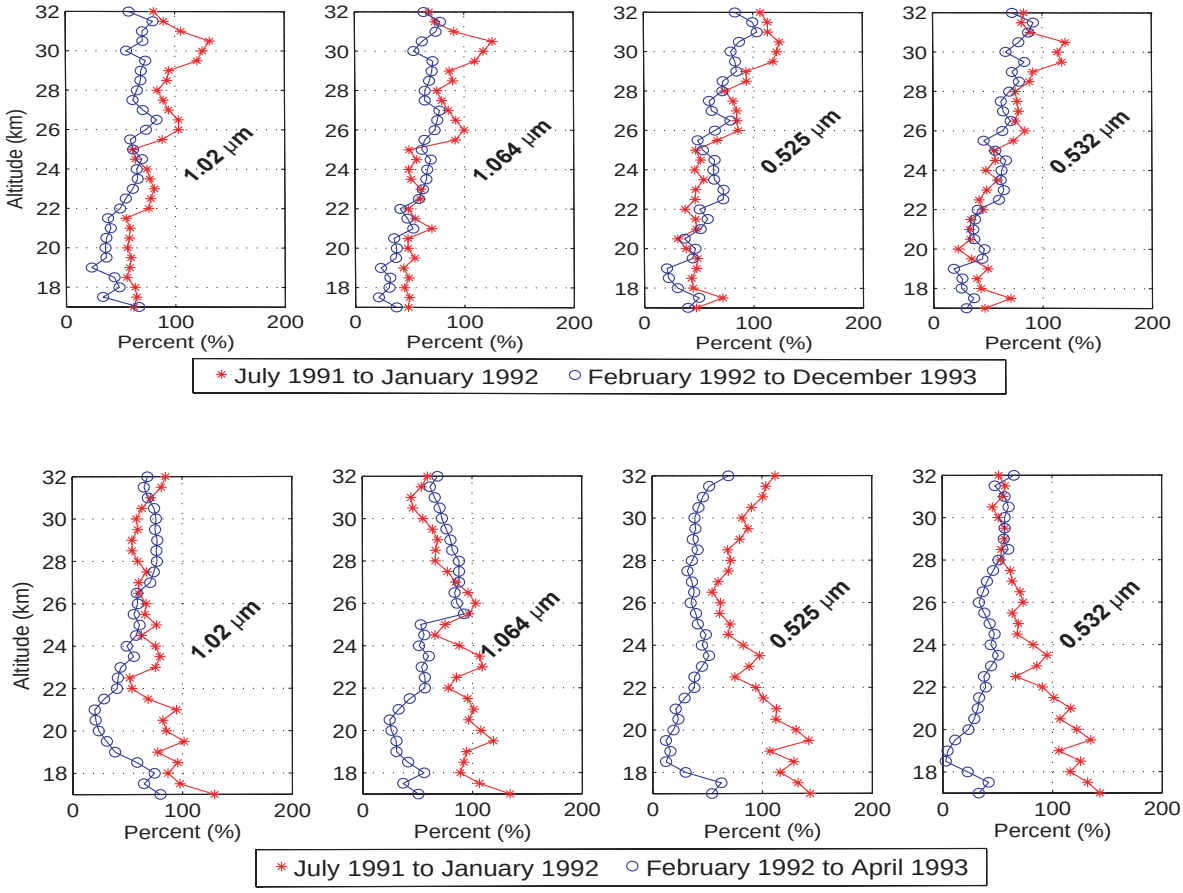

Figure 4.56: Mean absolute differences in % as function of altitude for Hampton (upper row) and Mauna Loa (lower row) between SAGE extinctions and lidar -derived extinctions (time windows indicated in upper right corner). Coefficients used for converting lidar backscatter profiles at 0.532 and 0.694 µm to SAGE II extinction profiles at 0.525 and 1.020 µm are from Thomason and Osborn [1992], those for 0.532 µm and 1.064 µm are from Jäger and Deshler [2002].

By comparing SAGE II sunset/sunrise coincident aerosol extinction profiles as well as one and two day consecutive lidar aerosol backscattering measurements, the magnitude of the time variability of aerosol extinction due to the Mt Pinatubo aerosol cloud has been obtained. That variability reached values between 50 and 150% absolute differences at the core of the cloud for the initial, heterogeneous period, for time lapses of 12 to 48 hours. The degree of agreement between SAGE II extinction profiles and lidar-derived extinction after the eruption is dominated by the magnitude of this variability [Antuña et al., 2003].

The test of the two sets of backscatter-to-extinction coefficients does not reveal appreciable differences since the magnitude of the differences associated with them is lower than the magnitude of the aerosol extinction variability [Antuña et al., 2003]. Before SAGE II - lidar data assimilations are used in stratospheric studies, one should carry out further comparisons between the aerosol extinction profiles measured by SAGE II and lidar derived aerosol extinction profiles, especially under background conditions.

4.5 Conclusions

In this chapter we have presented a fairly complete picture of the stratospheric aerosol. We have not included a number of interesting data sets, nevertheless, we believe that we have generated a representative picture of the stratospheric aerosol. We have included results from eight satellite borne instruments and a large number of other instruments, including both balloon borne and aircraft borne particle counters and ground based and aircraft borne lidar systems.

A significant amount of work was carried out to generate comparisons between the derived products of several instruments. This is difficult to do because the parameters measured by the various instruments differ; even in cases when the same physical quantity is studied, (as for example, extinction) it is usually observed at different wavelengths by different instruments.

The comparisons of the properties of the stratospheric aerosol as determined from the various instruments used in this assessment enable us to draw some general conclusions. First of all, it might be noted that the quality of the agreement is strongly dependent on the altitude and on time. Nevertheless, in general, the aerosol extinctions agree to within 20-60 %. This value depends on whether the comparison is direct (as for SAGE-POAM) or not (as for SAGE-HALOE where the comparison involves modeling and is dependent on the wavelength and assumptions on indices of refraction). Further issues are the coincidence criterion and the comparison methods.

Surface area densities do not agree as well. This is probably due to the differences between the retrieval algorithms and the fact that the various instruments are not sensitive to the same size range of the particles. In general, during periods of high aerosol loading there is agreement in the surface areas calculated from the data obtained from SAGE II, HALOE and the OPC. Disagreements are significantly greater during periods of low aerosol loading, for reasons that have not been clearly determined. It would seem that for periods of high aerosol loading, the calculated aerosol surface areas from any one of the instruments are probably appropriate for use in chemical and radiative studies. Surface areas obtained during periods of low aerosol loading should be treated with care. Finally, it must be noted that, for all measurements, inference of surface area density is carried out assuming a known composition (i.e. known refractive index) for the particles, leading to an additional uncertainty (bias) in the surface area.

In this chapter we have also presented a record of the stratospheric aerosol in which the gaps in the satellite record have been filled in by using lidar and other measurements. The assumptions made in the gap filling procedure have been carefully described. This generates a nearly complete record of the stratospheric aerosol for a period of almost 25 years.